RAPPORT

Nr. 3/2021

Monitoring glaciers in mainland Norway and Svalbard using Sentinel

Liss M. Andreassen (ed.), Geir Moholdt, Andreas Kääb, Alexandra Messerli, Teodor Nagy and Solveig Havstad Winsvold

Copernicus Glacier Service Norway

UiO University of Oslo

Norwegian Polar Institute

NVE Rapport nr. 3/2021

Monitoring glaciers in mainland Norway and Svalbard using Sentinel

Published by:	Norwegian Water Resources and Energy Directorate (NVE)
Editor:	Liss M. Andreassen
Authors:	Liss M. Andreassen, Geir Moholdt, Andreas Kääb, Alexandra Messerli, Teodor Nagy and Solveig Havstad Winsvold
Cover photo:	Sentinel-2 image of Edgeøya, Svalbard, from 1st August 2020 after an unusually warm period where most winter snow melted away from the glaciers and ice caps. Photo: /Copernicus Sentinel data 2020/
ISBN:	978-82-410-2103-9
ISSN:	1501-2832
Print:	NVE
Number printed:	30

Abstract: In this report we evaluate the suitability of data from the Sentinel 1&2 satellites for monitoring glaciers in mainland Norway and Svalbard.

Key words: Sentinel, remote sensing, satellite, glacier velocity, crevasses, glacier lakes, glacier outlines, snowlines, surge

Norwegian Water Resources and Energy Directorate
Middelthuns gate 29
P.O. Box 5091 Majorstuen
0301 Oslo

Telephone: 22 95 95 95
Email: nve@nve.no
Internet: www.nve.no

February, 2021

Copernicus Bretjeneste Norge

Norges vassdrags- og energidirektorat
2021

Contents

Preface

The project Copernicus Glacier Service ('Copernicus bretjeneste' in Norwegian) is a cooperation between the Norwegian Water Resources and Energy Directorate (NVE), the Norwegian Polar Institute (NPI) and the Department of Geosciences, University of Oslo (UiO). The project has been co-funded by the Norwegian Space Agency (NoSA) through national funding reserved for Norwegian implementation of the European Copernicus Program. The project has mainly focused on using optical imagery from Sentinel-2, but also Sentinel-1 and Landsat-8 and other sensors were considered.

Liss M. Andreassen has been the project leader and in charge of the NVE work, Geir Moholdt has been in charge of the NPI work and Andreas Kääb led the project work at UiO. Several colleagues, master/PhD.d. students and temporary project co-workers have also been involved in the project: Torgeir Ferdinand Klingenberg (NVE/UiO), Solveig H. Winsvold (NVE/UiO), Alexandra Messerli (NPI), Teodor Nagy (NVE), Bjarne Kjøllmoen (NVE), Kjetil Melvold (NVE), George Stanley Cowie (UiO/NVE), Josephine Maton (NPI), Aniek Lith (NPI), Marta Majerska (NPI), Ashley Morris (NPI), Jack Kohler (NPI), Mikhail Itkin (NPI), Bas Altena (UiO), Paul Leclercq (UiO), and Varvara Bazilova (UiO/NVE), all working with the Sentinel imagery. NVE would also like to thank Paul Weber for providing historical glacier extents, Ivar Peereboom and Astrid Voksø for updating NVE's GIS data model for the digital glacier inventory, and Nils Kristian Orthe and Heidi B. Stranden for work getting satellite and glacier data visible in NVE's Xgeo.no.

The work done at UiO was coordinated and co-funded by the ESA Climate Change Initiative project Glaciers CCI.

We would like to thank ESA for providing freely available Sentinel imagery and NoSA/Meteorologisk institutt for efficient data distribution through the Norwegian ground segment portal (satellittdata.no). We also want to thank the Norwegian mapping authority (Kartverket), and the NPI mapping section for providing freely available high resolution orthophotos for mainland Norway (www.norgeibilder.no) and Svalbard (toposvalbard.no). Landsat-8 and ASTER imagery was acquired via the Earth Explorer tool built by USGS.

Oslo, February 2021

Hege Hisdal
Director
Hydrology Department

Rune Engeset
Head of section,
Section for Glaciers, Ice and Snow

Summary

In the Copernicus Glacier Service project, we have used Sentinel satellite imagery to monitor glaciers and derive glacier products for mainland Norway and Svalbard.

Sentinel-2 data are well suited to derive periodic glacier products and for visual inspection of state of the stake of glaciers and glacier lakes. We used Sentinel-2 to derive updated glacier outlines for mainland Norway and Svalbard, map annual position of the marine calving fronts on Svalbard, determine glacier velocities, detect glacier crevasses and surges and delineate position of transient snowlines and glacier lake areas.

The major limitation for more usage of the Sentinel-2 data is cloud cover. Although our main focus in this project was the use of Sentinel-2 optical data, we also did some initial tests, demonstrations, and comparisons using Sentinel-1. Preliminary results suggest that Sentinel-1 radar data can be a supplement or alternative to Sentinel-2 data, in particular the detection and monitoring of glacier/snow facies, ice-velocity and surging.

Sammendrag

I prosjektet Copernicus bretjeneste har NVE, Norsk Polarinstitutt og Institutt for Geofag, Universitetet i Oslo brukt Copernicus Sentinel data til å overvåke og kartlegge endringer av breer og utarbeide breprodukter for breer på Norges fastland og på Svalbard.

Vi har lagt hovedvekt på å teste ut de optiske Sentinel-2A og 2B satellittene, men har også gjort noen tester med bruk av data fra de to Sentinel-1 radarsatellittene.

Sentinel-2 data er godt egnet til å kartlegge utbredelse av breene på Norges fastland, og på Svalbard kan de i tillegg brukes til årlig kartlegging av de marine kalvingsfrontene. Sentinel-2 data kan også brukes til å bestemme snølinjer, beregne brehastighet og finne områder med sprekker på breer. Sentinel-2 er også godt egnet til å overvåke sjøer som er i kontakt med bre og kan forårsake plutselige flommer (jøkullaup).

En begrensing med Sentinel-2 er at mange av bildene som tas er dekket av skyer, både på fastlandet og på Svalbard. Sentinel-1 har et stort potensial som supplement til Sentinel-2 for å følge med på utviklingen av norske breer framover., spesielt for å bestemme snølinjer og overflatetyper, beregne brehastighet og identifisere surgende breer.

List of abbreviations and acronyms

AAR	Accumulation-area ratio
BOA	Bottom-of-atmosphere
BRDF	Bidirectional reflectance distribution function
CIAS	Correlation Image Analysis Software
COSI-Corr	Co-Registration of Optically Sensed Images and Correlation
CPOM	Center for Polar Observation and Modelling
DEM	Digital elevation model
DTM	Digital terrain model
ELA	Equilibrium-line altitude
et al.	et alia, meaning 'and others'(used for multiple authors)
ESA	European Space Agency
ETM+	Enhanced Thematic Mapper Plus
GAO	Glacier area outline
GLIMS	Global Land Ice Measurement from Space
GLO	Glacier lake outline
GLOF	Glacier lake outburst flood
GNSS	Global navigation satellite system
GoLIVE	Global Land Ice Velocity Extraction
GPR	Ground penetrating radar
IMCORR	Image Correlation Software
ImGRAFT	Image Georectification and Feature Tracking Toolbox
ITS_LIVE	The Inter-mission Time Series of Land Ice Velocity and Elevation
L8	Landsat 8
MEaSUREs	Making Earth System Data Records for Use in Research Environments
NDSI	Normalized Difference Snow Index
NDWI	Normalized Difference Water Index
NIR	Near-infrared

NoSA	Norwegian Space Agency
NPI	Norwegian Polar Institute
NVE	Norwegian Water Resources and Energy Directorate
OLCI	Ocean and Land Colour Instrument
OLI	Operational Land Imager
RGB	Red-green-blue (colour composite)
RGI	Randolph Glacier Inventory
S1	Sentinel-1
S2	Sentinel-2
SAR	Synthetic Aperture Radar
SCR	Snow cover ratio
SenDiT	Sentinel-2 Displacement Toolbox
SLA	Snowline altitude
SWIR	Short-wave infrared
TIRS	Thermal infrared sensor
TM	Thermatic Mapper
TOA	Top-of-atmosphere
UiO	University of Oslo
WMS	Web Map Service

1 Introduction

1.1 Background

Glaciers are particularly sensitive to changes in climate and one of the main contributors to recent sea level rise globally (e.g. Wouters et al., 2019). Glacial surges are common in Svalbard, where a glacier in shorter periods can advance substantially, moving at velocities many times faster than normal, and causing increased crevassing (e.g. Sund et al., 2009; 2014) (Fig. 1-1). Glacier crevasses can be dangerous for both tourists and personnel conducting glaciological field work (Fig. 1-2). Glaciers can be hazardous and may cause glacier lake outburst floods (GLOFs) and serac falls (Fig. 1-3). The snowline of glaciers and ice caps can be used as a proxy for glacier mass balance (e.g. König et al., 2004). Glacier datasets of outlines, calving fronts, glacier facies and velocity are important input for many types of analysis and modelling, and valuable in glacier change studies (e.g. Nuth et al., 2013; Winsvold et al., 2014; Schellenberger et al., 2015; Farinotti et al., 2017).

Figure 1-1. Part of the Nathorstbreen glacier system in southern Svalbard during surge in 2013. Note the difference between the heavily crevassed surfaces due to surge in the foreground, and the smooth and even surface of the quiescent phase glaciers in the background. Photo: Monica Sund.

The goal of the Norwegian project Copernicus Glacier Service is to use Sentinel imagery to monitor glaciers in mainland Norway and Svalbard. The Norwegian water resources and energy directorate (NVE) and Norwegian Polar Institute (NPI) are responsible for operational monitoring of glacier mass balance in Norway and Svalbard, respectively.

Figure 1-2. Glacier hiking in crevassed and snow-covered terrain at Nigardsbreen, in June 2018. Photo: Jostein Aasen

Medium resolution optical satellite sensors such as Landsat-8 and Sentinel-2 have proven to be invaluable for observations of the cryosphere. The project aimed to evaluate how optical imagery from the Sentinel-2 satellites could be used to derive operational information about glacier state and glacier changes. Radar data from Sentinel-1 and data from other optical (e.g. Landsat) and radar sensors (e.g. Radarsat) have also been used when relevant.

Glacier products that were assessed were:

- Glacier outline, area and calving front
- Glacier surface type and snow line
- Ice velocity
- Glacier crevasses and surge
- Glacier lakes

Figure 1-3. Rundvassbreen, an outlet of Blåmannsisen has had many GLOF events. Here is the lake almost emptied after an event in September 2019. Note the ice blocks marking the previous lake extent. Photo: Cecilie R. Amundsen.

1.2 Study area

The study area in the Copernicus Glacier Service is the glacierized area over mainland Norway and Svalbard. Glaciers in mainland Norway cover an area of ca. 2700 km^2, about 0.7% of the land area (Andreassen et al., 2012). The 40 largest glaciers cover 2/3 of the total area. The six largest glaciers are Jostedalsbreen (JOB), Vestre Svartisen (VS), Søndre Folgefonna (FOL), Østre Svartisen (ØS), Blåmannisen (BLÅ) and Hardangerjøkulen (HAJ) (Fig. 1-4) ranging in size from 474 km^2 to 71 km^2 (according to Andreassen et al., 2012). Mass balance measurements in Norway are currently conducted on a selection of 10 glaciers and 1 ice patch, and length change measurements on 30-40 glaciers (Kjøllmoen et al., 2020).

A recent review of glacier changes since the 1960s reveals overall retreat of the glaciers, great inter-annual variability of mass balance, and accelerated deficit and retreat since 2000 (Andreassen et al., 2020b). Some years with a positive (or less negative) mass balance after around 2010 can be attributed to variations in large-scale atmospheric circulation. For a sample of 131 glaciers the overall change in surface elevation was −15.5 m for the ∼50-year period. Converted to a geodetic mass balance this gives a mean mass balance of -0.27 ± 0.05 m w.e. a−1. (Andreassen et al., 2020b).

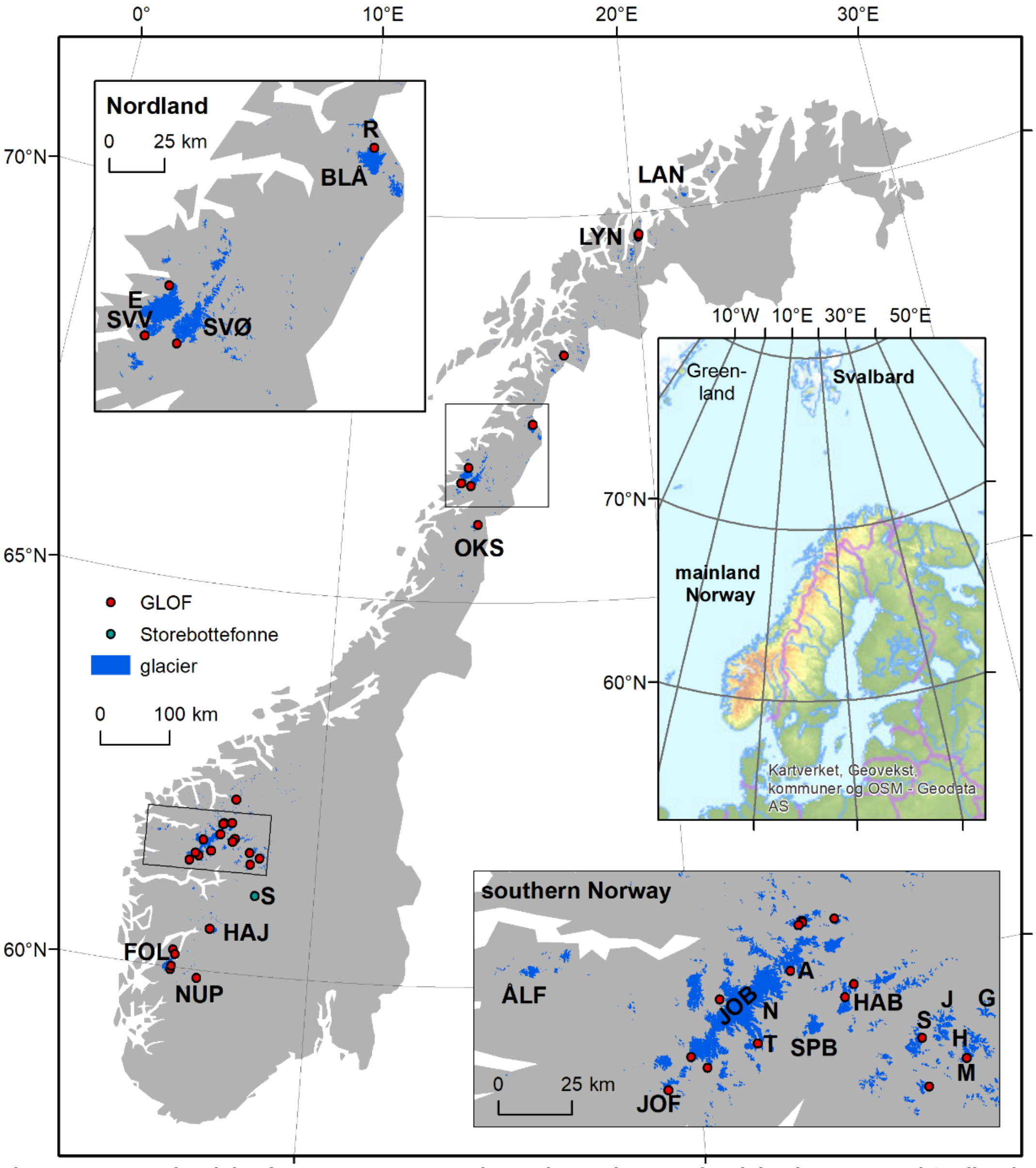

Figure 1-4. Map of mainland Norway. Inset map shows the study area of mainland Norway and Svalbard (see figure 1-4 for Svalbard map). Two other insets show close-ups of some of the glaciers mentioned in the report. Main map abbreviations: FOL: Folgefonna, HAJ: Hardangerjøkulen, S: Storebottefonne, OKS: Okstindbreen, SV ØV: Vestre and Østre Svartisen, Blå: Blåmannsisen, LYN: Lyngen, LAN: Langfjordjøkelen. Inset southern Norway abbreviations: ÅLF: Ålfotbreen, JOB: Jostedalsbreen, JOF: Jostefonn, T. Tunsbergdalsbreen, N: Nigardsbreen, A: Austdalsbreen, HAB: Harbardsbreen, SPB: Spørteggbreen, J: Juvfonne, H: Hellstugubreen, M: Memurubreene, G: Gråsubreen. Nordland abbrevations: SVV: Vestre Svartisen, SVØ: Østre Svartisen, E: Engabreen, BLÅ: Blåmannsien, R-Rundvassbreen.

In the last complete mapping in the 2000s, Svalbard glaciers and ice caps (Fig. 1-5) covered ~57% of the archipelago with a total area of 33,775 km^2 (Nuth et al., 2013) and an ice volume of roughly 6000 km^3 (Fürst et al., 2018). About 60 % of the total glaciated area on Svalbard drains into tidewater glaciers (Blaszczyk et al., 2009), terminating into the sea as grounded ice-tongues with a marked cliff in front (Fig. 1-6). Typical Svalbard glaciers are characterized by low velocities (<10 m a^{-1}) with glacier beds often frozen to the underlying permafrost (Björnsson et al., 1996). Some glaciers like Kronebreen near

Ny-Ålesund have a relatively steady fast-flow (Schellenberger et al., 2015) whereas other rapidly flowing glaciers are often associated with episodic glacier surging (Fig. 1-1). Marine frontal ablation (sum of frontal melt and calving) is an important part of mass losses on Svalbard, but atmospheric glacier surface melting is still the main control of the overall mass balance. Various geodetic methods have been used to estimate the total glacier mass balance of Svalbard, with typical values ranging from -5 to -15 Gigatons per year (-0.15 to -0.45 m w.e. a^{-1}) for different periods during the last few decades. In-situ mass balance measurements from a selection of reference glaciers also indicate a negative mass balance since the 1960s, with a slightly increasing trend since 2000 (Schuler et al., 2020).

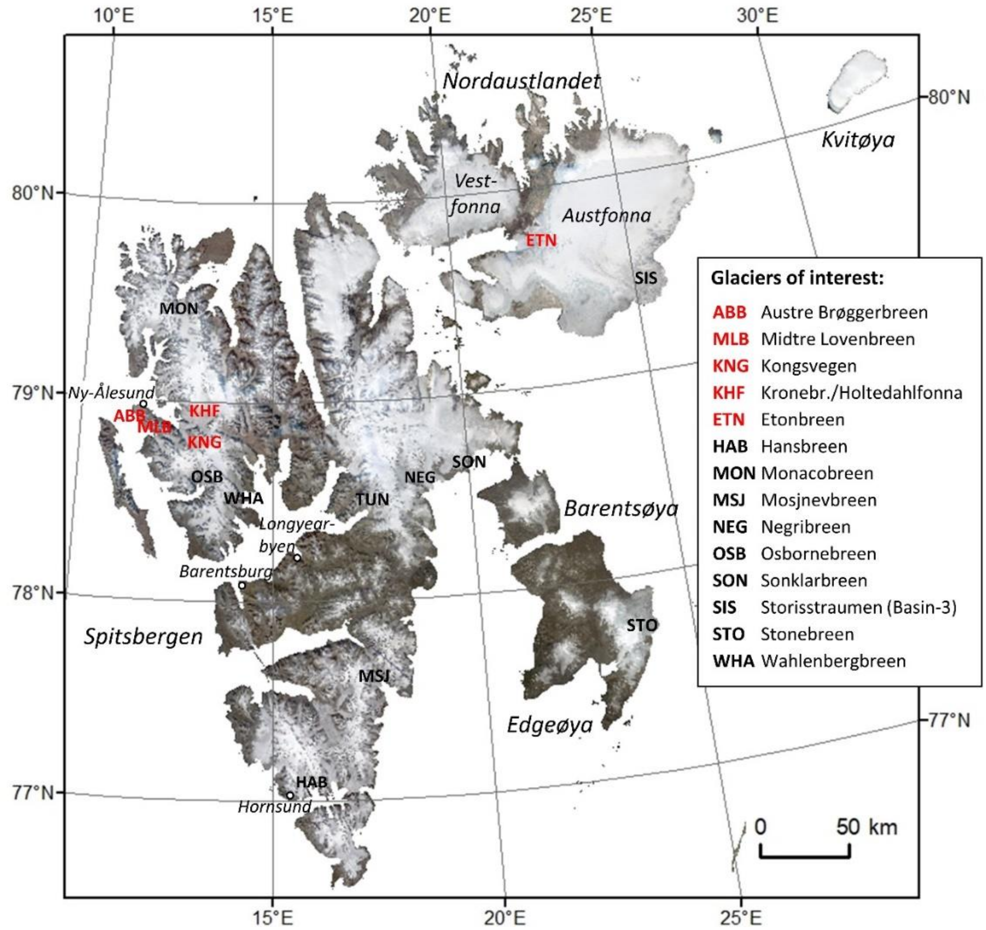

Figure 1-5. Overview map of Svalbard, showing glacier-covered areas (white), main islands and settlements (italic names) and abbreviations of some key glaciers mentioned in the report. Glaciers with red letters are monitored by NPI for long-term mass balance, a climate indicator in the Environmental monitoring of Svalbard and Jan Mayen (MOSJ). The image mosaic is made from Landsat-8 imagery, courtesy USGS.

Figure 1-6. Participants of the "ESA Cryosphere Remote Sensing Training Course 2018" admiring the glacier calving front of Tunabreen in Tempelfjorden, Svalbard, 14 June 2018. Photo: Geir Moholdt.

1.3 About this report

The report is separated into 6 chapters. Chapter 2 gives a short overview of data sources and quality. Chapter 3 describes analysis and evaluation of Sentinel data for deriving the planned glacier products. In chapter 4 we describe data download and data visualization through web map services and xgeo, and other data storage. We draw conclusions of our Sentinel-related experiences in chapter 5 and give an outlook for possible further work in chapter 6.

2 Data

Sentinel-1, -2 and Landsat-8 are excellent instruments to use for mapping and monitoring of glaciers (e.g. Winsvold, 2017). The satellite imagery from these radar and optical sensors are free and open, and have high temporal, spatial and radiometric resolution compared to earlier similar satellite sensors. However, it can also be challenging to use these data together in multi-sensor applications due to differences in the sensors and the processing algorithms (Altena and Kääb, 2017).

In the Copernicus Glacier Service project we have focused primarily on satellite data from Sentinel-2 (optical), but also used data from Sentinel-1 (radar) and Landsat 8 (optical). In this section we give a brief overview of the Sentinels, Landsat as well as other data used. We also describe how we have facilitated the use of Copernicus data, and we test the geometric performance of Sentinel-2.

2.1 The Sentinels

The word *Sentinel* can be used both as a noun and verb, and means (someone who) watch or guard over. The *Sentinels* are a family of missions developed by the European Space Agency (ESA) in the EU Copernicus programme (Fig. 2-1). The missions cover different temporal and spatial resolutions and both radar and multi-spectral imaging instruments for land, ocean and atmospheric monitoring. The Sentinel-1 and Sentinel-2 missions we use in this report are each based on a constellation of two satellites to fulfil revisit and coverage requirements.

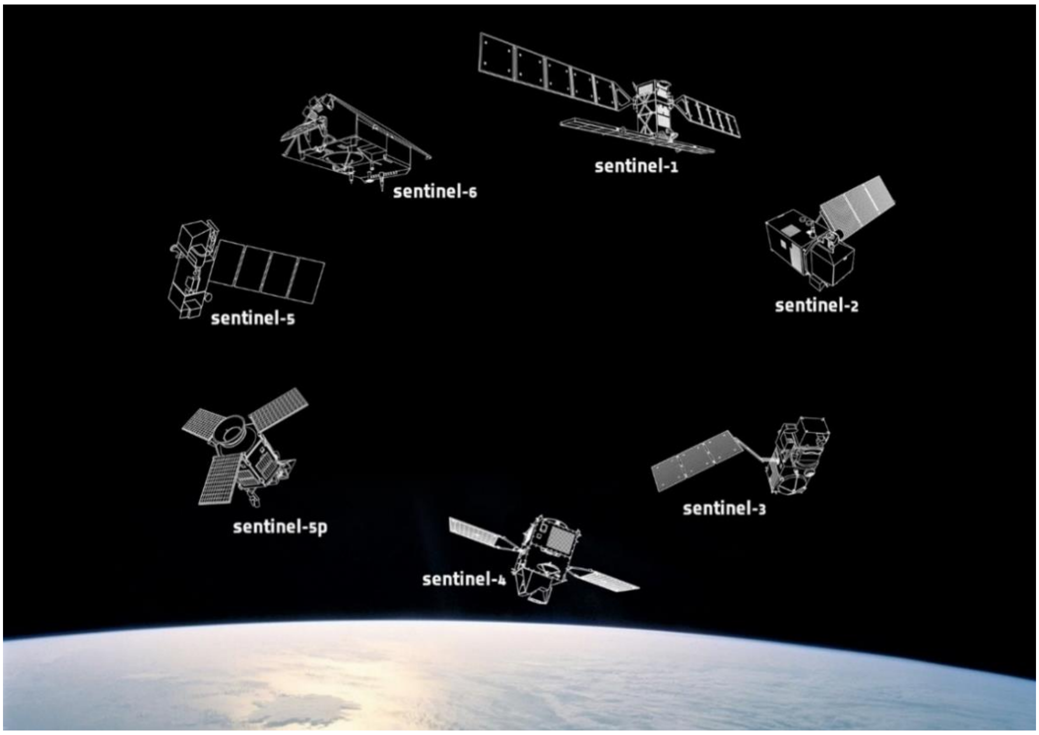

Figure 2-1. The Sentinels consist of six missions. In this report we use Sentinel-1 and Sentinel-2. Source: © ESA.

Sentinel-1 is a polar-orbiting, all-weather, day-and-night radar imaging mission for land and ocean services. Sentinel-1A was launched on 3 April 2014 and Sentinel-1B on 25 April 2016. Both were taken into orbit on a Soyuz rocket from Europe's Spaceport in French Guiana. (Source: ESA). Sentinel-1 is a C-band synthetic aperture radar (SAR) sensor. Sentinel-1A and Sentinel-1B together can provide a repeat frequency of six days from the same nominal orbit.

Sentinel-2 is a polar-orbiting, multispectral high-resolution imaging mission for land monitoring to provide, for example, imagery of vegetation, soil and water cover, inland waterways and coastal areas. Sentinel-2 can also deliver information for emergency services. Sentinel-2A was launched on 23 June 2015 and Sentinel-2B followed on 7 March 2017. (Source: ESA). The Sentinel 2A-2B constellation yields an observation every five days at the equator and more frequently in higher latitudes from the same nominal orbit. Sentinel-2 currently provides the highest ground resolution (10m) of freely available satellite imagery.

2.2 Landsat

The Landsat program is a series of multispectral satellites provided by the U.S. Geological Survey (USGS). The first satellite was launched in 1972 and Landsat has the longest continuous global record of the Earth's surface.

Landsat-8 that has relatively similar properties as Sentinel-2. It carries an operational land imager (OLI) and thermal infrared sensor (TIRS) and has nine reflective wavelength bands designed for land use, with the highest ground pixel resolution being 15m for the panchromatic band (Loveland and Irons, 2016). The revisit time is 16 days.

The Landsat missions have been excellent in providing freely available imagery covering mainland Norway and Svalbard for decades now. Landsat data was used for the previous glacier and glacier lake outline inventories (Andreassen and Winsvold, 2012; Winsvold et al., 2014; Nuth et al., 2013). In this work, we mainly used Landsat-8 imagery for mapping glacier lakes, glacier outlines and calving fronts for years prior to the Sentinel era or to supplement and compare with Sentinel data when the missions overlap.

2.3 Comparison of Sentinel-2 and Landsat

Comparing Sentinel-2A and Sentinel-2B satellites with Landsat 5, 7 and 8 shows an improved spatial and temporal resolution of Sentinel 2 (Table 2-1). Many of the glacier features such as crevasses, ash layers or boulders can be on the order of few meters wide and therefore using the bands with highest possible resolution is favourable (Fig. 2-2). The ground swath width is 185 km of Landsat, and 290 km of Sentinel 2 (Table 2-2), which cause larger off-nadir viewing angles and thus larger potential ortho-rectification errors (Kääb et al., 2016). Sentinel-2 carries no thermal instrument, in contrast to Landsat-8. 8

Figure 2-2. Comparison of imagery of Tunsbergdalsbreen tongue and terminus. To the left Landsat 8 (L) band 8 image at 15m resolution, to the right Sentinel-2 (S) band 8 image at 10m resolution, both from 22 August 2017. More crevasses at better resolution are visible in the Sentinel-2 image.

Sentinel-2 has several characteristics that makes it suitable for glacier mapping including four visible and near-infrared (VNIR) bands with 10 m spatial resolution, compared to 30 m (15 m for pan) for Landsat 8 (Fig. 2-3). Sentinel-2 also has six VNIR and short-wave infrared bands (SWIR) with 20 m resolution, compared to 30 m for Landsat 8.

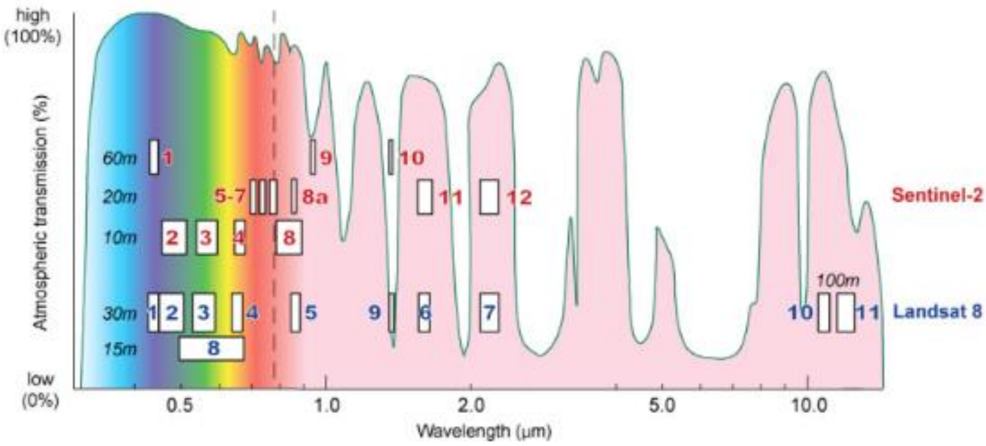

Figure 2-3. Comparison of spectral bands of Landsat-8 and Sentinel-2 with respective wavelength and resolution. Figure from Kääb et al. (2016).

Sentinel imagery are typically displayed in red-green-blue (RGB) colour composites or as single bands. In this report we used natural and false combinations using the NIR and SWIR bands (Fig. 2-4). Single bands such as NIR (Fig. 2-2) or blue (Fig. 2-4) were also used in this report. Hereafter we denote the combination NIR-Red-green as false 8-4-3 and SWIR-NIR-Red as false 11-8-4.

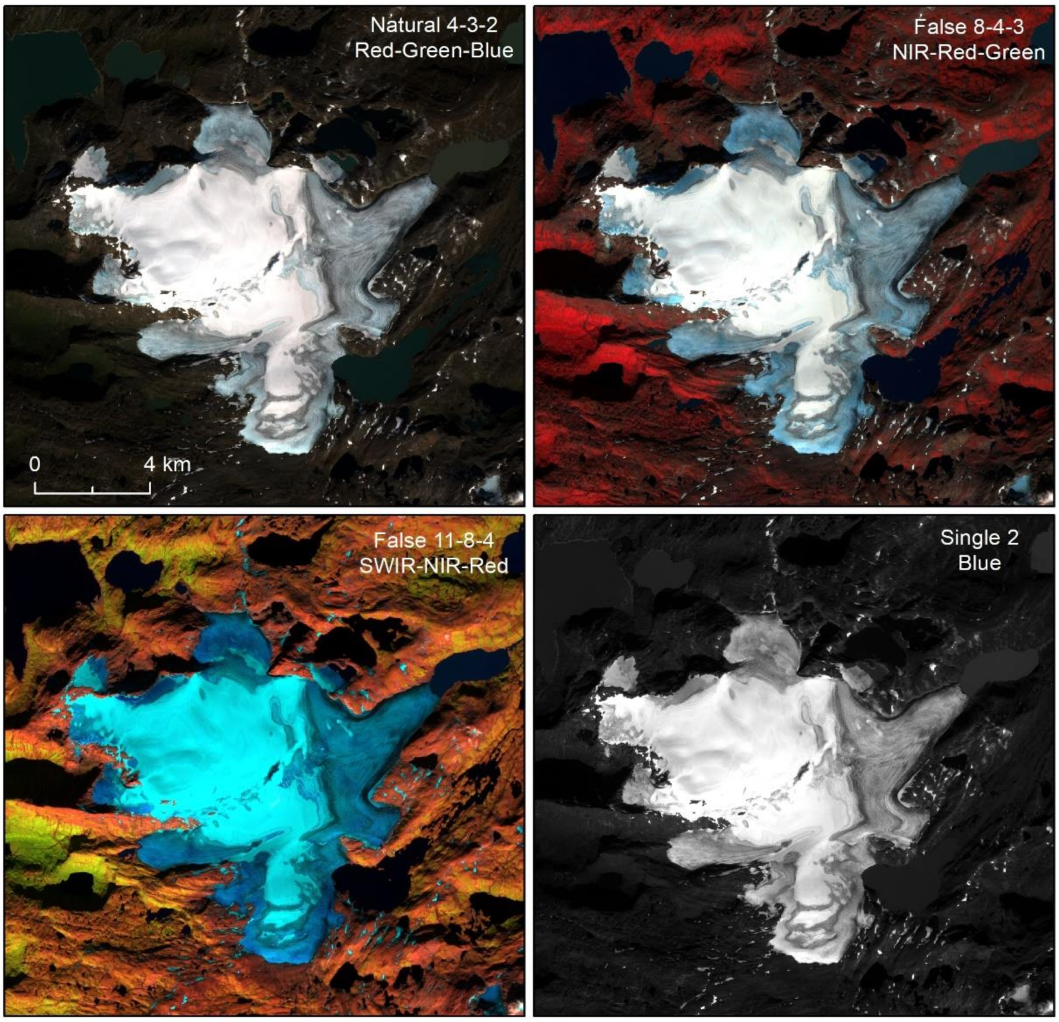

Figure 2-4. Blåmannsisen, Nordland, displayed in three different band combinations and as single band. Glacier ice appear turquoise is the false 11-8-4 (SWIR-NIR-Red), light blue in false 8-4-3 (NIR-Red-Green) and light blue-grey in natural colours. Note also how the colours of lake and vegetation varies. /Copernicus Sentinel data/

Table 2-1. Spectral band wavelength ranges (in µm) of the optical sensors that are used for glacier mapping. The spatial resolution (in m) is color-coded: 10 (green), 15 (blue), 20 (grey), and 30 (black). NIR: near infra-red, SWIR: short-wave infrared, Pan: panchromatic. TM: Landsat 5 Thematic Mapper, ETM+: Landsat 7 Enhanced Thematic Mapper Plus. Modified from Paul et al. (2016).

Band	**Number**				**Landsat**			**Sentinel-2**
Band	TM	ETM +	OLI	MS I	TM	ETM+	OLI	MSI
Blue	1	1	2	2	0.45–0.52	0.45–0.52	0.45–0.51	0.46–0.52
Green	2	2	3	3	0.52–0.60	0.53–0.61	0.53–0.60	0.54–0.58
Red	3	3	4	4	0.63–0.69	0.63–0.69	0.63–0.68	0.65–0.68
NIR	4	4	5	8	0.76–0.90	0.76–0.90	0.85–0.89	0.78–0.90
SWIR	5	5	6	11	1.55–1.75	1.55–1.75	1.56–1.66	1.57–1.66
SWIR	7	7	7	12	2.08–2.35	2.09–2.35	2.10–2.30	2.10–2.28
Pan	-	8	8	-	-	0.52–0.90	0.50–0.68	-

Table 2-2. Comparison of Landsat 8 and Sentinel-2 parameters. Data adapted from Loveland and Irons (2016) and Li and Roy (2017).

Parameter	**Landsat 8**	**Sentinel-2**
Highest resolution band	15m	10m
Number of bands of highest resolution	1	4
Revisit time	16 days	5 days (S2A and S2B)
Altitude	705 km	786 km
Ground swath width	185 km	290 km
Release year	2013	2015 (S2A), 2017 (S2B)
Local time of image acquisition	Ca. 10:00 (mainland) 12-14 (Svalbard)	Ca. 10:30 (mainland) 12-14 (Svalbard)

2.4 Other data

2.4.1 Orthophotos

Orthophotos are orthorectified aerial imagery and were used for validation and testing. 'Norge i bilder' means 'Norway in imagery' and is a website displaying orthorectified aerial imagery over mainland Norway: norgeibilder.no. The orthophotos were used for directly as a web map service (wms) or for viewing and downloading from norgeibilder.no. The imagery was useful, especially for glacier lake and glacier outline mapping. New imagery was available during the project, such as imagery from 2019 covering glacier regions Folgefonna, Hardangerjøkulen and Møre in southern Norway. Some of the newer orthophotos were less useful due to large amounts of seasonal snow, here older imagery could be more informative. Some of the orthophotos were downloaded and used in illustrations in this report.

All of Svalbard was surveyed with high-resolution stereo-imagery during the summer months of 2008-2012 and forms the basis for the NPI orthophoto products that can be viewed directly on *toposvalbard.no* or as a WMS product (see http://geodata.npolar.no). These orthophotos were important supporting information for many purposes in the project, especially for finer glaciological interpretations in the glacier outline mapping with Sentinel-2.

2.4.2 Digital terrain models

Surface elevation models are commonly referred to as both digital elevation models (DEM) and digital terrain models (DTM). In this report, both terms are used and means digital elevation of the surface. The Norwegian mapping authorities and the NPI use the term DTM for their datasets of surface elevations. The version we used for checking the orthorectification of Seninel imagery over mainland Norway was the 10 m resolution

DTM from the Norwegian Mapping Authority, which was produced using photogrammetric methods (Kartverket, 2018). Since then, more elevation data have been produced and we will use the newest available DTM10 for deriving glacier characteristics of the updated glacier inventory. NVE has also collected laser-scanning data of glaciers independently for detailed glacier studies (e.g. Andreassen et al., 2020b), and they have been submitted to the mapping authorities to be use in updating the national DTM and are available for viewing and download from hoydedata.no.

The main digital elevation model (DTM) used for Svalbard in this project was the NPI "S0 Terrengmodell" (doi:10.21334/npolar.2014.dce53a47), based on aerial stereo-imagery from 2008-2012. The S0 DTM is available as 5 m resolution tiles or a 20 m mosaic product. Parts of Southern Spitsbergen is still under production, so rather than using older data here, NPI made a second mosaic with missing areas filled with data from ArcticDEM (Porter et al., 2018). This mosaiced DTM (doi: 10.21334/npolar.2020.a660ff0c) was provided to the Norwegian Space Agency and ESA for implementation in the additional DTERRENG processing of Sentinel-2.

Jack Kohler at NPI has further used ArcticDEM strip data from 2013-2019 to make annual DTM mosaics that have been used to estimate glacier elevation changes and mass balance, as well as to improve ice thickness estimates for the annually mapped glacier calving fronts (Section 3.1.2). For this purpose, we also relied on near-glacier ocean bathymetry data from the Norwegian Mapping Authority and an observationally constrained bedrock model of the ice-free topography of Svalbard (Fürst et al., 2018). Up-to-date ice thickness at the calving fronts can then be calculated by subtracting the merged bedrock model from the annual ArcticDEM mosaics.

A third type of surface elevation data that were used on Svalbard is CryoSat-2 radar altimetry (2010-2020) and ICESat-2 laser altimetry (2018-2020). These data provide very accurate elevation reference for given times, but the spatial coverage is incomplete. Ashley Morris at NPI led a project-related study (Morris et al., 2020) to assess glacier thickness changes and mass balance for the whole of Svalbard, showing increased mass loss during the 2011-2017 CryoSat-2 period with respect to the 2003-2009 ICESat period. The CryoSat-2 results also showed evidence of ice-dynamical thinning and surging, consistent with mapping of ice velocity and calving fronts.

2.4.3 Time lapse camera

Time-lapse cameras have become popular to monitor rapidly changing glacier environments. A network of time-lapse cameras was installed on two mountain ridges next to Kronebreen in 2014 to study glacier hydrology, ice dynamics, calving and subglacial meltwater plumes in the fjord, all described by How et al. (2017). In 2017, a similar camera (Canon 600D) was set up on a mountainside overlooking a glacier lake called Setevatnet, located in an ice-moriane zone between the glaciers Uvêrsbreen and Kongsvegen near Ny-Ålesund. The time-lapse camera takes a snapshot every 30 minutes and has captured several cycles of glacier lake filling and outburst flood (GLOF) during the last few years. In this project, the terrestrial image time series has been combined with Sentinel-2, Landsat-8 and ArcticDEM strips to study GLOFs of Setevatnet back to year 2014. This work is described in more detail in Section 3.5.2.

2.4.4 Glacier velocity measured with differential GNSS

Glacier velocity stake data was used to compare the results of feature tracking for glaciers (chap 3.2). For mainland Norway, data from three stakes on Engabreen (SVV), Nigardsbreen (JOB) and Rembedalskåka (HAJ) (see figure 1-1 for location) were used. See Nagy et al. (2019) and Nagy and Andreassen (2019a) for details. For Svalbard, GPS-measured stake velocities were used for comparison with satellite-derived velocities for fast-flowing parts of Kronebreen and Austfonna. These in-situ GPS measurements are further described and presented by Dunse et al. (2012; 2015) and Schellenberger et al. (2015).

2.4.5 Radarsat

For validation of Sentinel-1 derived ice velocities we also used velocities as derived from repeat ultrafine beam Radarsat-2 data. Radarsat-2 is comparable to Sentinel-1 but has the possibility for high-resolution modes that enable visibility of more details, such as crevasses, and thus better resolved ice velocities (Schellenberger et al., 2015). Radarsat data are commercial, not freely available, and need to be tasked so that no background data are available.

2.5 Facilitate use of Copernicus data

We needed to ensure that the remote sensing data we use for deriving our glacier products are of good spectral and geometric quality. A part of the Copernicus Glacier Service project was therefore to test the geometric performance of Sentinel-2, in particular effects from orthorectification errors (see chap 2.6). Further, the Sentinel-2 satellite images themselves are valuable for many qualitative analyses. This can for example be to observe changes in a glacier lake over time, or getting information about the end-of-season snowline. Satellite images were therefore included in the IT-structure at NVE and NPI, and customised visualization tools of Sentinel-2 imagery can thus be included in the GIS-systems for further glacier analysis (combined with other geographic information). Standardization and sufficient metadata structures are also defined in this section.

2.6 On Sentinel processing and Satellittdata.no

Sentinel-2 data, which is orthorectified with a Norwegian DTERRENG DTM is available as a Top-of-atmosphere (TOA) L1C product with no atmospheric correction. The Sentinel L2A Bottom-of-atmosphere (BOA) product is available as a non-DTERRENG standard orthorectified product. However, Sentinel-2 L2A products are made available with atmospheric and topographic correction, including optional Bidirectional Reflectance Distribution Function (BRDF) corrections, all of which partly eliminate reflectance differences in multi temporal acquisitions by accounting for different cloud and sun illumination conditions. Sentinel-2 L1C products are converted to Sentinel-2 L2A by ESA, using the Sen2Cor processor (Main-Knorn et al., 2017). To make use of the geometrically most accurate product (DTERRENG), only Sentinel-2 L1C imagery is used for all glacier products in mainland Norway and Svalbard.

2.7 Geometric performance of Sentinel-2

In Norway, glaciers are usually located in mountain regions with high elevation and steep topography. Therefore, one has to consider the geometric challenges that can arise when using remote sensing data. If the geolocation accuracy is low, this will affect all glacier products derived from satellite imagery, causing displacements in the results. Kääb et al. (2016) performed geometric and radiometric tests on Level 1C Sentinel-2A imagery from the commissioning and ramp-up phase. They defined three error budgets that can affect the geometric quality of the satellite images:

1) Relative geo-locational precision mainly related to random noise (can also be systematic e.g. “jitter”)
2) Higher order offset patterns that are scene or system specific geolocation biases (e.g. shifts, rotations or deformation of entire scenes that arise from errors in position measurements or orientation parameters).
3) Vertical errors in the digital elevation model (DTM) used for ortho-rectification of satellite images.

The first error budget, the **geo-locational precision**, is usually hard to remove from the satellite images. However, it is possible to remove such errors by applying the mean, or similar robust calculations, on several satellite images close in time. Additionally, errors due to sensor motion (“jitter”) have successfully been removed from ASTER satellite images by applying specific algorithms to them (Girod et al., 2017). These algorithms have not been tried out on Sentinel-2 imagery as the jitter in the imagery was found only on a few occasions and is non-systematic. **Absolute errors** identified in the second error budget term can be corrected for by co-registering the images. ESA is preparing a reference GRID for geo-location and multi-temporal registration that will improve these geo-locational biases for each relative orbit (Gascon, 2016). However, geo-location discrepancy may persist between satellite images from different relative orbits. The geometric quality of satellite images is highly dependent on the terrain model used for ortho-rectification (third above error budget term). The focus of the Copernicus Glacier Service was to test the third error budget term (vertical errors in the DTM), as this can be derived by comparing Sentinel-2 images ortho-rectified with different DTMs. The terrain model used for ortho-rectification of Sentinel-2 images between 2015-2020 was the PlanetDEM90 (https://planetobserver.com/global-elevation-data/). Vertical errors in the terrain model propagate into horizontal errors in the Sentinel-2 image, especially in steep regions and towards the edges of the wide swath (290 km). We also use Landsat 8 imagery within the Copernicus Glacier Service. Reconstructed vertical DTM errors in Landsat 8 (< ~50-60 m) were found to be smaller than those in Sentinel-2 (~100 – 200 m) (Kääb et al., 2016). Sentinel-2 data has larger geometric errors compared to Landsat 8. This is as a result of the combination of a lower quality DTEM and a larger opening angle (Kääb et al., 2016). The horizontal shifts in Landsat 8 imagery are less than those in Sentinel-2 imagery, as a better terrain model is available to process Landsat 8 imagery.

In the following sections, we present three tests illustrating how the geo-location error problem was detected and how it can be solved (Table 1). The tests are from Sentinel-2 imagery over mainland Norway, but consistent results were found for Svalbard, summarized in Section 2.7.4.

To determine the offset between the two images, the normalised cross-correlation image matching method was applied to a Sentinel-2 image pair with cross-track overlap using the CIAS software (Kääb and Vollmer, 2000; Heid and Kääb, 2012).

Table 2-4. Sentinel-2 images used in the geometric tests. Colours indicates which terrain model that was used in the ortho-rectification of the Sentinel-2 imagery. Orange: PlanetDEM90 and national DTM from the Norwegian Mapping Authorities. Red: PlanetDEM90. Green: national DTM from the Norwegian Mapping Authorities.

Test	Region	Tile	Rel. orbit 1	Rel. orbit 2	Date 1	Date 2	DEM/DTM
1	Lyngen, Troms	T34WDC	R051	-	2016-06-30	-	SKDTM vs. PlanetDEM90
2	Folgefonna, southern Norway	T32VLM	R094	R051	2017-09-16	2017-09-23	PlanetDEM90
3	Seiland, western Finnmark	T34WED	R065	R108	2017-09-04	2017-09-07	SKDTM

2.7.1 Offsets between PlanetDEM and national DTM (Test 1)

In the first test we compared a Sentinel-2 satellite scene ortho-rectified with both the PlanetDEM90 and the national terrain model from the Norwegian mapping authority for the same date and relative orbit. The Sentinel-2 image used is from 30 June 2016 and the tile number is T34WDC from the relative orbit 51. The further away from nadir, the larger differences there are between the reflectance values from the Sentinel-2 images with different DTMs (Figure 2-5). A zoom in on Manndalen in Troms shows lateral offsets of up to 30 metres (Figure 2-6). The vectors show the direction and magnitude of the offset and are calculated using image matching (Kääb and Vollmer, 2000; Heid and Kääb, 2012). This test highlights the large elevation differences between the two terrain models leading to corresponding lateral offsets. Figure 2-5 also demonstrates the geo-locational biases due to the 12 pushbroom modules. These are visible as stripes every 20 km (from error budget no. 2). Figure 2-7 shows the relative displacements between the two Sentinel-2 images in dx and dy directions for the entire tile. Most offsets are in cross-track direction perpendicular to the flight direction, as expected from theory.

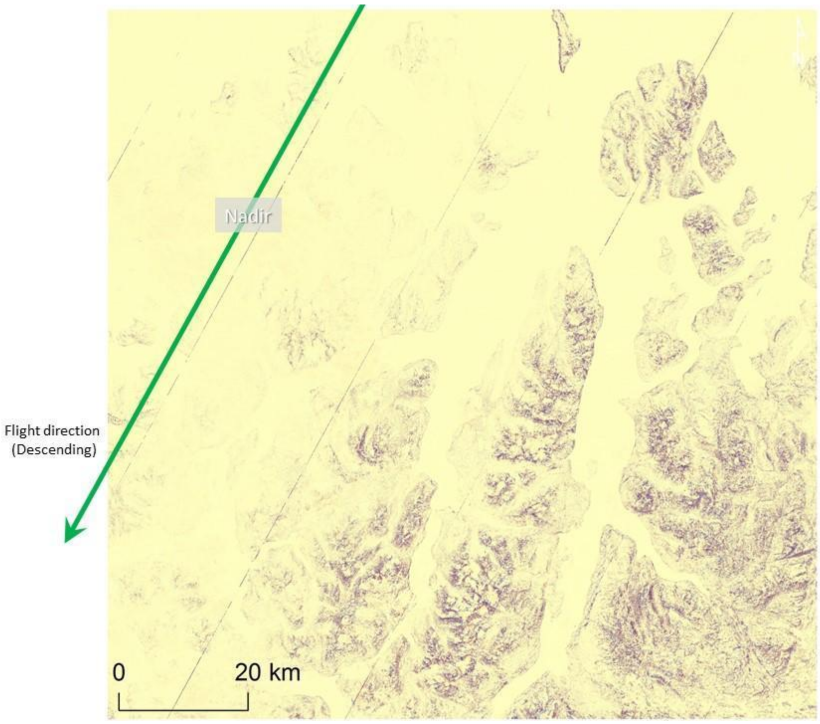

Figure 2-5. Difference image between a Sentinel-2 image ortho-rectified with PlanetDEM90 and the same Sentinel-2 image ortho-rectified with the national DTM (Band 8, NIR) for tile T34WDC (In northern Norway over Trømsø and the Lyngen Alps. Red and blue colors both indicate lateral offsets between the two satellite images.

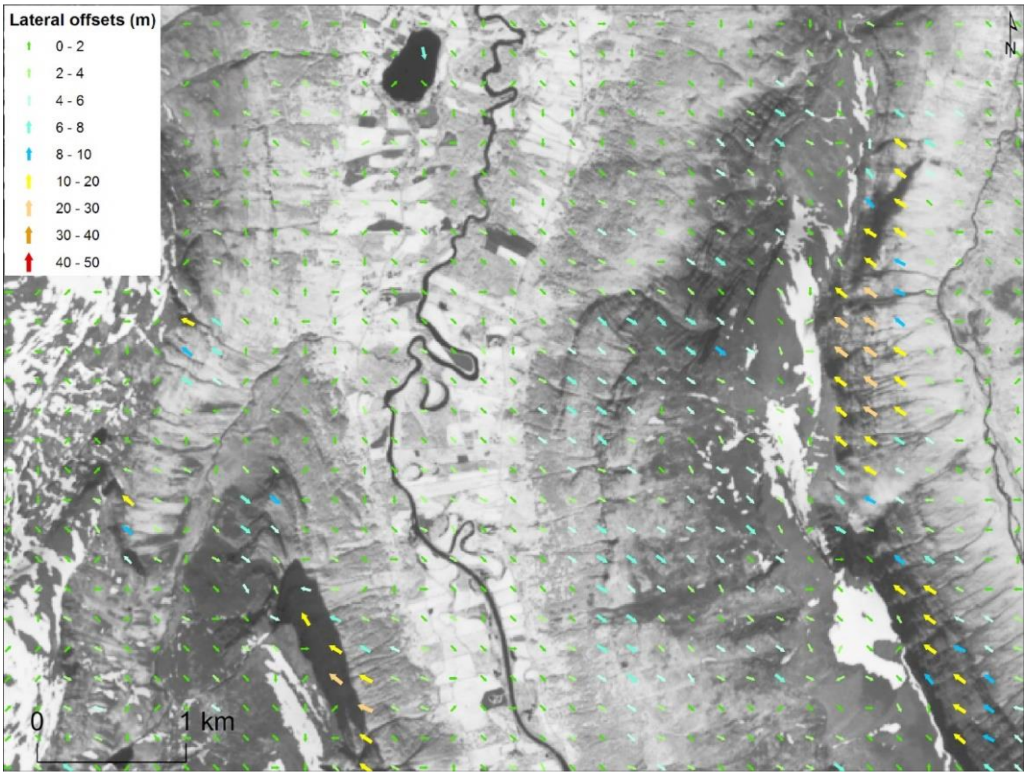

Figure 2-6. Lateral offsets between a Sentinel-2 ortho-rectified with PlanetDEM90 and the same satellite scene ortho-rectified with the national DTM. The subset is covering Manndalen in Troms.

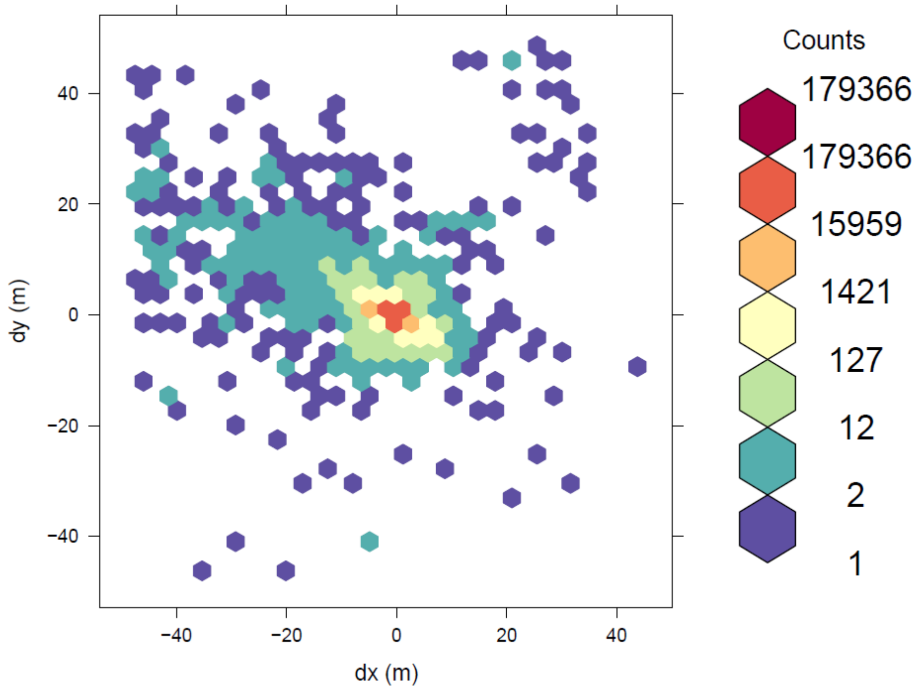

Figure 2-7. Relative displacements between the two Sentinel-2 images with different DTMs, in dx and dy directions for tile T34WDC. Flight direction roughly from upper right corner to lower left corner, perpendicular to the dominant direction of displacements that is roughly from lower right to upper left (negative dx and positive dy) in dy and dx direction.

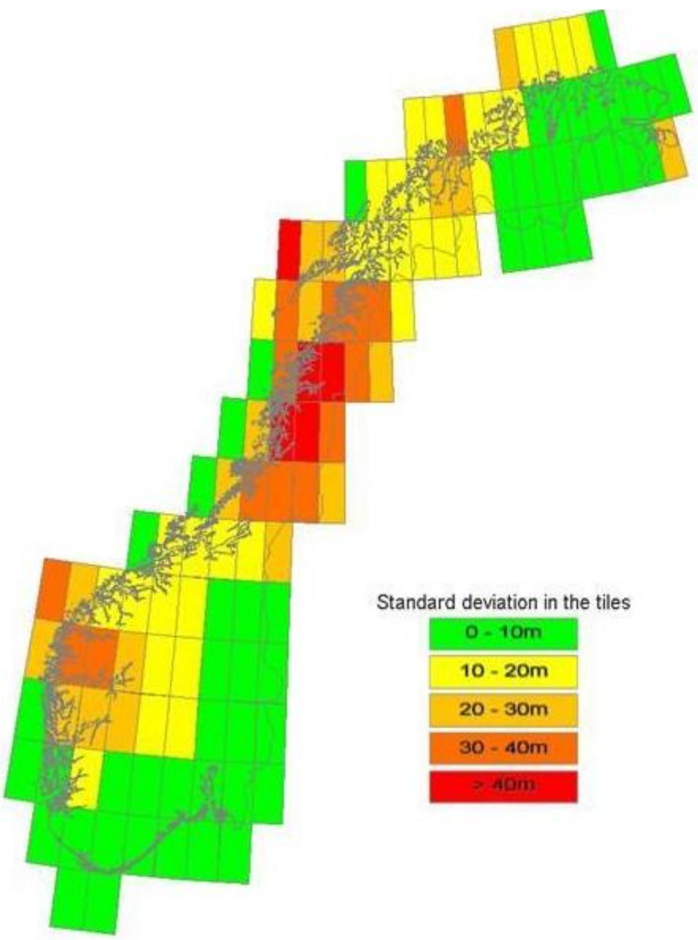

Figure 2-8. Standard deviation between the national DTM (10 m) and PlanetDEM90 (cut at the Norwegian border and the coastline). Figure provided by Ferdinand Klingenberg from the Norwegian Mapping Authorities.

2.7.2 Relative image offsets with PlanetDEM (Test 2)

Tests comparing Sentinel-2 tiles processed with two different DTMs were presented in the previous subsection (2.7.1). These tests revealed a problem with at least one of the terrain models. The national 10 m resolution DTM was produced using photogrammetric methods and is considered to be a high-quality DTM product (Kartverket, 2018). Figure 2-8 shows the standard deviation between PlanetDEM90 and the national DTM. In orange and red regions, the vertical errors in PlanetDEM90 can be as much as 100-200 metres. The PlanetDEM90 consists of two main DTM sources. For all areas up to 60 degrees north the SRTM DTM is used, for areas north of this latitude, DTMs derived from Soviet maps seem to be used over Norway (Kääb et al., 2016).

We investigated the orthorectification of Sentinel-2 with PlanetDEM90 further by using two Sentinel-2 images from different relative orbits and dates. It was then possible to investigate the offsets caused by the terrain model used in the ortho-rectification. It is important that the coherence between the images is not lost. We therefore used images with only one week separation, from 16 September 2017 (relative orbit 94) and 23 September 2017 (relative orbit 51) (Table 2-4). Figure 2-9 indicates lateral offsets up to 40 meters on top of the mountain (orange arrow).

2.7.3 Geometric test of Norwegian DTMs (Test 3)

A result showing a geolocation accuracy better than one pixel is sufficient (i.e. 10 m for Sentinel-2 and 30 m for Landsat 8) (Kääb et al., 2014). Test 3 on the geometric quality of Sentinel-2 images used the national DTEMs from the Norwegian mapping authority and the Norwegian polar institute. Figure 2-10 shows lateral offsets between two Sentinel-2 images ortho-rectified with the national DTM, from two relative paths and dates covering the island Seiland in western Finnmark. Both images are from tile T34WED from 4 September 2017 (relative orbit 65) and 7 September 2017 (relative orbit 108) (Table 2-4). Yellow and green dots show lateral offsets less than 10 m. This is sufficient for glacier mapping in the Copernicus Glacier Service project. The red dots are either tidewater differences between the two images, or different illumination angles causing problems matching in shadowed regions and on the glacier. Offsets of up to 10 times larger have been detected using the PlanetDEM90 compared to the national DTMs. In addition, a more detailed DTM (10/20 m vs. 90 m) gives better result in steep and narrow topography, e.g. in gullies. Ortho-rectified Sentinel-2 images with national DTMs can still have large geometric errors in glacier regions, due to elevation changes induced by retreating and down-wasting glaciers. However, the offsets of < 10 m is sufficient.

The conclusions from these tests were that Sentinel-2 imagery should be ortho-rectified with national DTMs or another global DTM with similar high quality, a recommendation that is meanwhile being taken into account by ESA.

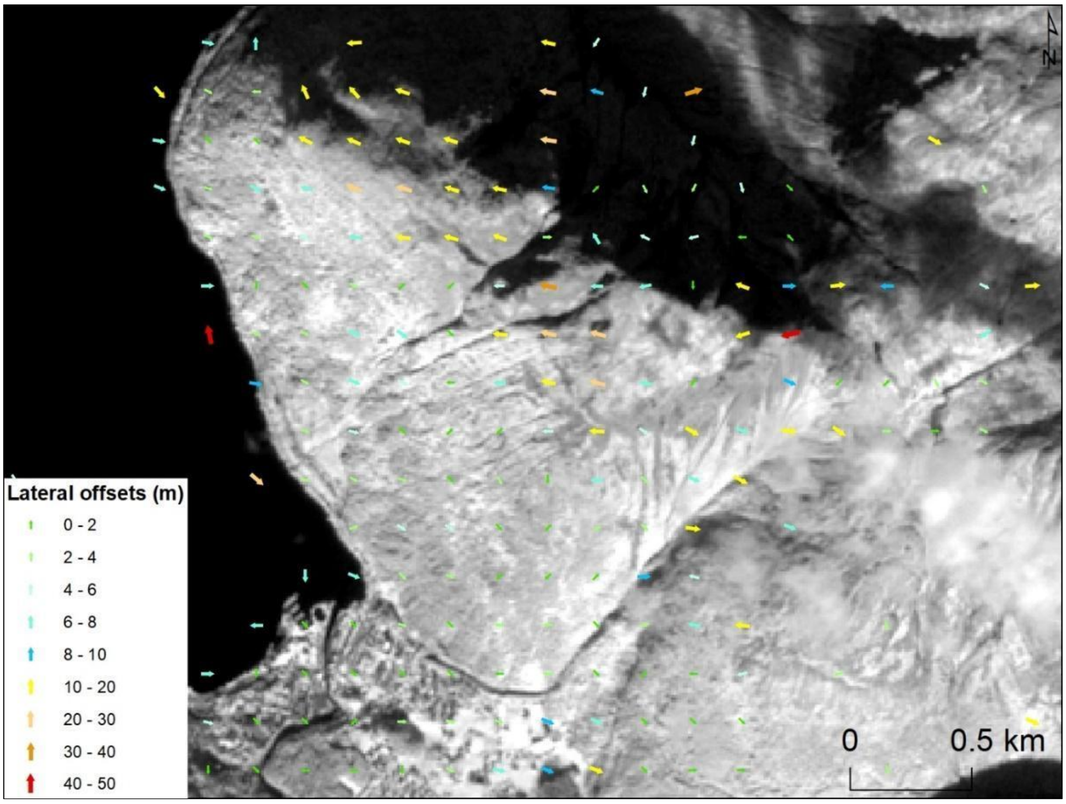

Figure 2-9. Lateral offsets between two Sentinel-2 tiles from different relative orbits (north of SRTM, 60 degrees north).

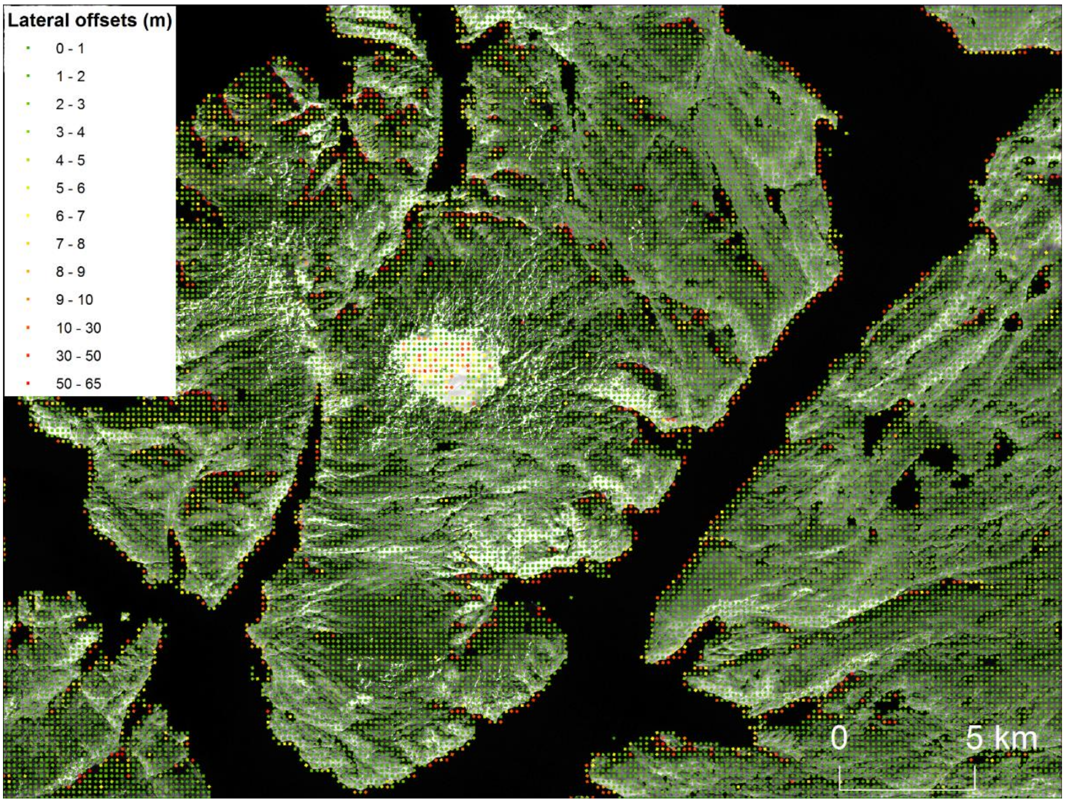

Figure 2-10. Lateral offsets between two Sentinel-2 tiles orthorectified using the national DTM from different relative orbits, three days apart (4 September and 7 September 2017).

2.7.4 Summary of tests on Svalbard

Similar geometric tests were also done for pairs of Sentinel-2 scenes on Svalbard. The results were consistent with mainland Norway, with horizontal offsets between near-coincident images from different relative orbits of up to 30 m (3 pixels) for the standard ESA products processed with PlanetDEM (test 2) and up to 10 m (1 pixel) for the DTERRENG product processed with national DTM (test 3). However, the orthorectification error on Svalbard is not only dependent on the intrinsic quality of the DEM, but also the acquisition time of the DTM because glacier elevation changes can be substantial, especially for marine-terminating and surging glaciers. To investigate this potential systematic issue, we compared PlanetDEM with the national NPI DTM (Fig. 2-11) and made some theoretical considerations on expected orthorectification errors.

The across-track image distortion (*dR*) due to surface topography (*dH*) for a pushbroom sensor like Sentinel-2 can be estimated from the simple relation $dR/R = dH/H$ where R is the horizontal distance from the satellite nadir ground-track and H is the altitude of the satellite. Considering a swath width of 270 km for Sentinel-2 and an orbit altitude of 786 km (Table 2.2), the maximum across-track distortion becomes dR = dH*(270/2)/786 = dH*17%. Hence, a potential DTM error of 100 m will transfer into a horizontal geo-location error of 17 m in the orthorectified product. This is within the range of errors that can be expected for the standard ESA product considering the elevation differences between the NPI DTM and Planet DEM in Fig. 2-8. Relative image offsets can be even larger in cases where opposite edges of images swaths are compared or in cases with extreme DTM errors due to glacier surging. However, these worst-case impacts can easily be reduced by using data from similar relative orbits or from swath center rather than edges.

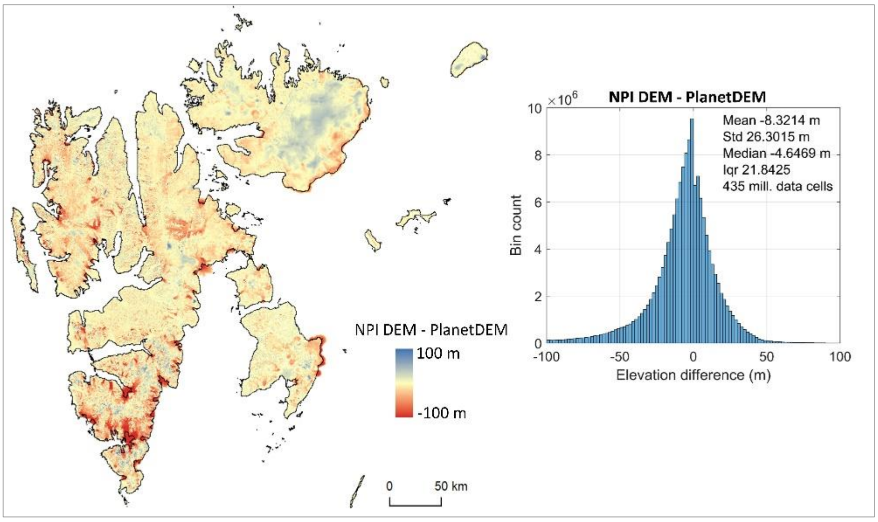

Figure 2-11. Elevation differences between the NPI DTM (DEM) from 2008-2012 and the PlanetDEM used in standard ESA processing. Elevation differences are largest for marine glacier fronts that have retreated and thinned. Source data for PlanetDEM were extracted from *viewfinderpanoramas*.org which is further based on digitized old maps.

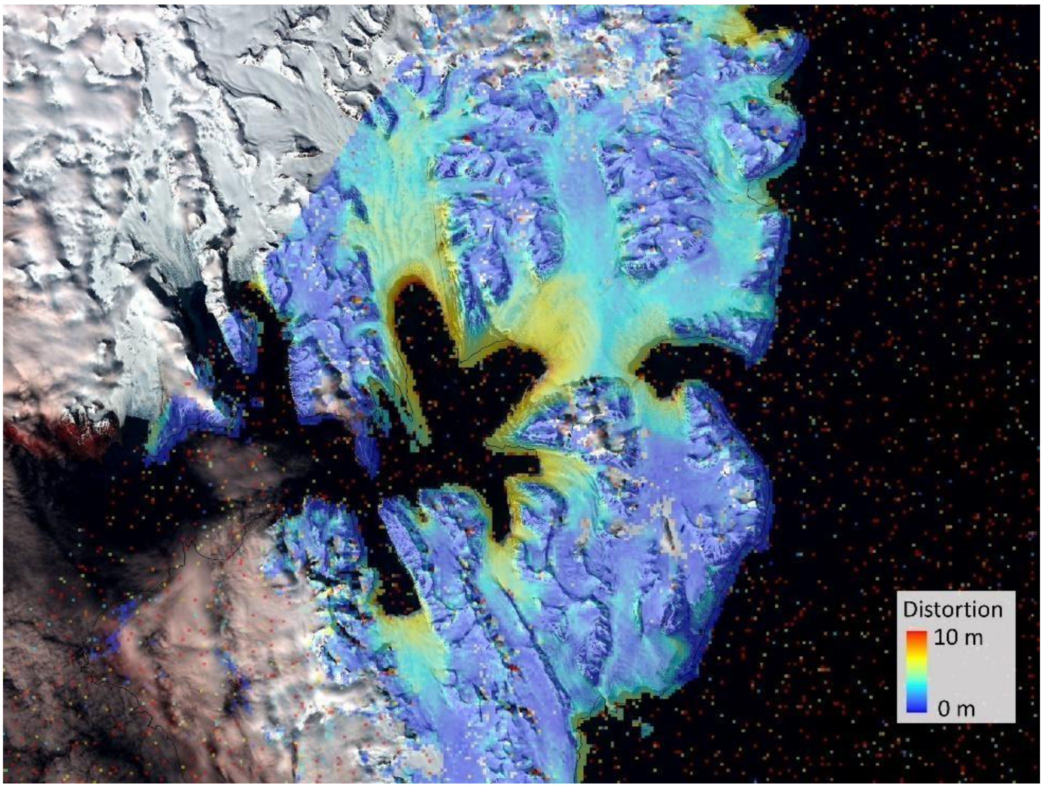

Figure 2-12. Horizontal offsets between two overlapping images acquired 50 mins apart on 30 June 2018 by Sentinel-2A and Sentinel-2B over Southern Spitsbergen (Image tile 33XWF, relative orbits S2A-R052 and S2B-R123). /Copernicus Sentinel data/

To test these theoretical considerations, we compared two near-coincident Sentinel-2A/B standard image products acquired from opposite viewing angles over a worst-case scenario area in Southern Spitsbergen where the largest DTM deviations were evident (Fig. 2-11). As expected, the results show a systematic pattern where relative image offsets are largest (10 m) at glacier tongues where substantial glacier retreat and thinning have occurred (Fig. 2-12). This issue is largely resolved for the DTERRENG product and likely also for future standard ESA products when a global DTM of higher quality gets implemented in the processing, but there may still remain some significant local errors due to glacier surging after the DTM acquisition time.

3 Glacier products

In this chapter, we describe the glacier products derived in the Copernicus glacier service. The methods used can differ for Svalbard and mainland Norway. This is due to Svalbard's larger glacier extent and volume, different glacier dynamics and climate compared to glacier regions in mainland Norway.

3.1 Glacier outlines, area and calving fronts

3.1.1 Background

Glacier outlines and associated attribute data, jointly referred to as *glacier inventory*, are baseline data for a range of glaciological and climatological applications, as well as for standard topographic maps. They are input data in local-to-global models of glacier mass balance and hydrology, and for satellite-based assessments of glacier volume changes and contribution to sea level rise. Most glacier mapping in the early days was done manually and published as paper maps and reports. Since the early 2000s, more advanced digital capabilities and higher availability of suitable satellite imagery made it possible to start collecting glacier inventory data at a global scale, facilitated by international initiatives like GLIMS (Raup et al., 2007). A major milestone was reached in 2012 when the first version of the globally complete Randolph Glacier Inventory (RGI) was released (Pfeffer et al., 2014). That was only possible through a communitywide collaboration where scientists came together to merge datasets to a common format and identify remaining gaps to be filled. NVE, NPI and UiO contributed to this effort by providing complete inventory data for mainland Norway, Svalbard and the Russian Arctic, respectively.

The first detailed list of the numbers and areas of glaciers in Norway was based on topographic maps at a scale of 1:100,000 and aerial photographs from the 1940s and 1950s for some areas (Liestøl, 1962). The first detailed glacier inventory of southern Norway was published in 1969 (Østrem and Ziegler, 1969). Identification of the glaciers was based on photographs from the period 1965–1968 as well as on topographic maps at scales of 1:50 000 and 1:100 000. A revised and extended glacier inventory for southern Norway was completed in the late 1980s based on aerial photography for the period 1969–1981 (Atlas88; Østrem et al., 1988). The first inventory of northern Scandinavia was compiled in the early 1970s as a joint inventory of glaciers in northern Norway and Sweden (Atlas73; Østrem et al., 1973). The inventory was based on maps and aerial photographs from the 1950s and 1960s. The first detailed overview of all glaciers was based on Landsat imagery from 1999-2006 (GI_{2000}) (Andreassen et al., 2012). Later two more inventories were created based on digitising of topographic first edition maps (GI_{n50}) and Landsat imagery from 1988-1997 ($GI_{1990)}$ (Winsvold et al., 2014). GI_{n50}, GI_{1990} and GI_{2000} become available as Glacier Area Outline (GAO) products of the CryoClim project. The GI_{2000} is part of the GLIMS database and the RGI.

The first complete glacier inventory of Svalbard was published as a report, "Glacier atlas of Svalbard and Jan Mayen" (Hagen et al., 1993). It was based on the official 1:100,000 scale topographic maps of NPI and updated with more recent aerial and Landsat imagery where needed. Glaciers and ice caps were separated into numerous hydrological basins with unique identification codes and basic glacier attributes such as name, area and length. However, since outline coordinates from were not preserved in the atlas, it was not until almost 20 years later that the first digital outlines became available as a Glacier Area Outline (GAO) product of the CryoClim and Glaciers_CCI projects supported by NRS/ESA. This was a multitemporal glacier inventory (Nuth et al., 2013) with one complete glacier inventory from the 2000s (GI_{00s}) based on various satellite imagery (ASTER, SPOT and Landsat) and two half-complete historical inventories based on digital maps made from aerial photography campaigns in 1990 (GI_{90}) and 1930-1970 (GI_{old}). The GI_{00s} data set was implemented in the international GLIMS and RGI databases and is still the reference point for most glaciological studies on Svalbard. It is however becoming more and more outdated due to glacier changes, especially along the marine margins, so in this project we have generated a new complete inventory from Sentinel-2 imagery of summer 2020. To further study and account for rapid changes of marine-terminating calving glaciers, we have also generated a calving-front product consisting of annual frontlines and estimated frontal ablation due to marine ice melting and calving. This latter work is specific to Svalbard and described in Section 3.1.2.

3.1.2 Data and methods

The glacier outline mapping and inventory work over mainland Norway and Svalbard have been done separately by NVE and NPI, for the most part using common data sources and methods. The first phase was to select suitable Sentinel-2 imagery, preferably from a selection of years with minimal snow cover during the summer and extended periods of clear weather. This was more challenging than anticipated with several unfavourable summers in the early years of Sentinel-2, but eventually we were able to obtain a suitable and complete image coverage for northern Norway in summer 2018 (Fig. 3-1), southern Norway in summer 2019 and Svalbard in summer 2020.

This is a major improvement from earlier Norway/Svalbard inventories where 7-10 years of data were needed. We also benefited from the higher resolution of Sentinel-2 (10-20 m bands) with respect to the alternative Landsat-8 (15-30 m bands), as well as the more accurately orthorectified DTERRENG product which we used whenever it was available, mostly in 2018-19, partly in 2020.

After selecting suitable images for each region, the next step was to apply a band-ratio thresholding method to produce an initial set of automatically generated glacier masks/outlines. This type of technique has been in use since the 1990s and adapted in various ways for different satellite sensors and glacier regions (e.g. Paul and Kääb 2005), including the previous inventory for mainland Norway (Andreassen et al., 2012). The previously used method was adjusted from the image band specifics of Landsat-8 to Sentinel-2 (Paul et al., 2016) and tested over s few sample areas to determine the most suitable threshold values to be applied in each region. We used the blue band 2 (B2_blue), the red band 4 (B4_red) and the shortwave infrared band 11 (B11_swir) to make a binary glacier mask which was converted to vector outlines that were further edited based on various criteria. This automated part of the mapping can be summarized as follows:

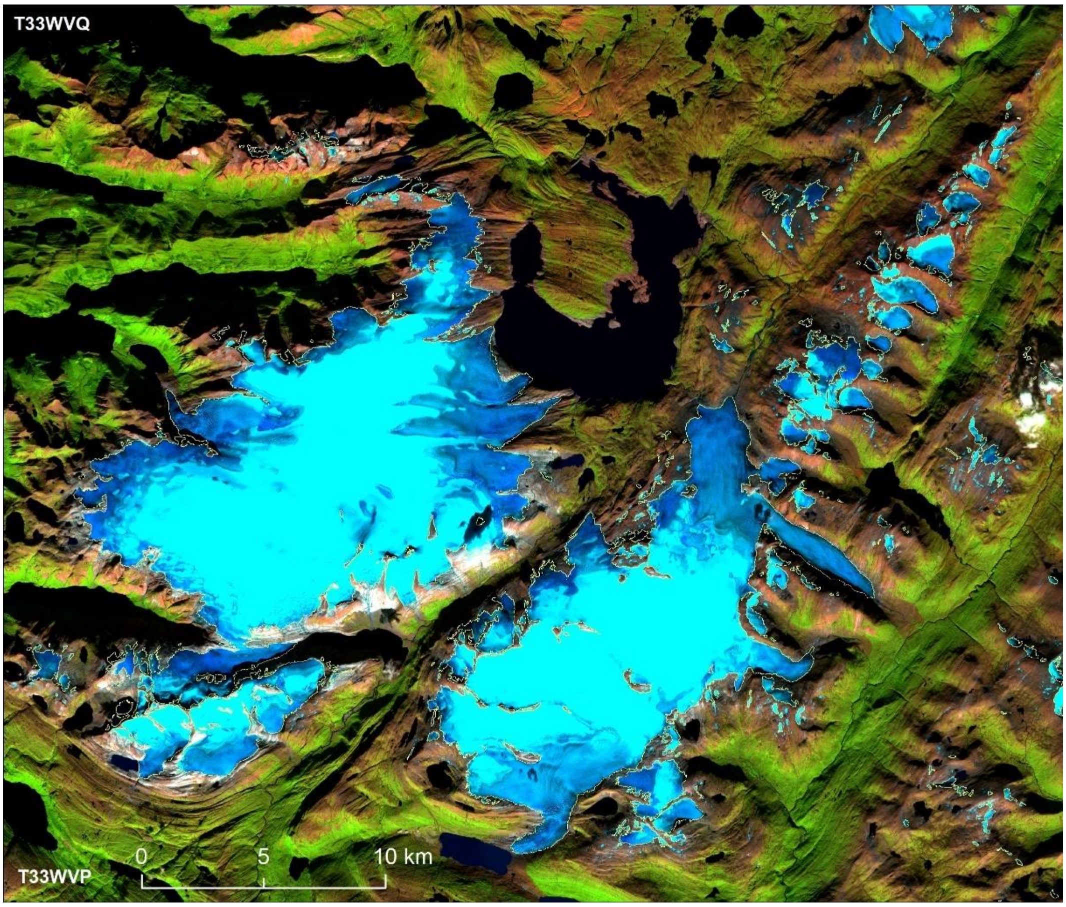

Figure 3-1. Sentinel-2 scenes (false 11-8-4) from two tiles (upper tile is T33WVQ and lower tile is T33WVP) covering Svartisen, Nordland. Both scenes were acquired 8 September 2018 and were used to derive the glacier outlines (in yellow) of this part of mainland Norway. /Copernicus Sentinel data/

- Make initial binary glacier mask: B4_red / B11_swir > ratio_threshold (e.g. 5)
- Apply threshold based on the blue band: B2_blue > blue_threshold (e.g. 1700)
- Apply median filter (3x3 pixels) to reduce noise
- Convert to vector outlines (polygon shapefile)
- Remove sea-ice and ocean polygons by land mask (Svalbard) and lakes and ocean polygons (Norway)
- Remove polygons and polygon holes smaller than minimum sizes (e.g. 1000 and 900 m^2)
- Remove snow-filled gullies based on area-perimeter ratio (Svalbard)

On Svalbard, the raster masking was done tile-by tile (100x100 km areas) and then mosaiced for each satellite overpass to make continuous along-track glacier masks in full 270 km swath-width, before converting to vector outlines. This is less relevant for mainland Norway where glaciers are more scattered, and most glacier regions are covered by a few tiles.

This automated procedure was repeated for all selected Sentinel-2 images to generate a catalogue of different glacier outlines. The best outlines for each glacier region were then used as starting point for manual checking and editing based on the source imagery as well as other suitable scenes from the image catalogue. Higher resolution orthophotos from different times were used to aid the interpretations in difficult areas such as steep terrain with shadows and areas with debris-covered ice, which are often misclassified in the automated procedure. Previous glacier inventories and maps/DTMs were also used as supporting data.

The further inventory process consisting of manual editing, outline validation, drainage divide delineation and extraction of glacier attributes was done somewhat differently for mainland Norway and Svalbard due to their different glaciological characteristics. This is the most labour-intensive part of the work and is described separately in the two sub-sections below.

3.1.3 Mainland Norway

The most labor-intensive task was to find the suitable threshold and manually check the glacier outlines. We also created an updated lake inventory by manual digitizing the lakes that were detected (see chapter 3.5). A particular challenge in mainland Norway is large snow fields and snow separate from glaciers. The orthophotos used to validate result had varied snow conditions and were not so useful in some regions. Another problem was clouds (Fig. 3-2). Here we often had to select outlines from an earlier image, this may result in more snow on the glacier margins. This was done interactively by checking outlines for each glacier, replacing or adding outlines from earlier imagery if the later image only partly mapped the glacier or completely missed it.

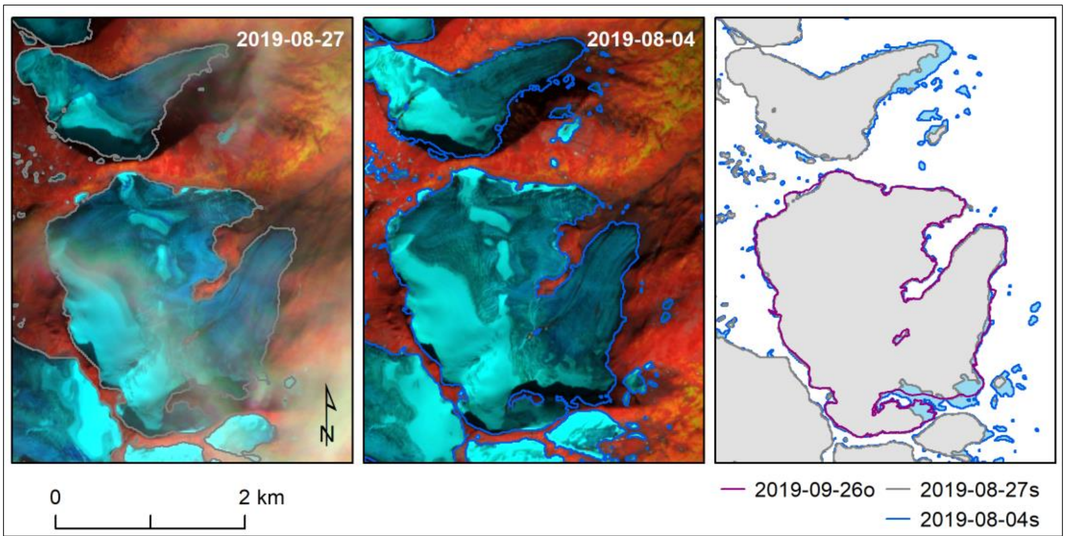

Figure 3-2. Sentinel-2 imagery (false 11-8-4) showing cloud over Storbreen (2636) in Jotunheimen. The purple line is the outline derived from an independent orthophoto of Storbreen, the grey and blue outlines are results of the automatic derived outlines from 4 and 27 August 2019. The image from 4 August has more seasonal snow, but still detects the overall glacier outline. /Copernicus Sentinel data/

When going through the glacier we also tried to score the glaciers based on Leigh et al. (2019) and as in GI_{2000}, dividing the polygons in glaciers, possible snowfield/ice patches and snow (Fig. 3-3).

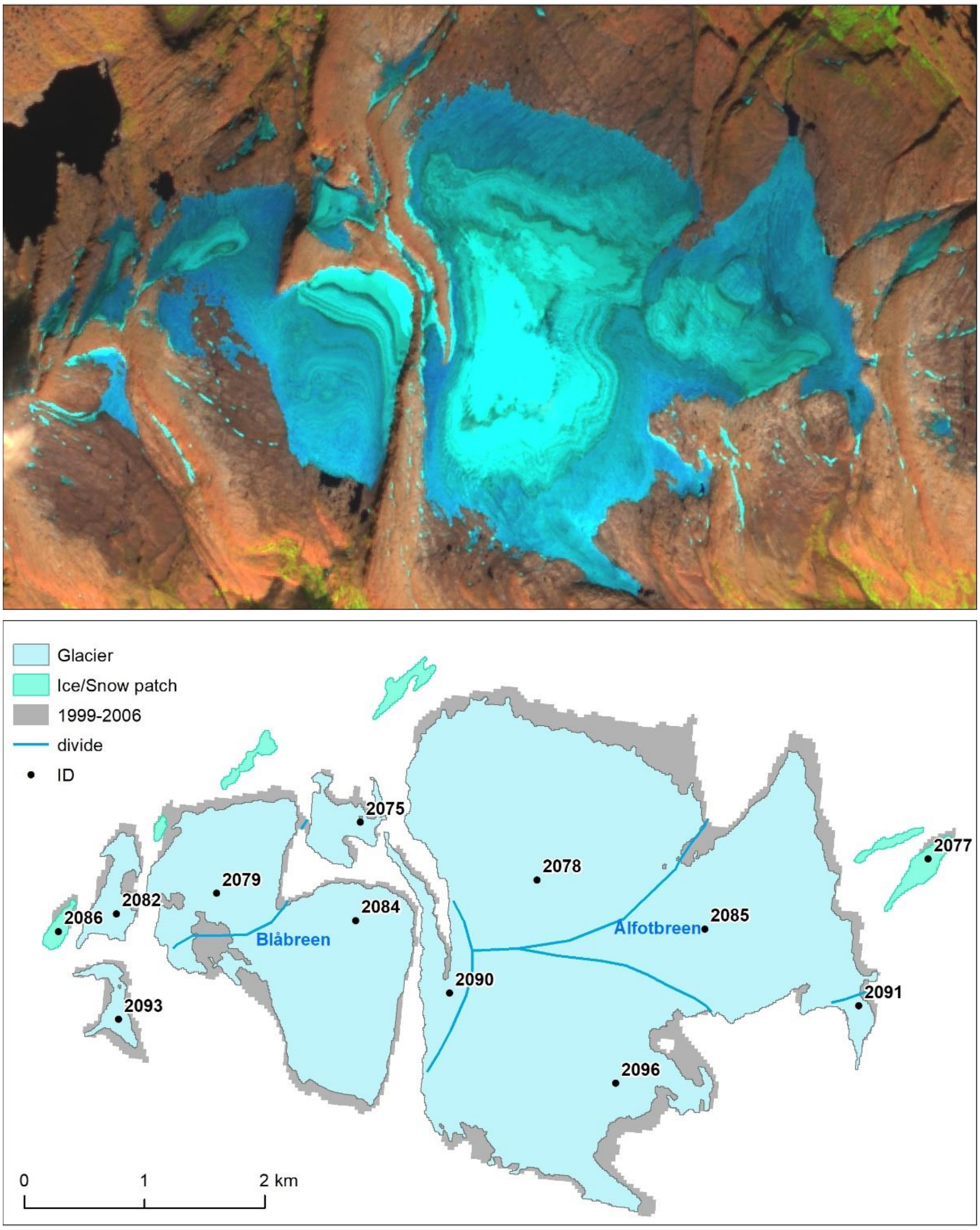

Figure 3-3. Sentinel-2 scene (false 11-8-4) of 15 August 2019 (above). Resulting glacier outlines of Ålfotbreen and Blåbreen and surrounding glaciers and ice patches (below). Previous glacier mask from 2006 showed in grey, and previous IDs points and ice divides are also marked. /Copernicus Sentinel data/

In addition to the overall mapping of glaciers outlines for 2018 and 2019 for mainland Norway, we also tested the use of Sentinel to map ice patch extent and changes since the GI_{2000} or available orthophotos from the last 10-20 years (Andreassen et al., 2020a). Not all the ice patches were included in the GI_{2000} due to their small size. Results showed that ice and snow patches down to 0.01 km^2 could be mapped using Sentinel-2, steep terrain and dark ice can be a challenge for both small patches and larger glaciers.

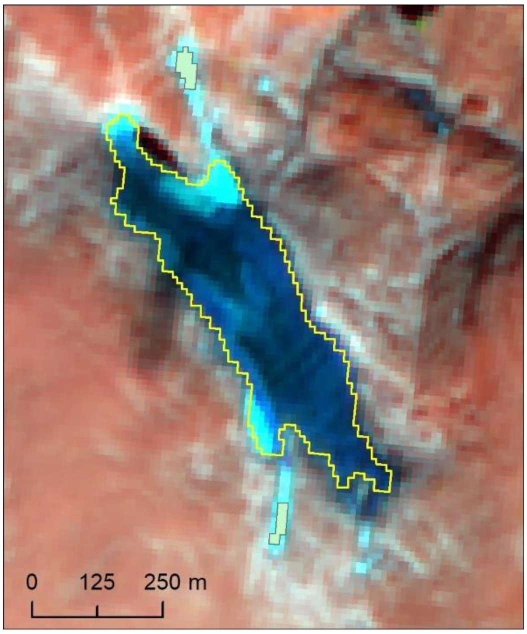

As a result, many more ice patches and smaller glaciers have been mapped in the new inventory. One example is Storebottefonne in Hemsedal having a 2019 mapped area of 0.1 km^2 (Fig. 3-4). This is of course not a newly formed ice patch, but it is outside the glacier regions covered in previous glacier inventories. This will now be included as an ice patch with Glacier ID in the new inventory that will be available from NVE's digital glacier inventory.

Figure 3-4. Sentinel-2 image (false 11-8-4) of Storebottefonne, Hemsedal, one of the numerous 'new' glaciers and ice patches mapped in the new inventory. Yellow line as automatically mapped by the band ratio method. This polygon was classified as an ice patch, two smaller polygons marked as snow. /Copernicus Sentinel data/

Results show an overall glacier retreat of glaciers in mainland Norway, as illustrated for Hardangerjøkulen that shrank from 71.3 km^2 in 2003 (GI2000) to 64.1 km^2 in 2019 (Fig. 3-5). Additional 0.7 km^2 from the southwestern part is now detached from the main glacier, thus the overall glacier area is reduced by 9%. In the Copernicus glacier service project we also provide recent and historical outlines derived from Landsat imagery, historical maps and geomorphological landforms (Stokes et al., 2018; Leigh et al., 2020, Weber et al., 2019; 2020ab) (Fig. 3-5).

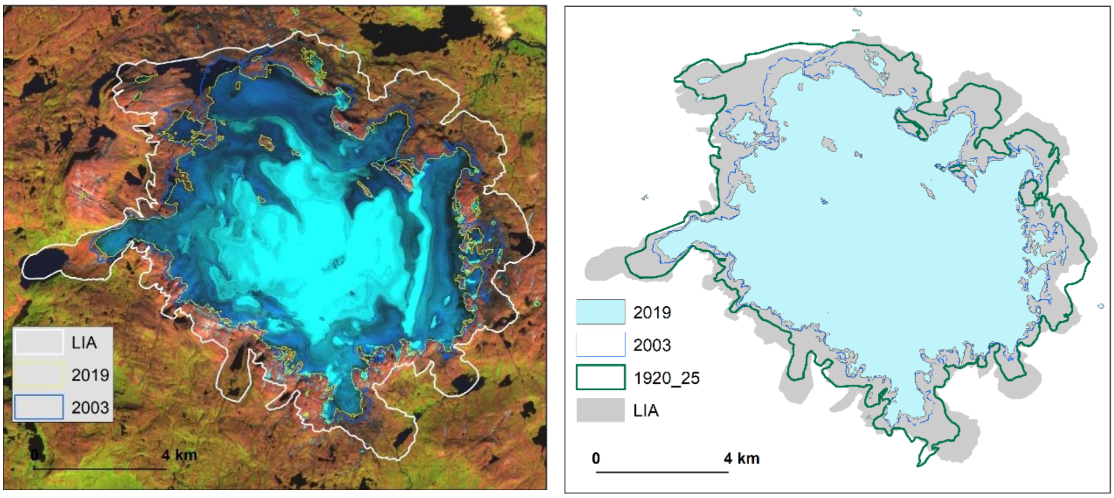

Figure 3-5. Sentinel-2 image (false 11-8-4) of Hardangerjøkulen showing new and previous outlines, 2003 is GI2000. Historical outlines of little ice age extent (LIA) and from topographic maps 1920_1925 are from Weber et al. (2019). Resulting polygons to the right. /Copernicus Sentinel data/

3.1.4 Svalbard

Before the manual editing, the automated outlines for Svalbard were split up into separate vector layers for the outer perimeter (large polygons), the nunataks (small polygons) and the drainage divides (lines inherited from the previous inventory). These three layers were then edited separately based on the best available Sentinel-2 imagery from summer 2020, as well as supporting data from Landsat-8, orthophotos and DTMs. In some areas, the automated outlines could be used efficiently (Fig. 3.6), whereas in shady areas and for debris-covered glaciers, they were not capable of detecting the whole glacier area, and it was also difficult to interpret glacier extent from the Sentinel-2 images themselves.

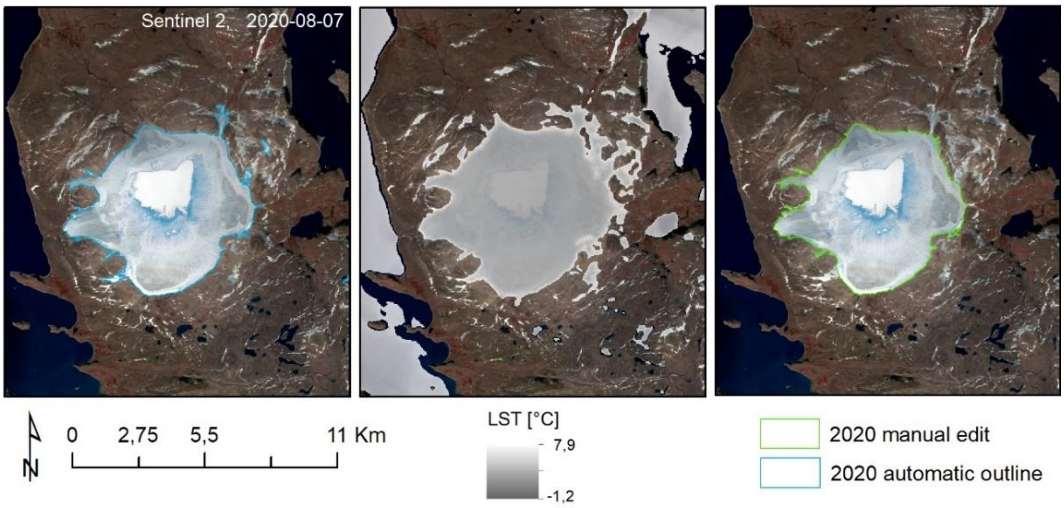

Figure 3-6. Example of an ice cap, Ahlmannfonna on Nordauslandet, where the automated method for glacier outlines performs well (left) and few manual adjustments need to be made for the final inventory (right). The middle image shows Landsat-derived land-surface temperatures (LST) below 7.9°C which was used as a threshold for icy areas, but in this case also including some surrounding areas, as well as lakes and the ocean. /Copernicus Sentinel data/

To better separate between areas containing ice and not, we attempted to use land surface temperatures (LST) derived from the Thermal Infrared Sensor of Landsat-8 (TIRS band 10, 30 m resolution). We used images acquired between 27 July and 3 August 2020, an exceptionally warm period on Svalbard with temperatures >20°C measured in Longyearbyen. This heat wave resulted in a sharp temperature contrast between atmosphere-heated land surfaces and snow/glacier surfaces near the melting point (Fig. 3-7). To use LST as an aid in the glacier outlining, we experimented with different glacier masking thresholds and found that a 7.9°C cut-off gave a good balance between being too inclusive (e.g. cold shadow areas without ice) and too exclusive (not including actual glacier areas). We did not generate automated outlines from this LST-based glacier mask, but used it visually to edit or replace erroneous outlines from the band-ratio method in areas where the distinction between glacier and land areas were unclear.

The automatically generated nunatak outlines contained many medial moraines that had to be deleted or manually cut off from the nunataks themselves. Debris-covered glacier fronts and shady glacier cirques were the most challenging areas to correct for the perimeter outlines (Fig. 3-8). Finally, the outline and nunatak layers were joined to get the total glacier area. The glacier divides were copied from the previous glacier inventory and clipped to the current glacier extents. For surging glaciers or areas with a big increase in nunataks, the divides have changed and had to be adjusted manually with the help of a hydrological basin map generated by ArcGIS from the most recent ArcticDEM of sufficient quality. The resulting glacier inventory was overlaid with the attribute data from the previous inventory to inherit glacier ID's and names. Some glaciers had split into multiple units and got assigned new glacier ID codes following the convention of system of Hagen et al. (1993) and Nuth et al. (2013). Eventually, we will also make the inventory consistent with the global standards of GLIMS and Radolph Glacier Inventory for submission there.

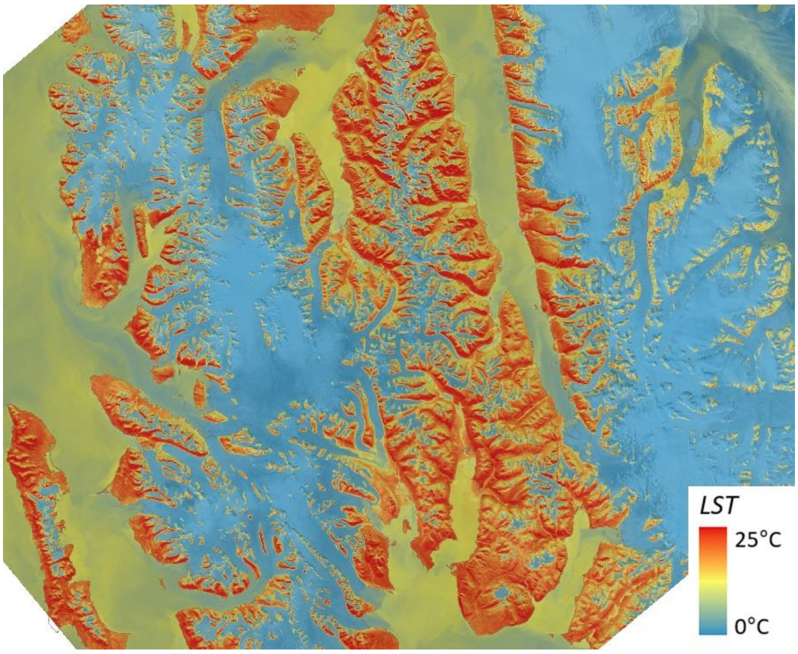

Figure 3-7. Land-surface temperature (LST) derived from Landsat-8 TIRS image on 27 July 2020, shown transparently on top of the OLI panchromatic image from the same acquisition. Ice and snow areas stand out due to their colder near-surface temperatures than heated bare-ground areas.

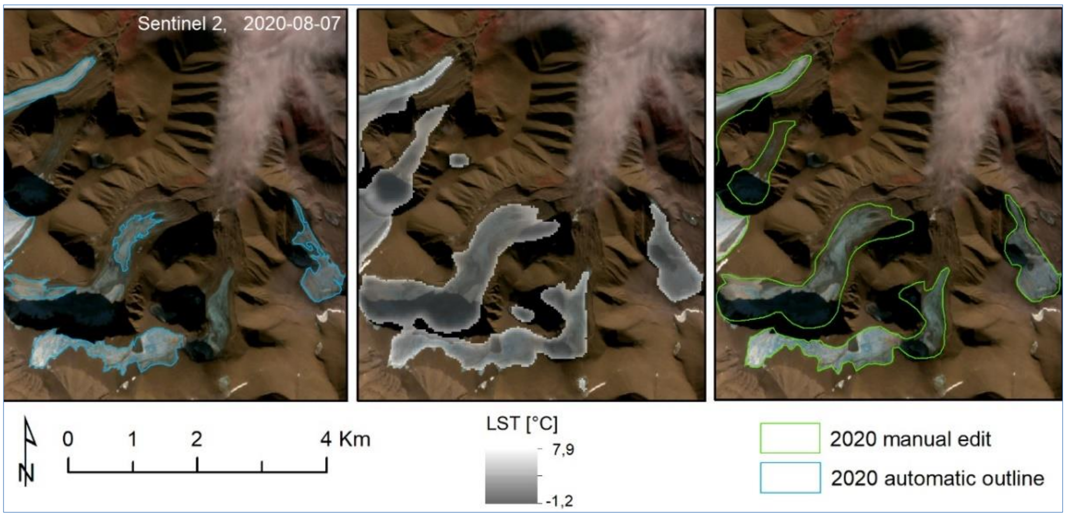

Figure 3-8. Example of shaded and debris-covered areas around Binnebreen in North-West Spitsbergen. The blue line (left) is the automatically derived outline. The middle image shows land-surface temperatures (LST) below 7.9°C which was used as a threshold for icy areas. The final green glacier outlines as shown in the right frame. /Copernicus Sentinel data/

The new 2020 glacier inventory has not yet been carefully analysed for glacier changes with respect to earlier inventories, but a substantial glacier retreat over the last 10-20 years is obvious (Fig. 3-9), especially along the western and southern coast of Spitsbergen. The only near-stable glacier areas are found on Nordaustlandet and at the northeastern tip of Spitsbergen. In total for Svalbard, the new glacier inventory indicates a current glacierized area of 32,000 km^2 whereas the previous digital inventory from the 2000s had a total of 33,800 km^2 and the analogue inventory of Hagen et al. (1993) a total of 36,600 km^2. Robust statistical comparisons of inventories are difficult due to different data sources, mapping methods and personal interpretations, but if we take the numbers as they are, Svalbard has lost ~5% of its glacier area during the last ~15 years.

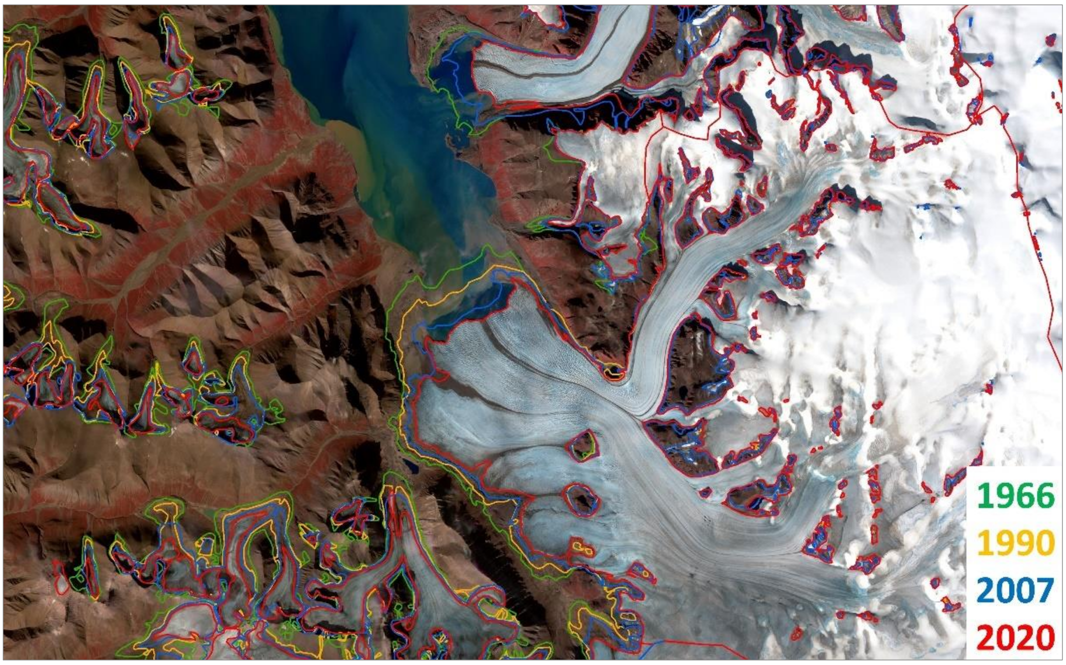

Figure 3-9. Comparison of the glacier extents from 1966 (GI_{old}), 1990 (GI_{90}), 2007 (GI_{00s}) and 2020 (new GI_{2020}) for the area around Wijdefjorden/Austfjorden, with Mittag-Lefflerbreen in the center. Glacier retreat and nunatak growth is evident for most areas. Background image is Sentinel-2 (False 8-4-3) from 31 July 2020. /Copernicus Sentinel data/

3.1.5 Calving fronts

More than half of the glacier area of Svalbard drains towards ocean-terminating fronts that ablate by ice calving and frontal melting below and above the waterline. This frontal ablation is a significant but poorly quantified part of the overall mass budget of Svalbard glaciers (Blaszczyk et al., 2009), as well as being important for the water circulation of Svalbard fjords and the habitat of marine mammals and seabirds (Lydersen et al., 2014). Glacier calving and frontal ablation is difficult to observe in the field due to unsafe access and few suitable viewpoints for time-lapse cameras or terrestrial lidar/radar. The near-daily acquisitions of Sentinel-1/2 over Svalbard offer a potential to monitor the glacier-ocean interface at a level of detail not possible before.

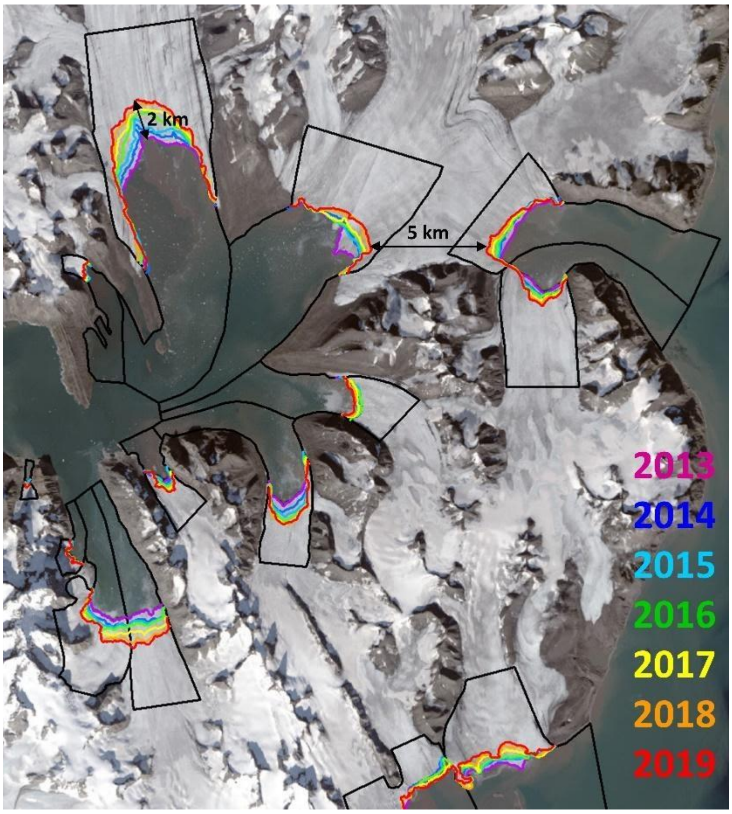

Figure 3-10. Annual front positions for the marine glaciers around Brepollen and Sørkapp Land in southern Spitsbergen. The black polygons outline the marine margins for glacier retreat/advance used in the automated calculations of glacier area changes and frontal ablation. Background image is a Landsat-8 mosaic from 2014.

In this project, we used Sentinel-2 to identify 204 marine-terminating glacier units that we outlined with reference polygons following the marine side-margins of each glacier within maximum boundaries of frontal advance and retreat (Fig. 3-10). Glacier frontlines were manually digitized from Sentinel-2 imagery acquired at end-of summer, defined as the period between 15 Aug. and 15 Sept. to make sure cloud-free coverage could be obtained for each glacier. These frontlines were then cut to the reference polygons and used to calculate glacier area changes and average advance/retreat rates from year to year (Fig. 3-11). We extended the annual time series back to 2012 by employing additional Landsat-7/8 and ASTER imagery. A somewhat longer summertime period was needed to cover all glaciers in years prior to the launch of Sentinel-2. The ASTER imagery had to be georeferenced to the land coastline to achieve sufficient accuracy.

To calculate changes in ice volume or mass, the thickness of the glacier front areas needs to be known or estimated. Most glaciers do not have direct radar measurements of ice thickness, so we relied on an observationally constrained model of ice thickness (Fürst et al., 2018) that we combined with the NPI DEM over land surfaces and available bathymetry data from the Norwegian Mapping Authority to interpolate a seamless bedrock elevation model. This bedrock model was then subtracted from annual ArcticDEM mosaics to derive ice thickness in the glacier front areas for any given year. Ice volume changes from advance or retreat could then be calculated by multiplying the frontal area changes with their average ice thickness.

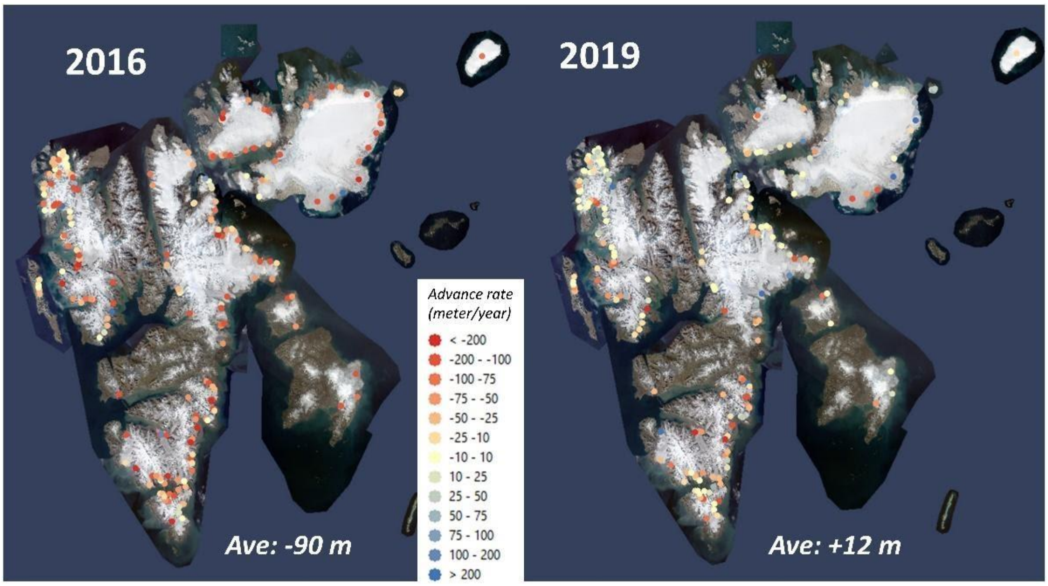

Figure 3-11. Annual advance rates (negative numbers imply retreat) for Svalbard calving glaciers in two very different years; 2016 and 2019. The distance-weighted average front advance was -90 m in 2016 and 12 m in 2019.

We further estimated ice discharge by defining cross-glacier transects, so-called flux-gates, near the glacier fronts on the upstream side where glacier velocity data could be retrieved (see Section 3.3.3). The volumetric discharge was estimated by integrating ice velocity multiplied by thickness across each flux-gate. The total frontal ablation could then be obtained from the sum of frontal volume change and discharge over the reference period. The results show that the discharge component is generally larger than the volume-change component, but that the latter varies more from year-to-year, likely because of a stronger dependency on varying seawater conditions. These aspects are being investigated further in a manuscript for submission to a peer-review journal.

A more detailed description of the calving front mapping and early results can be found in the internship report by Joséphine Maton (2020). The calving front positions for 2012-2020 are published in *svalbardkartet.npolar.no* and as vector lines with attributes on the NPI data center. The data have already been used by biologists to study how GPS-tagged seabirds use glacier fronts as foraging areas, and by the NPI mapping department to add updated calving front locations to their online map services. We have also combined the glacier fronts with the land-based parts of the coastline in topographic maps to produce updated land/glacier coastlines for each year. This is highly needed as many glacier fronts have changed by more than a kilometer, even several kilometers for a few surging glaciers like Nathorstbreen and Storisstraumen (Fig. 3-12). Altogether, the calving front monitoring shows that Svalbard glaciers are strongly influenced by the ocean and have lost a total marine glacier area of 157 km^2 during the 2012-2020 period.

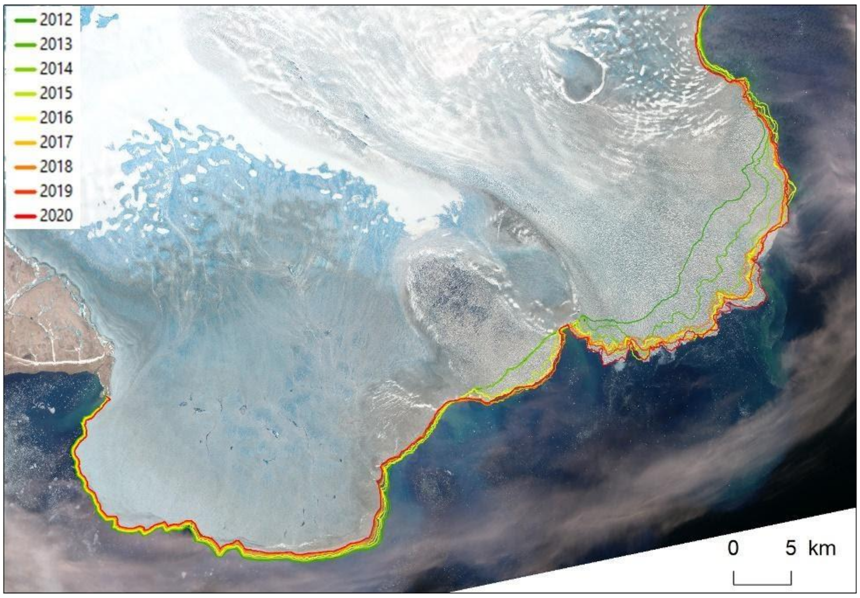

Figure 3-12. Calving front changes for two contrasting glacier basins on Austfonna ice cap; the retreating Bråsvellbreen (left) and the surging Storisstraumen (right). The image is from Sentinel-2, 26 July 2020. /Copernicus Sentinel data/

3.2 Glacier facies and snowlines

3.2.1 Background

The annual surface mass balance, equilibrium line altitude (ELA), snow line altitude (SLA), snow cover ratio (SCA), and accumulation area ratio (AAR) are calculated from direct field measurements on selected glaciers in mainland Norway and Svalbard. The mass balance data are submitted to the World Glacier Monitoring Service (WGMS) and published in their data reports (e.g. WGMS, 2020). NVE's data are also made available in annual NVE reports (e.g. Kjøllmoen et al., 2020). Available in-situ AAR and SLA data from reference mass balance glaciers have been compared with observed mass balance (Dyurgerov et al., 2009) with the aim of using ELA/SLA and SCR from remote sensing to infer mass balance. The application of this method has been limited by a small amount of in-situ measurements. Field measurements can only be carried out for a relatively small group of glaciers world-wide due to logistical and financial monitoring constraints.

Satellite imagery has long been used to detect snowlines, already in the 1970s Landsat I imagery over ice caps was used to derive snowlines for Seilandsjøkelen, Norway (Østrem, 1975). The snow line altitude (SLA) of a glacier near the end of the ablation season may be considered roughly representative for the ELA unless super-imposed ice from refreezing of meltwater at the base of the snow/firn layer can be expected, which is often the case on Svalbard (e.g. König et al., 2004). SLA and SCR have been used as a proxy for glacier mass balance in many regions (e.g. Pelto, 2011; Rabatel et al., 2005; Kienholz et al., 2017). The Landsat satellite missions in particular have long been used for glaciological investigations such as SLA detection (e.g. Racoviteanu et al., 2019). Sentinel-2 satellite acquisitions have been identified as a useful resource for SLA and SCR mapping (Paul et al., 2016; Rastner et al., 2019).

Kelly et al. (1997) and Engeset et al. (2002) used ERS SAR imagery for monitoring of SLA over Hardangerjøkulen ice cap and over Svalbard respectively.

Snow and bare ice can be mapped with optical satellites using a range of band ratios, for instance Red/Short-wave infrared (SWIR) or Near-infrared (NIR) / SWIR (Paul et al., 2016). The resulting maps are subject to thresholding by which snow and ice pixels are isolated. However, differentiation of ice from snow is difficult with the standard band ratios applied for snow and ice mapping due to the similar shape of spectral curves of ice and snow resulting in very similar ratio values for both facies (Rastner et al., 2019). Therefore, single band reflectance values, preferably in the NIR have been used instead (e.g. Østrem, 1975; Rabatel et al., 2017; Racoviteanu et al., 2019). Methods to acquire SLA and AAR are not standardized and various approaches are used. Most of the studies have used manual delineation of the snow lines from either single band or composite imagery (formed from a three-band combination). Semi-automatic detection of a snowline relies on selection of a fixed threshold, which is applied across one or multiple scenes, typically using Landsat-8/Sentinel-2 band 8. The threshold is carefully chosen so that it maximizes the ability to differentiate between snow, ice and possibly firn within single or multiple scenes. Semi-automatic processing workflows have been proposed by Racoviteanu et al. (2019) and Rastner et al. (2019), accounting for identification and separation of areas under shadow, clouds, surface water, non-glacier covering snow, snow on glacier and ice. Regardless of the workflow, differentiation of firn from ice and snow remains difficult, and even more so if super-imposed ice also needs to be accounted for. Some studies have attempted to separate glacier facies including firn and super-imposed ice zones using radar (e.g. Konig et al., 2004; Thakur et al., 2017; Winsvold et al., 2018) and optical imagery (e.g. Kienholz et al., 2017).

Data and methods

In the Copernicus Glacier Service project we tested the use of Sentinel-1/2 and Landsat-8 for snow line and glacier facies detection. Sentinel-2 and Landsat were used for testing automated processing of snowline products for selected glaciers in Norway. Sentinel-1 was used for selected glaciers in mainland Norway and Svalbard (Winsvold et al. 2018).

A prerequisite for using Sentinel-2 imagery for snowline detection as an operational service is that usable imagery is available at the end of the season. Ideally, imagery should be cloud free over the glaciers at end-of-season when snow extent is at its minimum. Fresh snow on the glaciers makes it difficult to assess the ELA/SLA. For mainland Norway we assessed the availability of useful imagery in the time window 15 August - 10 October over the Sentinel era 2015-2019 for 12 mass balance glaciers that had been monitored by NVE in this period (Fig. 3-13).

The imagery was categorized according to cloud conditions (from full cloud cover to clear sky). The best end-of-season image for each glacier was identified and episodes of fresh snowfall and snow melting were marked. Results reveal that all the five summer seasons of 2015-2019 were dominated by imagery with partial or full cloud cover. Imagery with full cloud cover is the most common. The mean date for the last clear end-of-season image of all five seasons was 07 September. This is typically earlier than the date of the ablation measurements on glaciers that were conducted in the time window 9 September – 22 November in this 5-year period. The date for the best end-of-season image capturing maximum snow melting varies over the seasons and for the glaciers being as early as 15 August for Ålfotbreen and Hansbreen in 2019 or as late as 5 October for Langfjordjøkelen in 2017. The last clear end-of-season image is typically from a later date for glaciers in North Norway. Langfjordjøkelen, the northernmost of the glaciers, has a later end-of-season image date than all other glaciers in South Norway in all five seasons. This can be explained by more frequent image acquisitions in North Norway.

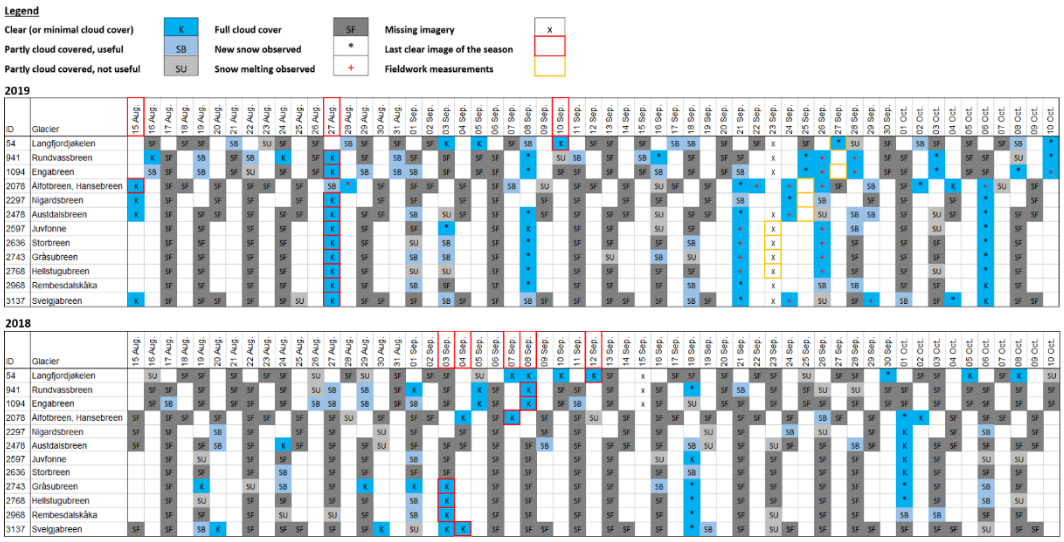

Figure 3-13. Overview of available imagery for snowline mapping in 2018-2019 for 12 monitored mass balance glaciers in mainland Norway. Glaciers are sorted from north (Langfjordjøkelen) to south (Svelgjabreen). Imagery is classified according to cloudiness and usefulness for snowline detection.

3.2.2 Snow cover monitoring on xGeo

XGeo (www.xgeo.no) is NVE's expert tool for notification and emergency. After an update in 2018, Xgeo now also displays satellite imagery and postprocessed imagery products of Sentinel-1, Sentinel-2 and Sentinel-3 missions. NVE has implemented its snow cover monitoring into a processing chain in xGeo. This was done as a part of the operational snow monitoring service. Snow cover products are available for visualization at 500m (S3 SLSTR) and 20m resolution (S2). The S3 snow products shows fractional snow cover (1-100%) for cloud free pixels, lakes are masked (value 'nodata'). The S2 snow product classify the pixels as either snow covered, snow free, lakes, or clouds (lakes are masked out nodata). The classification of S2 pixels is performed using SNOMAP algorithm (Hall et al., 1995), using Normalized Difference Snow Index (NDSI) and thresholding of band 8 for improved discrimination between snow and water. NDSI as suggested by Dozier (1989) has been used in multiple studies (Hall et al., 1995) and is using the green (band3) and SWIR (band11) bands (see Table 2-2 and Figure 2-3 for band wavelengths):

$$NDSI = \frac{Green - SWIR}{Green + SWIR}$$

SNOMAP algorithm classifies a pixel as snow if the following criteria is 'true':

NDSI > 0,4 and Band 8 > 0,11

The Sentinel-3 and Sentinel-2 snow cover products have been available from April 2018 and January 2019 respectively and are available in near real time with approximately 24-hour delay (status of February 2020).

To test whether the Sentinel-2 operational processing chain could be used for snowline detection on glaciers, we compared the Sentinel-2 product with a Sentinel-2 image of Hardangerjøkulen (Fig. 3-14). The Sentinel-2 snow cover product discriminates snow from terrain and water outside the glacier, but does not differentiate between ice, firn and snow on the glacier. Snow, firn and ice are all classified as snow with the SNOMAP algorithm. Therefore, the product as is cannot be used for discriminating glacier facies, but it can be used to detect snow and possibly glacier bodies or snow-covered glacier bodies. For automatic extraction of glacier facies in the operational service other algorithms must be applied.

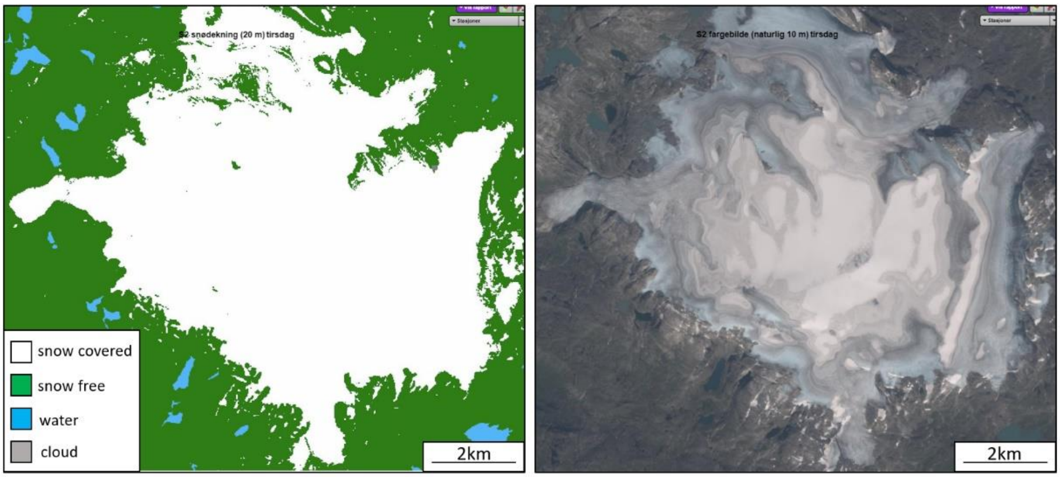

Figure 3-14. Xgeo visualization of Hardangerjøkulen based on Sentinel-2 image of 27 August 2019. To the left NVE's Sentinel-2 classified snow cover product at 20m resolution. To the right the natural Sentinel-2 image at 10m resolution. /xgeo.no/Copernicus Sentinel data/

3.2.3 Sentinel-1 for Svalbard and mainland Norway

To test the possibility of detecting snowlines and glacier facies, Sentinel-1 and RADARSAT-2 synthetic aperture radar (SAR) data over mainland Norway and Svalbard were used to derive multitemporal SLA and categorize snow and ice zones on the glaciers. This work is reported in detail by Winsvold et al. (2018). The results were compared to field measurements and optical Sentinel-2 acquisitions. The field measurements used for comparison included 2015 and 2016 measurements from Hellstugubreen, Storbreen, Austdalsbreen, Gråsubreen, and Nigardsbreen. Winsvold et al. (2018) demonstrated the possibility of tracking snowlines during the melt season from Sentinel-1A and 1B backscatter time series. Snowline data were found to be valuable for regionally extrapolating and estimating annual mass balance in areas without in situ measurements. Even though the temporal resolution of optical imagery has been increased with the twin Sentinel-2B satellite in orbit, maritime regions remain cloudy and hinder dense time series of medium-resolution optical imagery, and SAR time series can therefore act to fill data gaps. Additionally, high spatial resolution Sentinel-1 time series can be used to measure snowmelt parameters on glaciers like demonstrated for Kongsvegen glacier on Svalbard (Fig. 3-15).

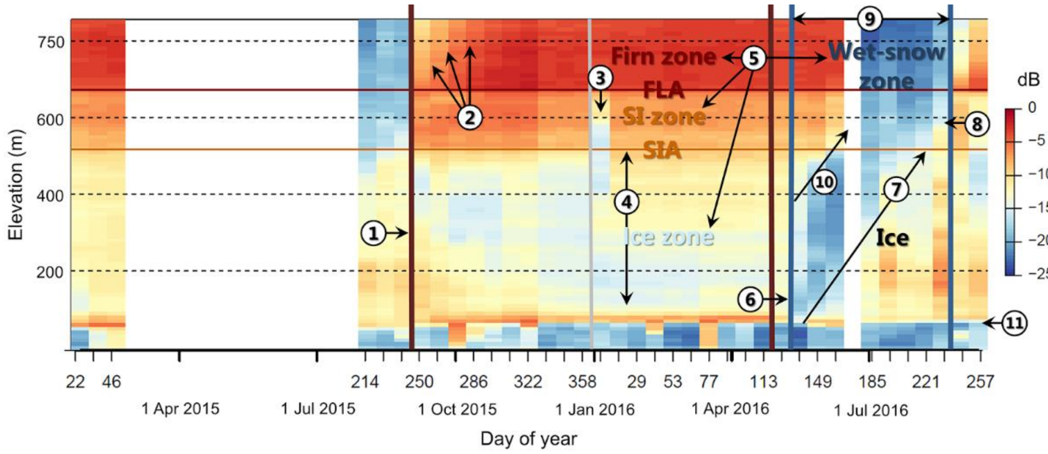

Figure 3-15. Time series of Sentinel-1A and 1B backscatter (dB) for a profile along Kongsvegen glacier on Svalbard. The numbers represent 11 possible glacier variables that can be detected: (1) onset of cold season; (2) freeze-up and the winter cooling of the firn area; (3) winter rain event; (4) change of surface properties after winter rain event; (5) glacier facies separated by firn line altitude and super-imposed ice altitude; (6) onset of melt season; (7) transient snow lines; (8) end of summer snow line altitude (SLA); (9) length of melt season; (10) surface dry-to-wet snow line; and (11) glacier outline or calving front. Figure from Winsvold et al. (2018).

3.2.4 Sentinel-2 for mainland Norway

To test the suitability of using Sentinel-2 for snowline mapping on glaciers in mainland Norway we used a semi-automatic approach with and without manual editing. Sentinel-2 imagery including NIR band 8 were downloaded from colhub.no and processed further with ArcGIS 10.5.1. system.

Snowline or snow area extraction can be performed semi-automatically, or manually. In the test regions, pixel values in the band 8 (NIR) of Sentinel-2 were inspected to find the best threshold for differentiating between snow, ice and possibly firn. Due to varying terrain and atmospheric conditions, range of values of snow, firn and ice was found to vary even within a single scene and therefore manual corrections were often necessary. Applying a fixed threshold worked best over larger glacier units such as plateau glaciers, with little influence of terrain induced shadows. As example, for Hardangerjøkulen a fixed threshold of 5000 was applied to detect division between snow and firn (Fig. 3-16). The glacier zones were mapped quite accurately by the fixed threshold, though manual corrections can still improve the result or be used to generalize the resulting snowline and firnline. The snow-covered area was 12.2 km^2 prior to correction and 12.1 km^2 after manual correction, representing only a ca. 1% overall difference. Applying a threshold of 3400 worked well do detect the ice-firnline, the firn area was 12.7 km^2 prior to correction and 13.0 km^2 after manual correction, a difference of ca. 2.5%.

Fixed thresholding did not performed as well over smaller-scale valley and cirque glacier units, in particular those facing North, West, or East direction (Fig. 3-17). Terrain induced shadowing results in very low values in band 8 values, usually in a range 0-1000 and thus well under optimal thresholds for detection of snowlines and firnlines. Even in case of cloud-free imagery and additional atmospheric correction (such as for Sentinel-2 L2A products) manual correction of a vast majority of outlines was needed to provide useful results (Fig. 3-17). Identification of snowline and firnline in shadow is therefore time-demanding, requires careful consideration and results can be uncertain. Using results from fixed thresholding is not to be recommended without careful inspection and manual correction of each glacier, regardless of how carefully the thresholding is applied. This particularly concerns smaller valley and cirque glaciers with large variations in topography, usually facing north, east, or west. Examples of such areas are Lyngen, Sunnmøre, or parts of Jotunheimen.

Additionally, supraglacial debris in form of moraines (lateral, medial, terminal), as well as fresh snow (regularly or irregularly distributed) pose a significant challenge for snowline and firnline identification. Firnline, as identified on Hardangerjøkulen (Fig. 3-16), was not as easy to identify in other regions, neither by fixed thresholds nor manual digitization. In many cases firn cannot be visually differentiated from snow and therefore only the snowline can be mapped.

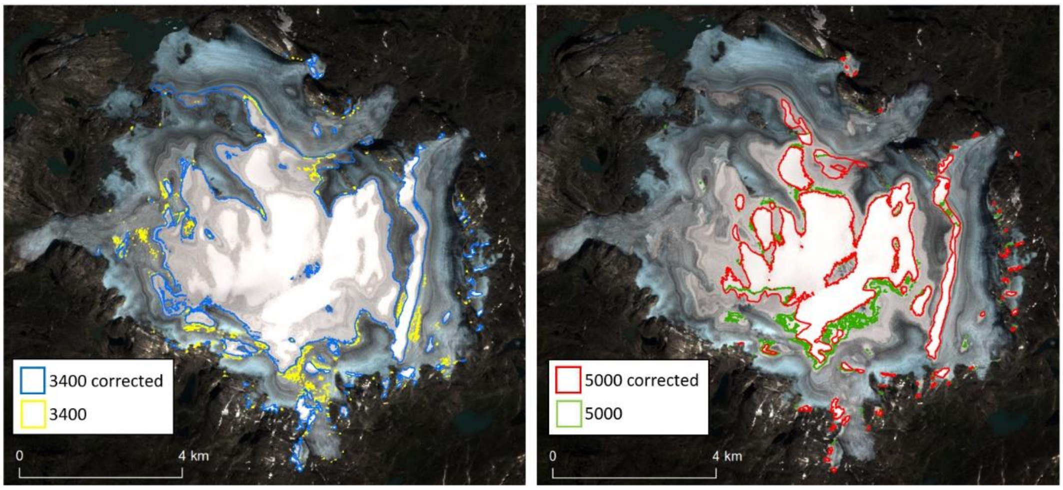

Figure 3-16. Firnline (left) and snowline (right) outlines mapped using a fixed threshold of 3400 and 5000 and modified using manual correction over Hardangerjøkulen. Background image is a natural colour Sentinel-2 image from 27 August 2019. /Copernicus Sentinel data/

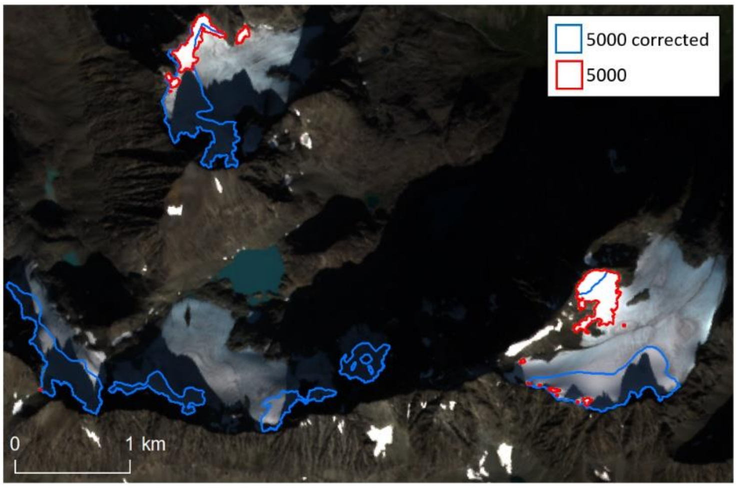

Figure 3-17. Detected snowline using a threshold of 5000 in band 8 (NIR) in red and manually corrected snowline in blue over selected north oriented cirque glaciers in North Lyngen. Note the heavily shadowed parts of the glaciers. Background image is a natural colour Sentinel-2 image from 1 September 2018. /Copernicus Sentinel data/

To assess performance of the semi-automatic thresholding on larger scale, it was applied to a Sentinel-2 scene from 1 September 2018 covering most of Lyngen peninsula and Kvaløya (tile T33WXT). This corresponds to glacier regions 4, 5, and 6 in the previous glacier inventory (Andreassen et al., 2012). After a visual inspection, a fixed threshold of 5000 was considered to differentiate best between snow and ice. Firn was not possible to visually detect and differentiate. The glacier area determined from the glacier outline mapping over Lyngen and Kvaløya was 91.0 km^2, considering only glacier bodies larger than 0.1km^2. The cut-off size was applied, as inclusion of smaller units would substantially increase manual correction time, and because the glacier units in northern Norway larger than 0.1 km^2 represent ca. 92% (ca. 872 km^2 out of 938 km^2) of all glaciers in northern Norway, therefore making up a representative selection. While some snow areas were detected successfully, most of the snow cover polygons needed to be either drawn from scratch or manually corrected. In some areas large corrections were needed and automatic results were not reliable (Fig. 3-17). The total estimated snow-covered area using a fixed threshold was 18.5 km^2 without manual corrections and 33.5 km^2 after manual corrections. Hence, using the semi-automatic method with thresholding led to marked underestimation of snow cover area.

Snowline can also be automatic mapped to track the changes in transient snowline through the season. This was tested for a selection of glaciers in Jotunheimen for three scenes with favourable cloud conditions from July and August 2019 (Fig. 3-18). A threshold of 4000 was selected after a visual inspection of the three scenes with a goal to differentiate snow from ice. The glacier sample has relatively little terrain induced shadowing, which posed little problem for this glacier sample in this period. Though imagery acquired at later dates such as in late September or later would result in more widespread shadowing and therefore increased uncertainty. The selected threshold detected the snowline well at all three dates and shows the snow cover depletion on the glaciers. The resulting snow cover area was 57.1 % (13 July 2019), 14.2 % (4 August 2019) and 7.0 % (27 August 2019) of the total glacier area (24.7 km^2). The snow covered area was underestimated in cirques where shadowing was prominent although thresholding performed well overall. This shows that snow coverage evolution can be monitored using an automatic method and a fixed threshold for some glaciers through the season. Manual digitization of snowlines may be a better option for glaciers, where a fixed threshold performs worse, especially in the case of smaller glaciers, north oriented glaciers or glacier parts influenced by shadowing.

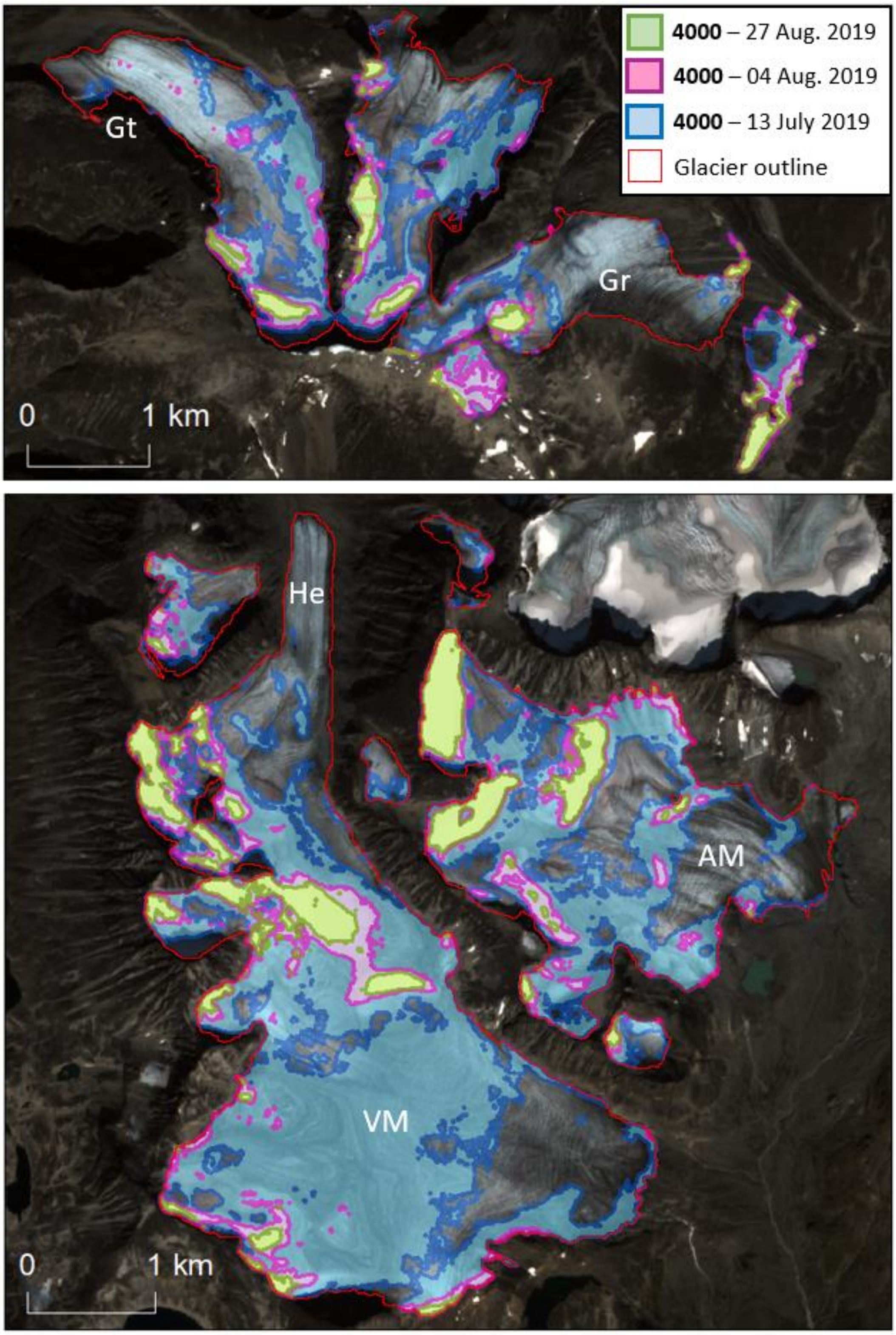

Figure 3-18. Snowline evolution on glaciers in Jotunheimen, using a threshold value 4000 on band 8 imagery from 13 July 2019, 4 August 2019 and 27 August 2019. Upper figure shows Grotbrean (Gt) and Gråsubreen (Gr) and lower figure Hellstugubreen (He) and Vestre (VM) and Austre Memurubre (AM). Background image is the Sentinel-2 image from 27 August 2019 in natural colours. /Copernicus Sentinel data/

3.2.5 Sentinel-2 for Svalbard

A similar semi-automated threshold mapping as for mainland Norway was tested on Svalbard for mapping snow- and firn areas. We selected Sentinel-2 band-8 images from summer 2020 when snow cover was at a minimum due to record-warm temperatures. Thresholds for firn and snow were decided by visual inspection and applied to a GIS-based script to derive separate outlines for snow- and firn areas, with plausible results (Fig. X). We also tried to identify and map super-imposed ice zones, but delineation proved to be difficult due to high local variability of pixel-values across all bands. Applying the same thresholds to other Svalbard image tiles for the same period gave reasonable results for western and southern Spitsbergen, whereas snow-firn separation was more difficult in the northeast where melt-impacts were less pronounced. Although these analyses provided some useful results, it appears difficult to employ any operational monitoring of glacier facies based on Sentinel-2 due to persistent cloud-cover on Svalbard during the late summer, frequent summer snowfall events, and large gradients in climate and surface types.

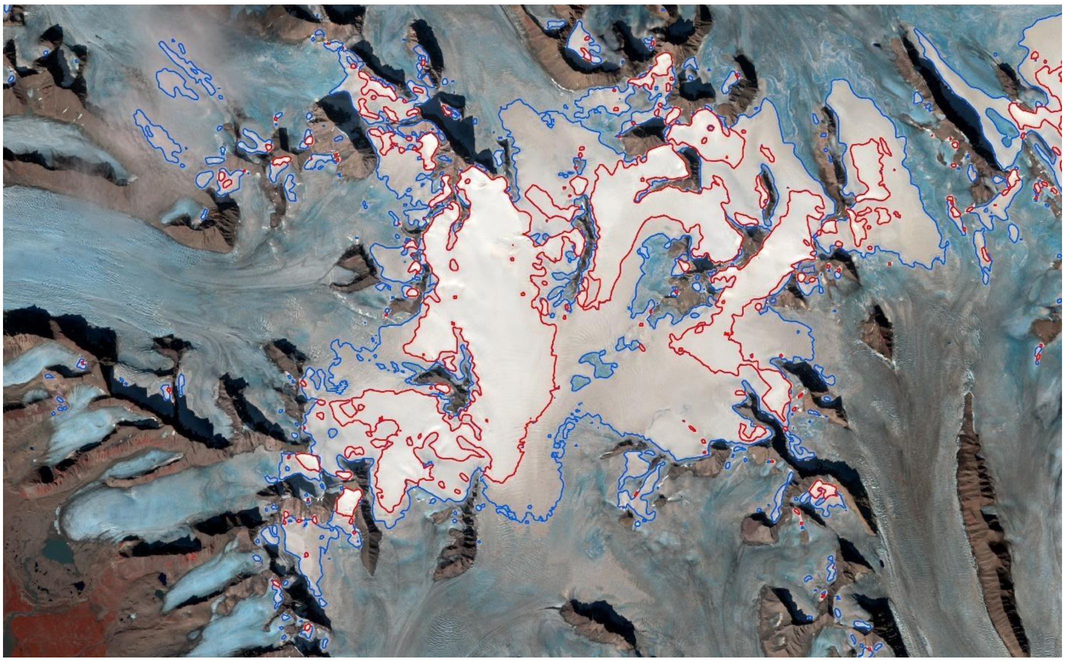

Figure 3-19. Semi-automatically generated maps of snow area (red) and firn area (blue) over Løvenskioldfonna south of Kongsfjorden, Spitsbergen. The bright white surface is expected to be remaining winter snow, whereas the browner non-ice surface is expected to be firn from earlier years. The areas were separated by band-8 thresholds of >5000 for snow and 3500-5000 for firn. The Sentinel-2 image is from 27 July 2020 (False 8-4-3). /Copernicus Sentinel data/

3.2.6 Snowline products

As demonstrated, the Sentinel-2 imagery is useful for a visual assessment of the snow characteristics of glaciers and can be viewed in Xgeo. Deriving automatic snowline products requires visual inspection and selecting a suitable threshold that needs thorough checking, and in many cases, manual corrections. Manual digitization is a possibility for deriving snowlines and glacier facies for the glaciers of interest. Thresholding of imagery prior to manual correction can be considered for larger plateau glaciers.

In the Copernicus glacier project we offer selected products resulting from the work:

- Transient snowlines and snowzones for among others 10 mass balance glaciers for the period 2015-2019 using best end-of-season imagery. Snowlines and snowzones were manually digitized and images used are the best images closest to the end of ablation season.
- Transient snowlines and snowzones for a selection of glaciers in Lyngen and Kvaløya from 2018 and Hardangerjøkulen from 2019 using manual correction of automatically thresholded result. Transient firnline and firnzone were included for Hardangerjøkulen 2019.
- Transient snowlines and snowzones for a selection of glaciers in Jotunheimen. Snow zones were mapped using automatic thresholding for multiple dates in 2019.
- Snow- and firn areas for glaciers on Svalbard during summer 2020.

3.3 Glacier velocity

3.3.1 Background

The large amount of freely available repeat optical imagery nowadays enables deriving glacier velocities at a higher spatial and temporal resolution than ever before. Glacier surface velocity extraction from optical imagery using offset tracking/image matching is well documented in multiple studies and has been determined for entire glacierized regions (e.g. Dehecq et al., 2015; Mouginot and Rignot, 2015), and for single glaciers (e.g. O'Neel et al., 2005; Redpath et al., 2013). Challenges in mapping surface velocities using optical imagery have been insufficient satellite sensor resolution, slow movement of glaciers, lack of trackable features, cloud and snow cover, and finding optimal window sizes for the image matching. The basic method to derive displacements from optical data is cross-correlation between repeat images, called image matching or offset tracking. Different tools to perform the work use different implementations, algorithm variants, numerical solutions, and post-processing or outlier filtering.

Displacements can be derived in a very similar way from repeat radar images. Thereby the complex radar signal (phase + amplitude) can be exploited. However, under the maritime climate in Norway and Svalbard, the radar phase component does not typically show coherence over several days, so that the radar backscatter amplitude is most important for defining displacements. As a main difference to optical images, radar images have inherent noise (radar speckle) that requires use of larger windows compared to else equivalent optical images to derive displacements with a sufficient signal-to-noise ratio (SNR). Such use of larger matching windows results in a lower resolution of the velocity fields derived compared to optical images with same nominal resolution. The strong advantage of ice velocities from radar images is their weather and day-light independency: displacements can be measured also through clouds and during polar night.

3.3.2 Mainland Norway

The work on deriving glacier velocities from Seninel-2 imagery has been described in a separate report (Nagy and Andreassen, 2019a). Here we give a summary of main results but refer to the latter report for further details. Early results for three larger outlet glaciers in Norway, Nigardsbreen, Engabreen, and Rembedalskåka, were also described in Klingenberg (2017).

Previous studies of glaciers in mainland Norway are done for individual glaciers by using repeat aerial photography (Jackson et al., 2005; Wangensteen et al., 2006), time-lapse cameras (Messerli and Grinsted, 2015) and field techniques and stake measurements (e.g. Liestøl, 1967; Østrem et al., 1976).

Data and methods

For the new glacier surface velocity product derived for Copernicus Glacier Service we used exclusively optical imagery from Sentinel-2. To derive surface velocities, presence of features such as crevasses is crucial and more features generally lead to higher likelihood of results.

To acquire displacement information from the Sentinel-2 imagery, we used the Sentinel-2 Displacement Toolbox (SenDiT) (Nagy et al., 2019). SenDiT is a semi-automatic, open-source toolbox optimized for retrieval of displacement maps from Sentinel-2 bands with 10m ground resolution. The toolbox uses the Image Correlation software (IMCORR) (Fahnestock et al., 1992) and its structure is described in detail by Nagy et al. (2019). The degree of flexibility of SenDiT is higher than that offered by other services such as CPOM, GoLIVE, and MEaSUREs, which provide velocity maps for fixed spatiotemporal parameters. The automated processing and the quick turnaround are superior to other feature tracking tools such as ImGRAFT, CIAS, or COSI-Corr. However, results obtained with SenDiT still need to be checked and postprocessed using manual filtering.

Selection of imagery

The feature appearance is determined by the ground resolution of the satellite sensor. The features most often seen on glacier surfaces in Norway were crevasses and crevasse induced shadowing, ogives, lateral and medial moraines, and rockslides (Fig. 3-19). Applying feature tracking on snow covered parts of the glaciers is difficult due to lack of differences in intensity values. Therefore, we looked for snow free parts (ablation areas) to get trackable features. The relative orientation of features is also important as features such as medial and lateral moraines that are stretched in the flow direction of glaciers were hard to track. On the other hand, crevasses, ogives, debris layers or ash layers that are perpendicular to the flow of the glacier were found to offer potentially good tracking targets (Fig. 3-21).

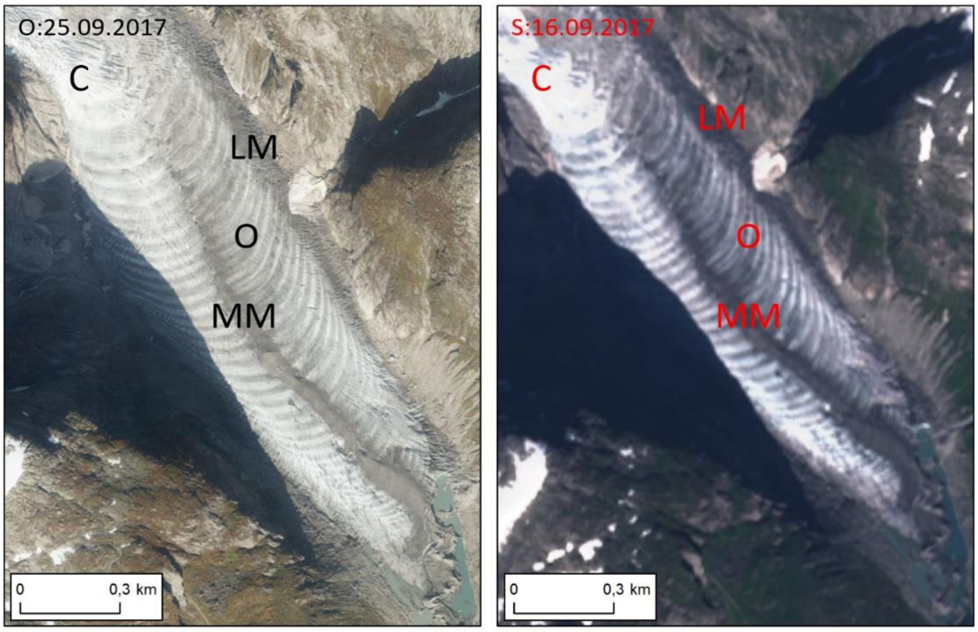

Figure 3-21. Illustration of visible surface features in orthophoto (left) and Sentinel-2 imagery (right) on Austerdalsbreen, outlet of Jostedalsbreen. LM: lateral moraine, MM: medial moraine, O: ogives, C: crevasses. /norgeibilder.no/Copernicus Sentinel data/

The time difference between the two paired images must be long enough to observe displacement, yet short enough for the features not to change and maintain similarity. Due to the varying nature of glacier surface velocity, a variable pair time span was used. The ideal time window was chosen after visually assessing the speed of the glaciers. Large time spans may result in decorrelation of the features through change of pattern, change of extent, or complete disappearance due to snow. Commonly, selected time spans were on the order of weeks and months for fast moving glaciers and months to a year or two for slower moving glaciers. Though, many of the glaciers were too slow or lacking features to acquire any results (e.g. Gråsubreen). To compare the imagery and derive velocity on a yearly scale, it is ideal to use images from the similar periods of the year, as the same features tend to become visible on the surface at certain time during the seasons.

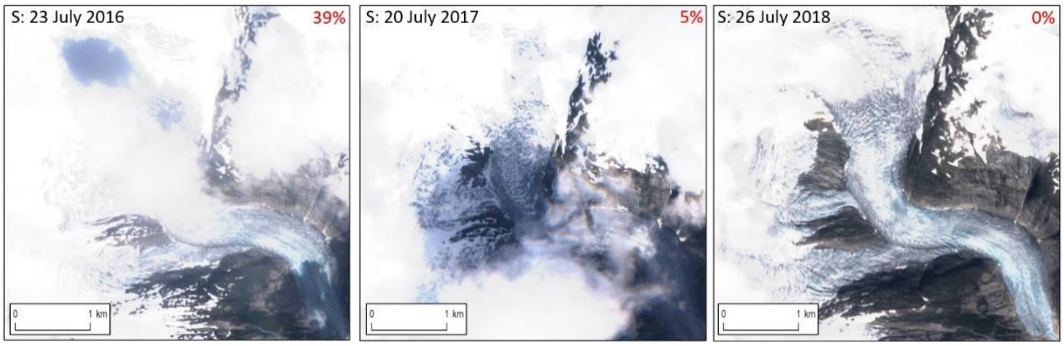

Figure 3-22. A comparison of feature visibility and snow cover on Nigardsbreen, outlet of Jostedalsbreen, using Sentinel-2 images from July in the period 2016-2018. Clouds cover part of the tongue on 20 July 2017. Note also cloud and cloud shadow on 23 July 2016. Overall cloud percentage of the scene given by ESA is in red. /Copernicus Sentinel data/

However, the time of appearance of a feature will vary due to interannual variations in summer melt, winter accumulation and cloud conditions (Fig. 3-22). Clouds over the glaciers remains a problem when using optical imagery for glacier surface velocity mapping as optical sensors cannot collect surface reflectance through clouds. Manual selection is laborious but is often better than using strict cloud percentage thresholds to avoid omitting potentially good images that can have little or no cloud cover over the glaciers of interest, despite a high overall cloud percentage for the scene (calculated by ESA). The cloud cover over Nigardsbreen was more prominent in a 2017 acquisition with overall 5% cloud cover, than in a 2016 acquisition with 39% cloud cover (Fig. 3-22). many suitable scenes as possible regardless of ESA indicated cloud cover percentage.

Sources of error and postprocessing

When co-registering two images from the same relative orbit, the orthorectification error will get mostly eliminated. Using imagery from two different relative (neighbouring) Sentinel-2 orbits may lead to an error of several tens of meters at the glacier termini (Kääb et al., 2016; Nagy et al., 2019). Therefore, we only used image pairs composed of imagery from the same relative orbit. The relative co-registration accuracy of the two images in an image pair was the main source of error in the glacier velocity product. The error manifests itself as a relatively uniform and unidirectional shift, visible over the stable ground. The magnitude range of the co-registration error in the used image pairs was estimated from the stable area and used as the main error estimate for the given pair.

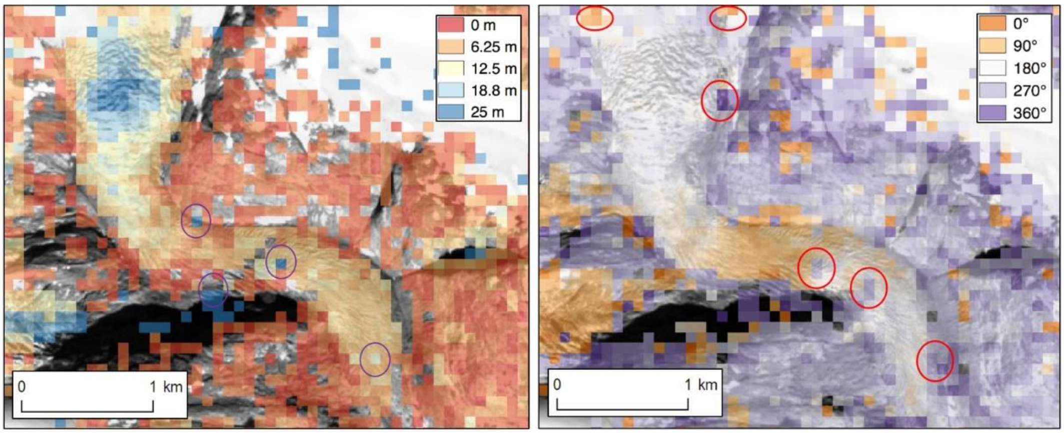

Figure 3-23. Maps of displacement magnitude and displacement direction over Nigardsbreen and adjacent areas of stable ground. Estimated displacement magnitude and direction in stable areas is 2-6m and 220-270°. The data was acquired from the Sentinel-2 pair 22 August 2017-16 September 2017 (25-day temporal difference). The outliers marked in purple (for displacement) and red (for direction) were removed from the final dataset.

Overall, we estimated a co-registration error to be most often in the range 2-8m for most image pairs, but we found a co-registration error reaching the magnitude of up to 12m for some of the pairs. It was necessary to filter the results manually as the glacier movement in a region or of an ice cap can differ both in magnitude and direction. The displacement magnitude and direction can also vary within a single glacier, e.g for Nigardsbreen where flow is fast and dominantly in N-S direction in the icefall upstream, while slower and in W-E direction further downstream (Fig. 3-23). To detect and remove outliers, the magnitude and azimuth of the displacement were used alongside with DEMs of the glacier areas, and high resolution orthophotos to understand the flow direction of the ice.

The derived glacier velocity dataset was manually filtered for each of the image pairs and for each glacier unit separately.

Glacier velocity product for mainland Norway

After dataset filtering, we kept ca. 24 300 point results over 91 glacier units (whereof 37 in northern Norway and 54 in southern Norway). Out of the 91 units, 53 units were part of the four largest ice caps in Norway (Jostedalsbreen, Vestre Svartisen, Søndre Folgefonna, Østre Svartisen). Jostedalsbreen itself had results for over 30 glacier units. The maximum velocity was 1.65 m/day for Nigardsbreen.

For the investigated period 2015 to 2018, the maximum number of multitemporal point measurements at one point was eight for certain points of Engabreen, Tunsbergdalsbreen and Austerdalsisen. These glaciers have some of the longest and widest outlets, a large number of distinct crevasses, large accumulation basins, and they move relatively fast due to steep terrain. Therefore, they are likely to provide spatiotemporally dense observation series. The final glacier velocity product has results mainly over the snow-free and/or feature rich parts of the glaciers (Fig. 3-24). See Nagy and Andreassen (2019a) for further results.

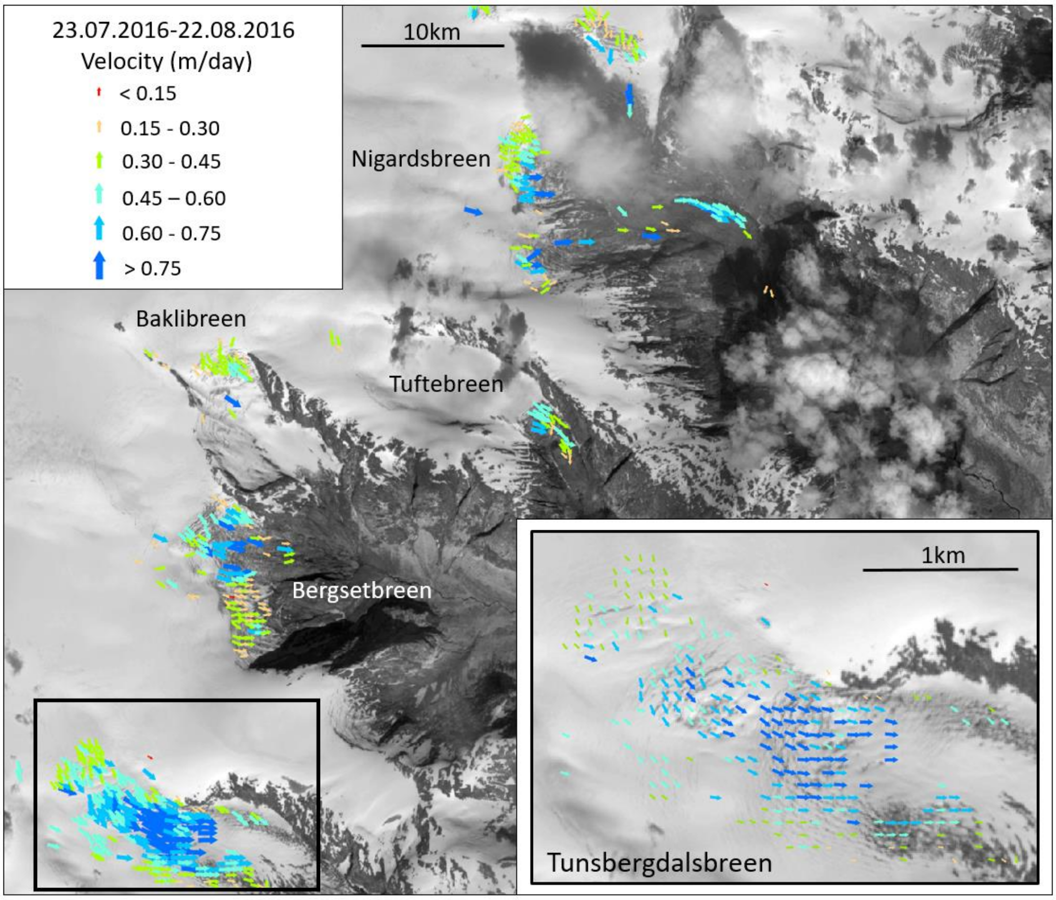

Figure 3-24. Glacier velocity calculated from the pair 23.07.2016-22.08.2016 over selected glacier arms of Jostedalsbreen. Background image is band 8 Sentinel-2 image from 23.07.2016 at 10m ground resolution. The results shown are filtered and obtained mostly from ablation areas and/or areas with trackable features (mostly crevasses). /Copernicus Sentinel data/

3.3.3 Svalbard

Sentinel-2 ice velocities

Velocity mapping with Sentinel-2 on Svalbard was done with the ImGRAFT feature-tracking toolbox developed by Messerli and Grindsted (2015) on the principles of template matching with normalized cross correlation. The toolbox was originally written in Matlab, but was also translated into the Python language during the project to make it freely available. With ImGRAFT as a core, it is easy to batch-process a large number of image pairs, but issues with cloud cover, mismatches and noise still remain. We found that the spring period (April/May) often performs better than the summers due to more stable weather and surface conditions, with minimal impact from snowmelt. Data from winter and autumn are hampered by large mountain shadows due to the low angle of the sun, as well as fresh snow on glacier ice in the autumn.

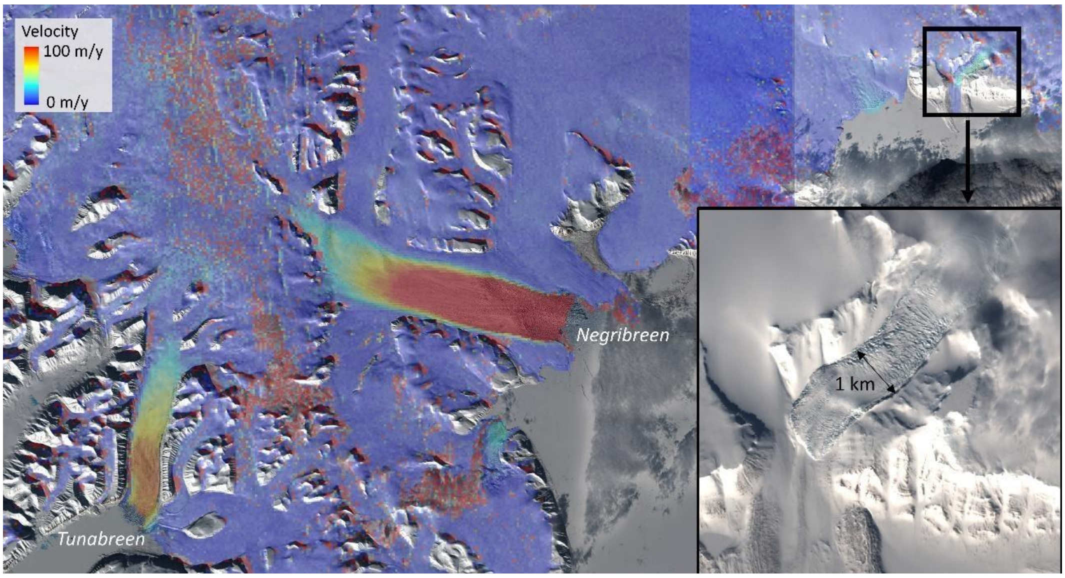

Figure 3-25. Glacier velocities derived from Sentinel-2 images acquired on 7 and 24 April 2018 over a region between Isfjorden and Storfjorden, central Spitsbergen. Rapid glacier flow appears clearly for the two surging glaciers Tunabreen and Negribreen, whereas it is less obvious but still visible for the smaller Ganskijbreen (black frame) where the image itself (inset) from 24 April reveals an ongoing surge with heavy crevassing and strong shearing. /Copernicus Sentinel data/

In this project, we chose to focus our Sentinel-2 velocity mapping on a selection of surging glaciers, as well as testing Sentinel-2 for Svalbard-wide velocity mapping. Our results show that glacier surging can be readily detected and monitored with Sentinel-2 (Fig. 3-25) although the long winter darkness and frequent cloud cover in summer limits the number of suitable image pairs that can be found. The geometric accuracy of Sentinel-2 (see Section 2.7) is not so critical for surge monitoring where velocities are high, but for slower flowing glaciers it easily becomes an issue for obtaining significant velocities. For example, a one-pixel (10 m) orthorectification error in one of the 17-day repeat images in Fig. 3X would translate into a velocity error of 0.6 m per day, which is higher than the typical velocity of non-surging glaciers on Svalbard. Due to this accuracy limitation, we therefore limited our velocity analyses to image pairs from the same relative orbit (i.e. similar geometrical error) or images corrected by national DEMs (i.e. subpixel accuracy).

Unfortunately, this also limited the number of comparable image pairs dramatically because of frequent cloud cover and data gaps in the national-DTM processing.

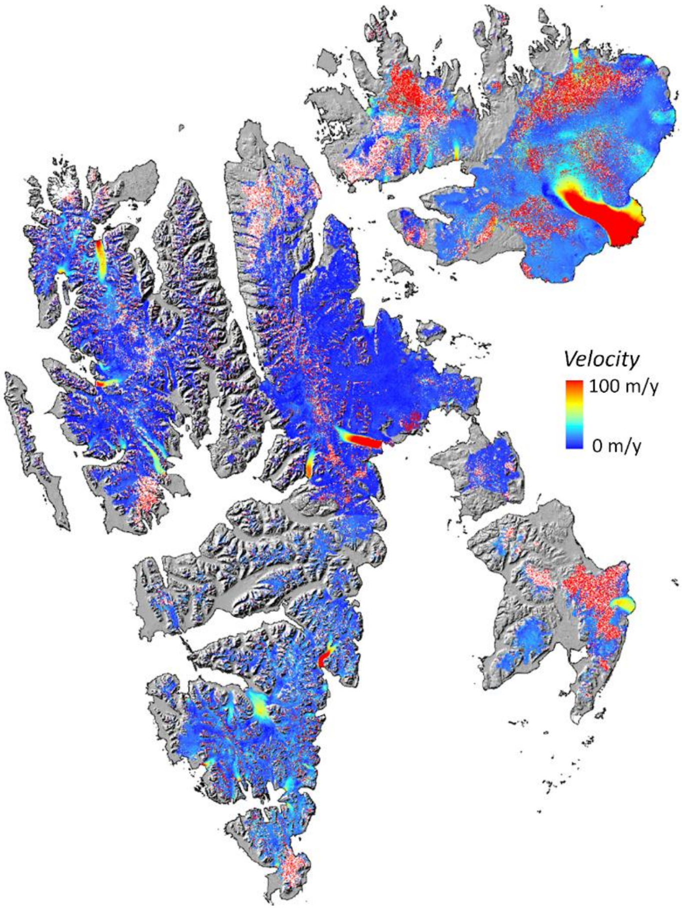

Figure 3-26. Svalbard-wide glacier velocities derived from Sentinel-2 using 1-3 week repeat scenes from April 2018. Many surging glaciers stand out (e.g. Storisstraumen, Negribreen, Stonebreen, Mosjnev-breen, Monacobreen), but glacier velocities are also significant for other glaciers, especially the front area of calving glaciers.

We tested Svalbard-wide processing for a clear-weather period during April 2018 (Fig. 3-26). The processing was optimized towards fine resolution (100-200 m) velocity mapping in fast-flowing areas with many features, at the cost of more mismatches and noise in the higher areas where surface features are fewer with better performance for larger matching templates (e.g. 500 m, 50 pixels). Better results could likely have been achieved by an adaptive template-size strategy like the JPL auto-RIFT processor by Gardner et al. (2018) which has been applied to the entire Landsat archive for Svalbard in the ITS_LIVE project (https://its-live.jpl.nasa.gov/). These Landsat-based velocities are freely available on an annual basis and were combined with our Sentinel-2 results for the ice discharge and frontal ablation calculations in Section 3.1.5. We further plan to implement velocities from Sentinel-1 which gives more consistent results for Svalbard.

Sentinel-1 ice velocities

Svalbard-wide winter glacier velocities were derived from Sentinel-1 images once every winter using offset tracking procedures programmed in the Gamma Remote Sensing software (Schellenberger et al., 2016). The method is explained in general terms in section 3.3.1. Due to the large windows to be used for matching repeat radar images, small glaciers cannot be resolved. Also, the amount of tracking errors depends, in particular in the accumulation areas, on the weather conditions between the matched images. Snow fall, wind drift or surface melt can reduce the similarity of features over time and thus lead to errors. Figure 3-27 shows two Sentinel-1 derived velocity maps over Svalbard.

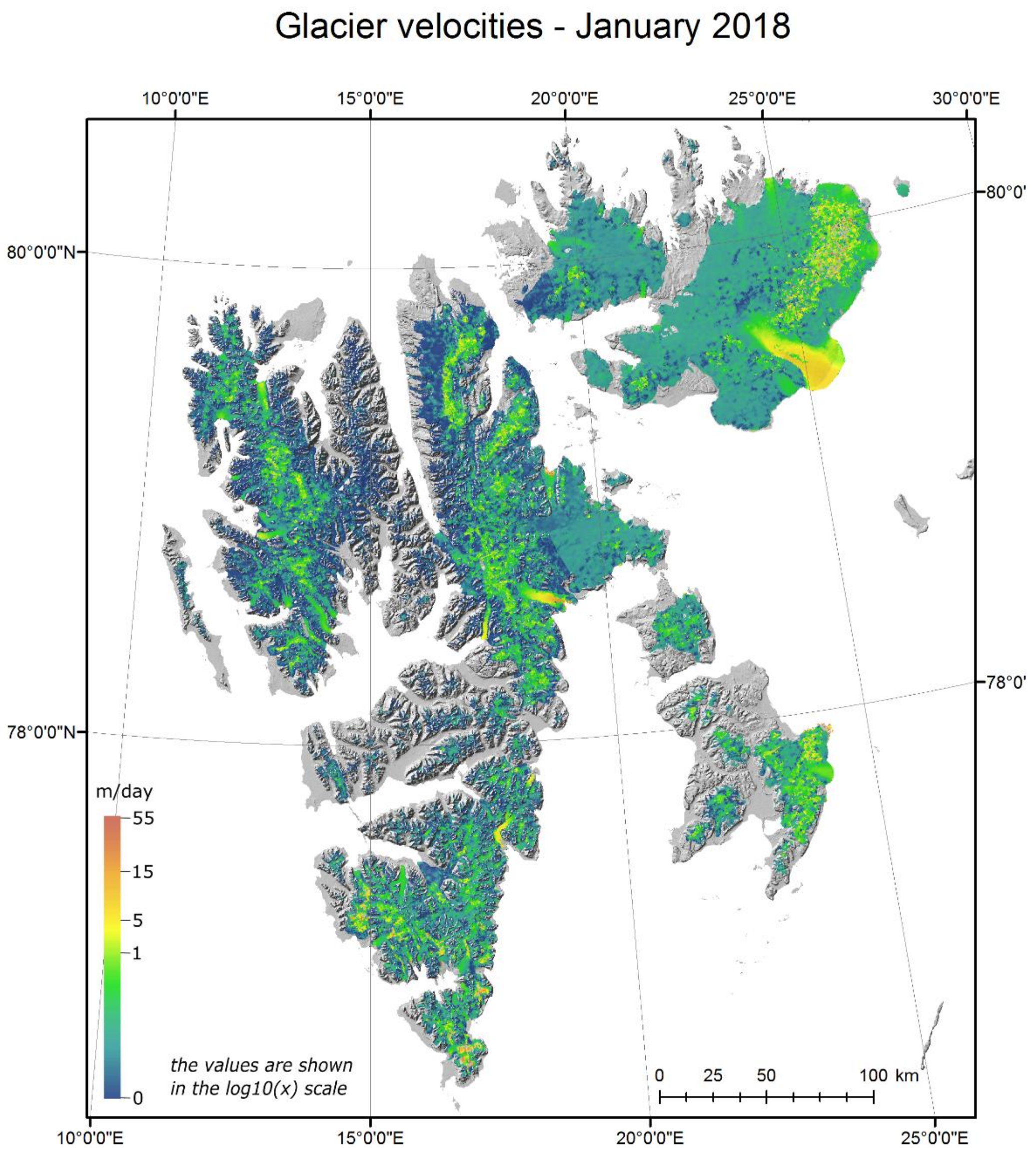

Figure 3-27a. Glacier speeds over 12 days from repeat Sentinel-1 data, Svalbard. 5-18 January 2018. Colour scales are shown a logarithmic scale to show speeds better. At several places surge activity increased end of 2019, compared to beginning of 2018, at some places surge activity decreased.

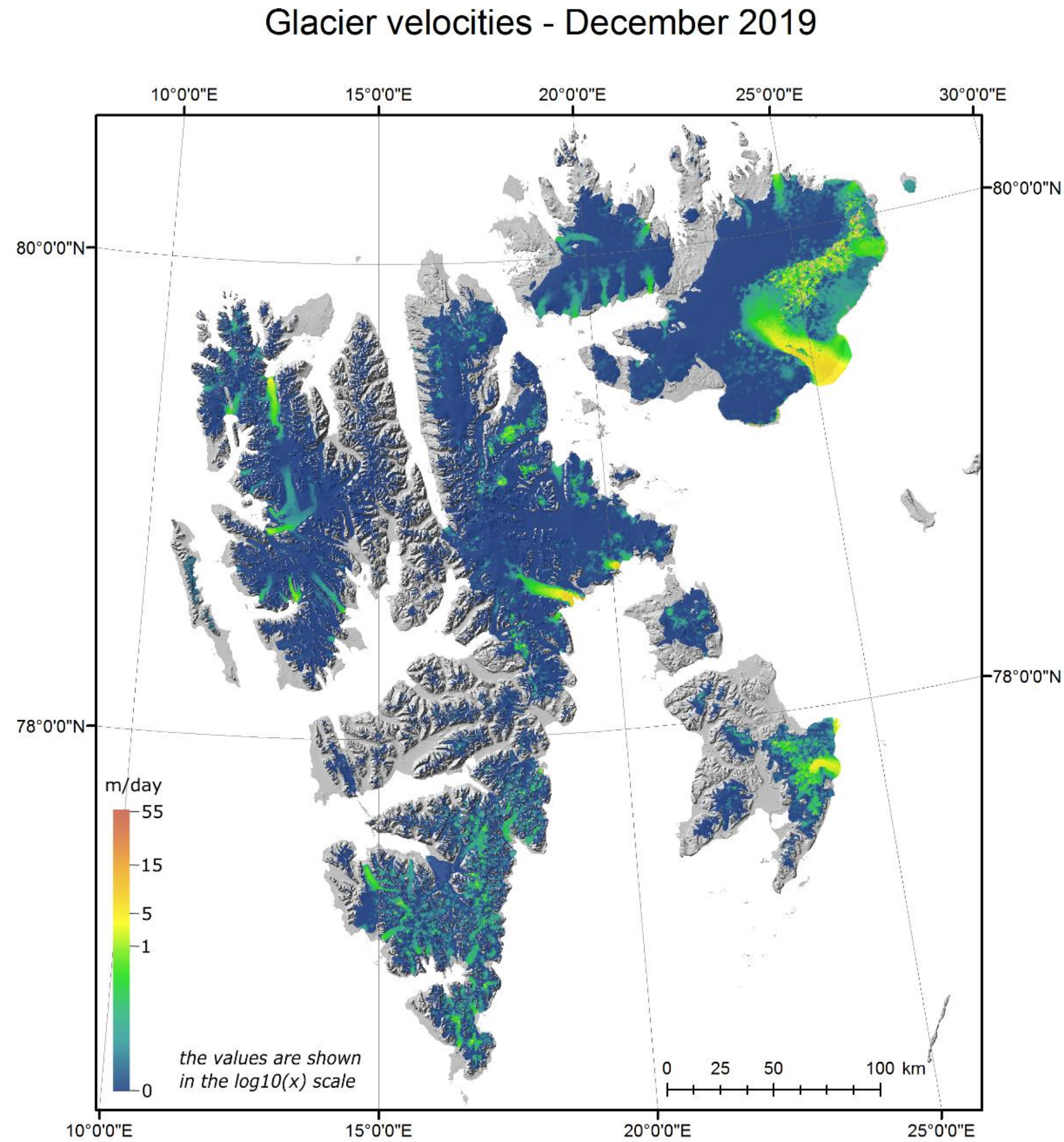

Figure 3-27b. Same as 3-27a, but for 9-21 December 2019. Colour scales are shown a logarithmic scale to show speeds better. At several places surge activity increased end of 2019, compared to beginning of 2018, at some places surge activity decreased.

3.4 Glacier crevasses and surges

3.4.1 Background

Crevasses are a common feature on glaciers, ice caps and ice sheets. A crevasse is a crack formed in glacier ice when tensile stresses exceed the tensile strength of the ice (Cogley et al., 2011). The crevasse distribution can reflect the pattern of glacier basal friction (Gong et al., 2018). Temporal monitoring of the crevasse pattern is also considered useful in studying glacier dynamics (Whillans and Tseng, 1995). Crevasses are used for feature tracking and displacement mapping (see chap. 3.3). The detection and mapping of crevasses are important for polar research safety (Zhou et al., 2008; Bhardwaj et al., 2016). Mountaineering accidents involving falling into a crevasse during walking, skiing, hiking or climbing are numerous and can be fatal. Jackson and Ragulina (2014) reported at least 10 deaths in mainland Norway due to a fall into a glacier crevasse, but also multiple non-fatal falls. To detect crevassing, ground based and airborne Ground Penetrating Radar (GPR) has been used (e.g. Luckman et al., 2012). Satellite imagery is used in only a few studies, examples of such are Bhardwaj et al. (2016) highlighting usefulness of optical satellite imagery for detection of crevasses from Landsat 8 imagery using the ratio of bands 10 and 6 and Gong et al. (2018) using Radon transform (see chap 3.4.3).

The Icelandic Association for Search and Rescue has mapped known crevasse areas on ice caps in Iceland (https://safetravel.is/crevasse-maps). The classification was based on high resolution SPOT5 imagery, Landsat imagery, Lidar data and aerial orthophotos and are irregularly updated. The purpose is to increase safety for those who have experience and are planning on traversing the glaciers, but users are warned that crevasses can appear with limited warning signs. In Svalbard and mainland Norway no coordinated map service of glacier crevasses exists so far.

Glacier surging is a phenomenon whereby glaciers suddenly increase in speed by at least one order of magnitude compared to their normal background speed, and in doing so transfers accumulated mass from the upper regions of the glacier downstream (Copland et al., 2003). Surge type glaciers occur in distinct pockets around the world, and it is thought that surge-type glaciers make up a high percentage of all the glaciers found on Svalbard (Jiskoot et. al. 2000, Copeland et. al. 2003). Surge-type glaciers are not found in mainland Norway. Surging takes place in a periodic cycle defined by two distinct phases; the dormant, stagnant retreating, phase, known as the quiescent phase, and the active, fast flowing and advancing phase, known as the surge. The quiescent phase can last from decades to centuries, and the active surge phase from a few months to a few years. Surging glaciers create a hazardous environment for people trying to navigate over them or in the area in the front of their terminus. This is due to the sudden and rapid opening of crevasses on the entire glacier surface as a result of the high tensile stresses, and advancement of surging glacier termini into the fjord. Increases in calving can lead to additional and more distal hazards that further hinder marine transport in the fjord region. With increasing numbers of tourists visiting Svalbard and making trips on land and by boat, there is an increased need to provide up to date monitoring of these dynamic surging catchments. This will allow the authorities to make informed decisions about safe travel routes over Svalbard and around the coast.

In the following we investigate how suitable Sentinel-2 data with 10 m resolution are for detecting crevasses in mainland Norway and Svalbard and how surging glaciers can be detected using Sentinel-data for Svalbard glaciers.

3.4.2 Mainland Norway

In mainland Norway, ski and hiking trails crossing the ice caps are open to the public and can attract tourists of varying level of experience in skiing or hiking on the glacier. Several outlet glaciers are used for glacier courses and commercial guided tours for tourists. Glacier termini relatively close to public roads are also frequently visited. Ski tours crossing the ice caps are popular. Whereas the ice cap Hardangerjøkulen has marked routes by the Norwegian Tourist Association for skiers in spring, others ice caps have no marked routes. Snow conditions and crevasse can also vary from year to year. NVE sometimes sends out press releases to the public when there is less snow than usual on the glaciers.

Crevasse mapping

To assess suitability of Sentinel-2 for crevasse mapping, we visually compared the terminal section of Nigardsbreen (Fig. 3-28) using both the orthophoto of a 0.25m ground resolution and Sentinel-2 image of a 10m ground resolution. A four-day difference between the acquisitions largely minimizes changes in the crevassing pattern. Within the area spanning ca. 200m from the terminus, only one crevasse (N1) was visually identified in the Sentinel-2 image from 22 August 2017. At least 80 crevasses of varying size were identified on the orthophoto from 26 August 2017. Alongside the crevasses, moulins or holes in the ground ice were also detected in the orthophoto. Crevasses identified in the orthophoto ranged in length from ca. 3m to 55m and in width up to ca. 4m. The crevasses were not likely long or wide enough to be visible in the Sentinel 2 image.

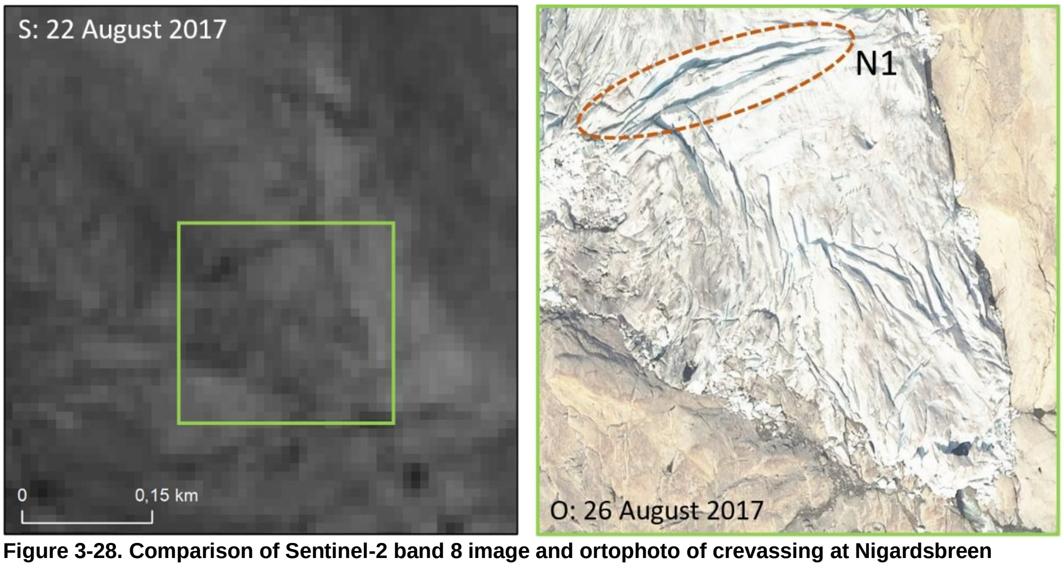

Figure 3-28. Comparison of Sentinel-2 band 8 image and ortophoto of crevassing at Nigardsbreen terminus using imagery acquired from August 2017. /Copernicus Sentinel data/norgeibilder.no/

At the terminus of Tunsbergdalsbreen (Fig. 3-29), five crevasses were identified in the Sentinel-2 image from 22 August 2017. They are seen in the orthophoto as crevasses T1-T5 and are up to ca. 8-12m wide at the surface, about the same order as dimension of a single pixel (10m) of S2 band 8. More than 20 other crevasses are visible on the orthophoto. Only the widest crevasses inducing shadowing and thus lowering the digital number could be distinguished visually. Narrower crevasses do not introduce enough to be distinguishable on the Sentinel-2 image.

To illustrate detectability of crevasses over the ice cap plateaus, the narrowest section Jostedalsbreen and the route used for crossing Jostedalsbreen on skis in spring (called ‘Josten på langs’) was looked at in detail (Fig. 3-30). At its narrowest, Jostedalsbreen is only ca. 2 km wide. Within this area crevassing is dominant. While it is possible to observe large crevasse zones in the Sentinel-2 imagery, many of the crevasses in the northern part of the area of interest are not visually detectable. Detectability also depends on the snow conditions in a given acquisition. The orthophoto from 2017 displays less crevasses than the orthophoto from 2010. Generally, the higher up the glacier the shorter time of ice exposure and fewer imagery for crevasse detection are available. This was also seen from the feature tracking results used for the glacier velocity mapping.

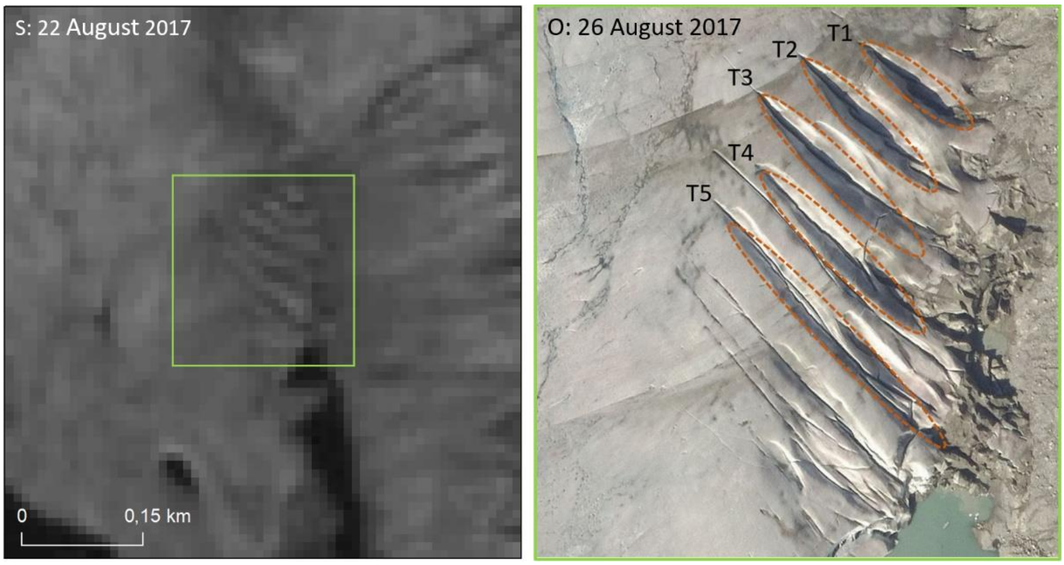

Figure 3-29. Comparison of Sentinel-2 band 8 image and ortophoto of crevassing at Tunsbergdalsbreen terminus using imagery acquired from August 2017. /Copernicus Sentinel data/norgeibilder.no/

Crevassed zones of the glaciers can also be taken from the ice velocity mapping results as most of the feature tracking features were crevasses (Fig. 3-24). Feature tracking based on other features, such as ogives used for Austerdalsbreen (Fig 3-21) or large boulders, should then be removed.

To sum up, Sentinel-2 does not have high enough resolution to be used for general crevasse mapping for glaciers in mainland Norway and we have therefore not produced any product for crevasses. The Sentinel-2 imagery can be used for identifying zones of crevassing using visual examination. Crevasse positions change over time and therefore mapping of individual crevasses only provide information for the time of mapping. Production of crevasse maps of Norway’s glaciers are possible using detailed ortophotos available at norgeibilder. This will require manual mapping that can be time consuming if individual crevasses are to be mapped. Moreover, orthophoto acquisitions are limited and not always that suitable due to fresh snow cover or much seasonal snow remaining. Other high-resolution optical imagery such as Pleiades, Planet or Spot may be suitable, but are not freely available.

A major limitation for producing crevasse maps, yielding all methods, is that the crevasse patterns change over time and may be incomplete or outdated. Thus, data should be linked with date and include warnings on the limitations.

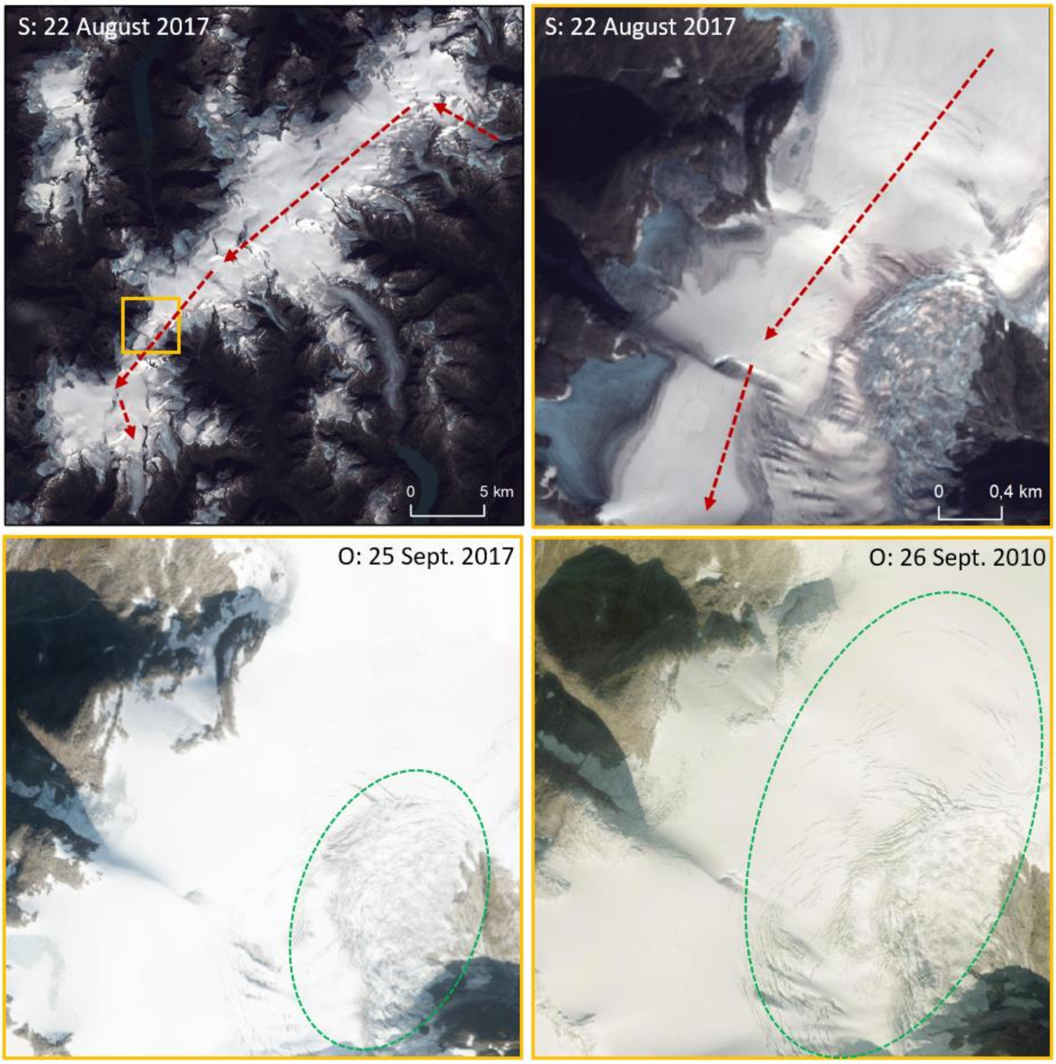

Figure 3-30. Jostedalsbreen crossing route (Josten på langs) approximated by a red arrow. The narrowest section of Jostedalsbreen in detail in a yellow frame. Visible crevassing at orthophotos in green. Orthophotos are of 0.25m (2017) and 0.5m (2010) resolution. Sentinel-2 image is a natural colour image from 22 August 2017. /Copernicus Sentinel data/norgeibilder.no/

3.4.3 Svalbard

Crevasse fields are clearly visible in many Setinel-2 images on Svalbard although individual crevasses often appear blurry, which can be improved by artificial intelligence (Fig. 3-31). Mapping out major crevasse zones is relatively straight forward to do, but detecting narrow or snow-covered crevasses higher up on a glacier is more challenging and, in many cases, not possible. More complete crevasse mapping for field-safety should therefore rather be done with ultrafine radar data such as Radarsat-2 where crevasse structures can be seen through the snow.

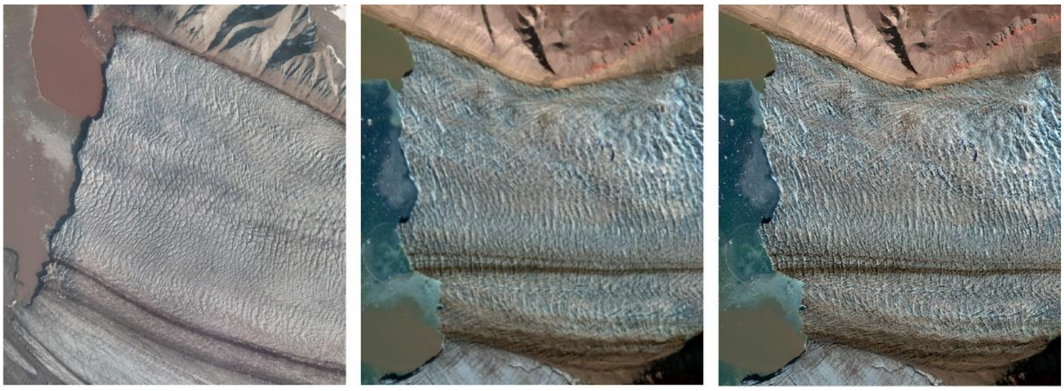

Figure 3-31. Example of crevasse field near the front of Kronebreen in Kongsfjorden for a sub-meter resolution orthophoto from 2009 (left), a Sentinel-2 image from 31 July 2020 (middle), and the same image enhanced by artificial intelligence using the web service of letsenhance.io (right). /Copernicus Sentinel data/

The mass balance year of 2020 was characterized by little winter snow in combination with an unusually warm summer over much of Svalbard. This caused a record-negative mass balance for the field-monitored glaciers near Ny-Ålesund, and much of the summer snow of Svalbard glaciers melted away and revealed hidden or unknown crevasses in several areas (Fig. 3-32). Most of these crevasses have likely been there for a long time, but have been invisible at the surface due to thick layers of snow and firn. To facilitate inspection of these images for a broader public, NPI has made an optimized Sentinel-2 mosaic of the summer 2020 imagery that is posted on toposvalbard.npolar.no as well as being available as a web-map-service (WMS).

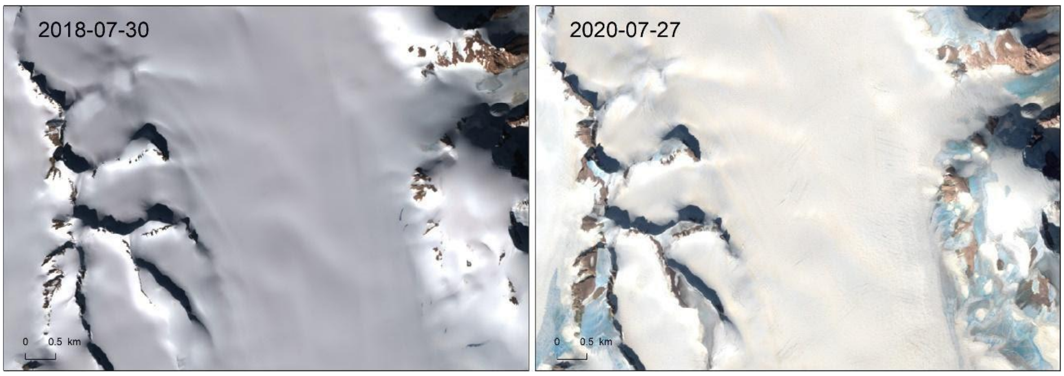

Figure 3-32. Two Sentinel-2 images from the same time of year in 2018 and 2020, covering the upper accumulation area of Holtedahlfonna at around 900 m elevation. A number of crevasses can be seen in the image from 2020 whereas it is difficult to see any of them in the image from 2018 when there was more snow/firn on the glacier. /Copernicus Sentinel data/

Crevasses can be detected automatically on Sentinel-2/Landsat 8 type images using Radon transform - a rotational filter detecting direction and strength of largest direction-dependent variation of greyscale at a given image point (Bas Altena, UiO; Gong et al., 2018). Figure 3-33 shows an example of such Radon transform for a Landsat scene over the surging Basin 3, Austfonna, Svalbard.

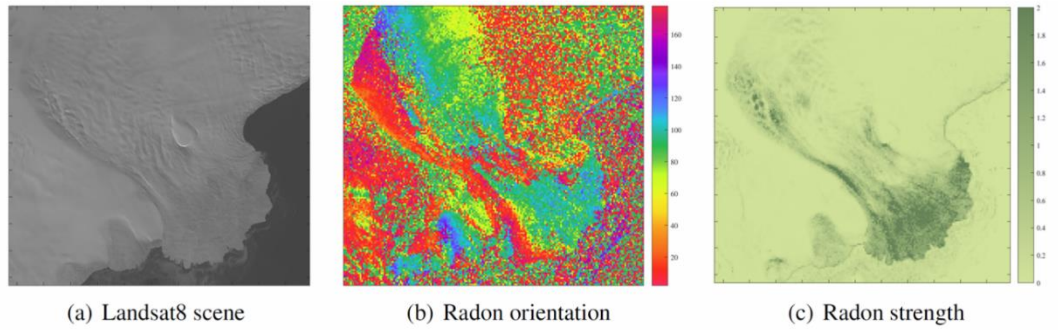

Figure 3-33. Austfonna Basin 3, Svalbard. Crevasse fields display particularly dominant directional greyscale variations. (Figure: Bas Altena, UiO; see Gong et al. 2018).

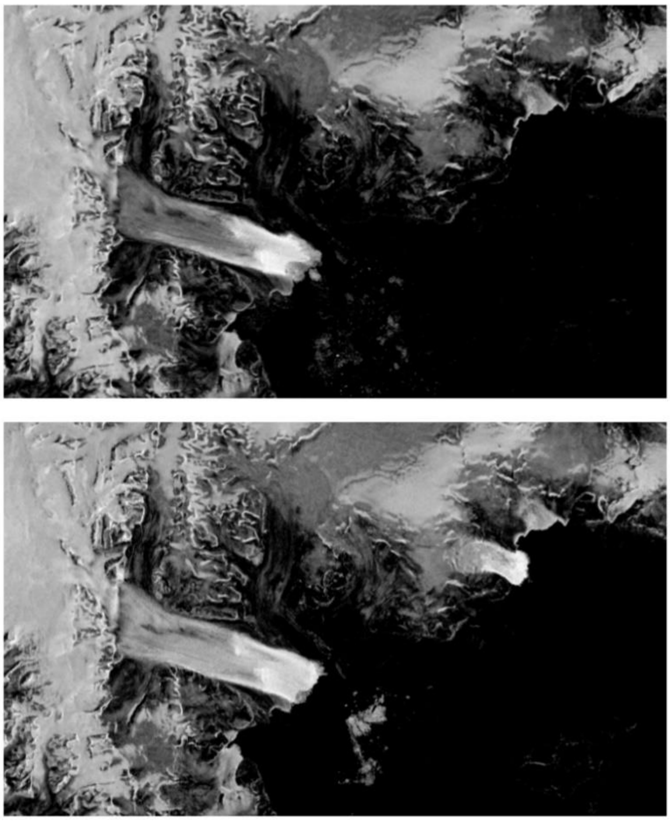

Figure 3-34. Sentinel-1 VH backscatter images over Negribreen (bright area to the middle left) and Sonklarbreen (upper right), Svalbard. Upper image: 2018-03-23, lower image 2020-03-18. While strong crevassing by the ongoing Negribreen surge (Haga et al., 2020) is visible by strong backscatter in both winters, a starting surge of Sonklarbreen causes strong backscatter only in the 2020 data.

Also radar images can be useful for detecting crevasse fields and their changes over time. Crevasse fields lead to increased radar backscatter and thus brighter areas in radar amplitude images. Such high-backscatter areas can thus point to highly crevassed areas. Changes over time of crevasse-induced strong backscatter areas indicate then changes in crevassing, on Svalbard mostly due to glacier surging. Increasing surge activity leads to increasing backscatter brightness and decreasing surge activity to decreasing backscatter

(Fig. 3-34). This correlation can be used to detect changes in surge activity over time (Fig 3-35).

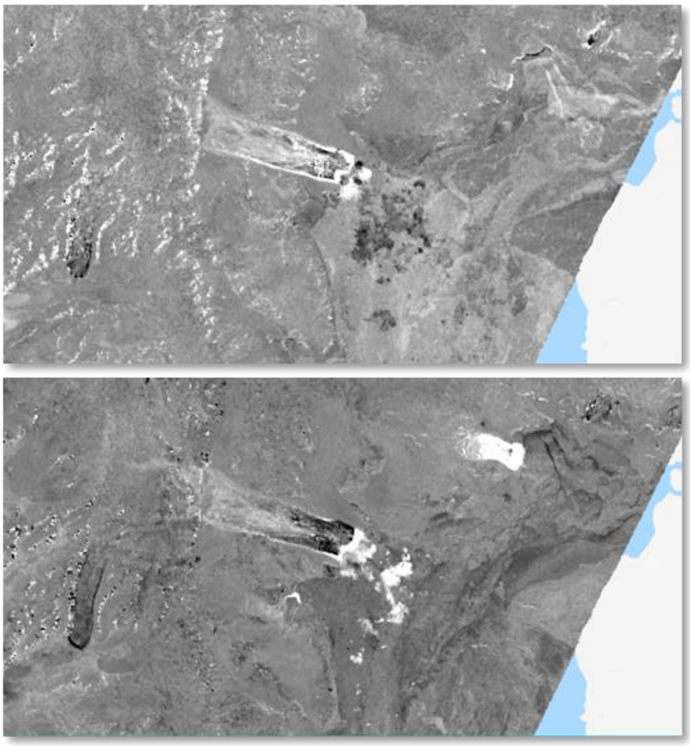

Figure 3-35. Differences between radar backscatter images between 2018-2019 (upper panel) and 2019-2020 (lower panel), Svalbard east coast (slightly large section than on previous Figure). Grey indicates no changes, black decreasing crevassing, and white increasing crevassing. Changes are well visible over Tunabreen (left), Negribreen (middle), and Sonklarbreen (upper right). (A. Kääb, P. Leclercq, unpublished work).

Finally, a brief test on surge mapping

Based on observed changes in ice velocity, surface elevation, crevassing and front position, a surge registry has been compiled at NPI. There are currently close to 40 glacier basins that are in a surging phase and another dozen that shows signs of activation (Fig. 3-36). This appears to be more than before, but it is difficult to conclude on this because our observational capability is so much better now with Sentinel-1/2 than it was just a decade ago.

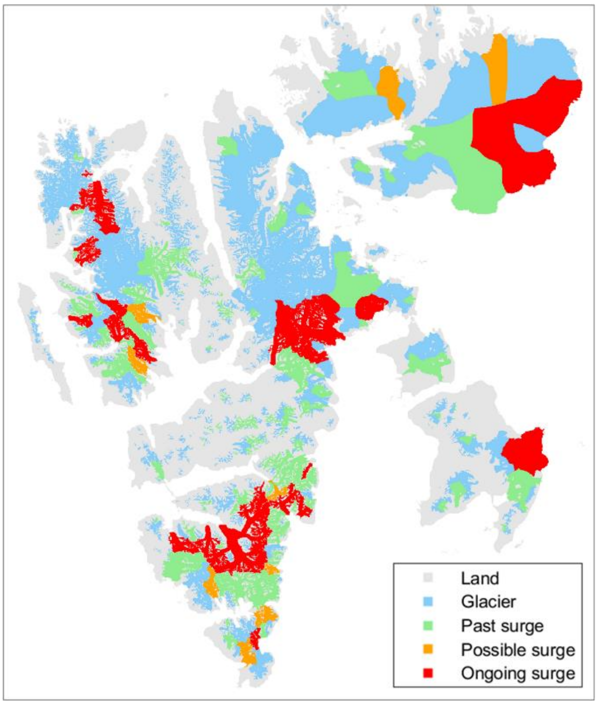

It is likely that many smaller surges were not detected in earlier decades. The influence of climate change on glacier surging on Svalbard is therefore still debated and a focus for ongoing research.

Figure 3-36. Overview of glacier basins with past surge, ongoing surge and possible surge (signs of activation). Surges have been detected through velocity changes, thickness changes, crevassing or frontal advances.

3.5 Glacier lakes

3.5.1 Background

A jøkulhlaup or Glacier Lake Outburst Flood (GLOF) is a sudden release of water from a glacier. GLOFs are the major hazard directly related to glacier lakes and can often lead to both personal and material losses. The water source can be a glacier-dammed lake, a pro-glacial moraine-dammed lake or water stored within, under or on the glacier. With continuing glacier shrinking, existing lakes can change, and new lakes can develop or disappear. Glacier lakes are sensitive to climate change and their mapping and monitoring improves our understanding of regional climate change and glacier-related hazards (Li and Sheng, 2012). Mapping of glacier lakes with optical satellite sensors has become common and has been applied to detect both proglacial and supraglacial lakes (Nie et al., 2017; Watson et al., 2018; Williamson et al., 2018). Mapping of changes in lake surface area has been done on seasonal (Watson et al., 2018) and near-daily scale (Cooley et al., 2019).

3.5.2 Mainland Norway

Glacier lakes in mainland Norway have long posed a threat due to frequent outburst floods, which were fatal in the past, resulted into material losses and new investigations (Liestøl, 1956; Jackson and Ragulina, 2014; Engeset et al., 2005; Kjøllmoen, 2018). Each year GLOF events are reported in NVEs annual glacier report (e.g. Kjøllmoen et al., 2020). Some of the sites with recent GLOFs are Nupsfonne (NUP), Demmevatnet (HAJ), Harbardsbreen (HAB) and Koppangsbreen (LYN) (See Figure 1-1 for locations). NVE's website http://glacier.nve.no/glacier/viewer/GLOF/en/ show all GLOF events registered in NVE's database. They can also be viewed in Xgeo and NVEs digital glacier inventory (see chap 4.1 and 4.2)

Two previous glacier lake outline inventories were conducted by NVE using Landsat 5 and Landsat 7 imagery from 1988-1997 and 1999-2006 respectively in the CryoClim project (Winsvold and Andreassen, 2012). In this project we created three new inventories from Landsat and Sentinel data from 2014, 2018 and 2019. The work on deriving glacier lake outlines from Seninel-2 imagery from 2018 is described in detail in a separate report (Nagy and Andreassen, 2019b).

Availability of images

Analysing the Sentinel-2 images revealed how snow and ice conditions can vary. For Jostefonni the lakes and lake perimeters had much remaining snow and ice in August 2015, while the lakes were completely snow and ice free in July 2019 (as early as 16 July 2019) (Fig. 3-37). The summer of 2019 was particularly warm in Norway, whereas the summer of 2015 was cold with a late onset of summer melting. The terrain induced shadowing is at its minimum during the summer solstice (~21/06) due to a high sun angle. The further the temporal distance from the summer solstice, the lower the sun angle, and the more widespread the shadowing becomes (Fig. 3-38). This is often problematic for glacier lakes lying north of a mountain ridge or in areas of prominent topography.

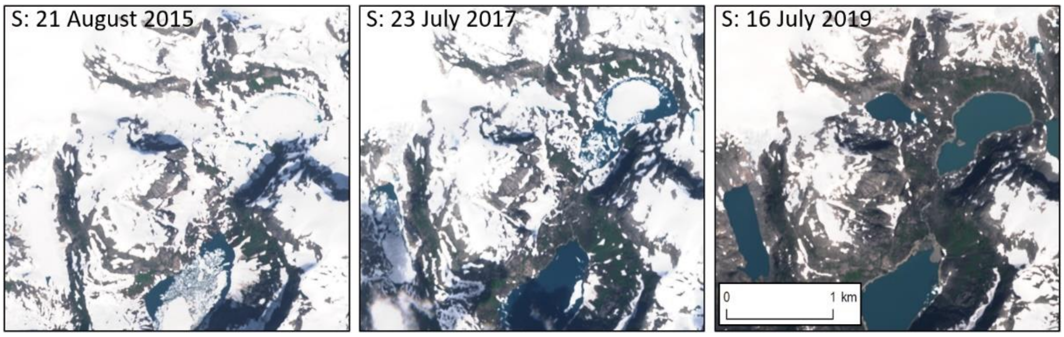

Figure 3-37. Sentinel-2 natural colour imagery of varying lake surface conditions in August 2015, July 2017 and July 2019 south of Jostefonni glacier. /Copernicus Sentinel data/

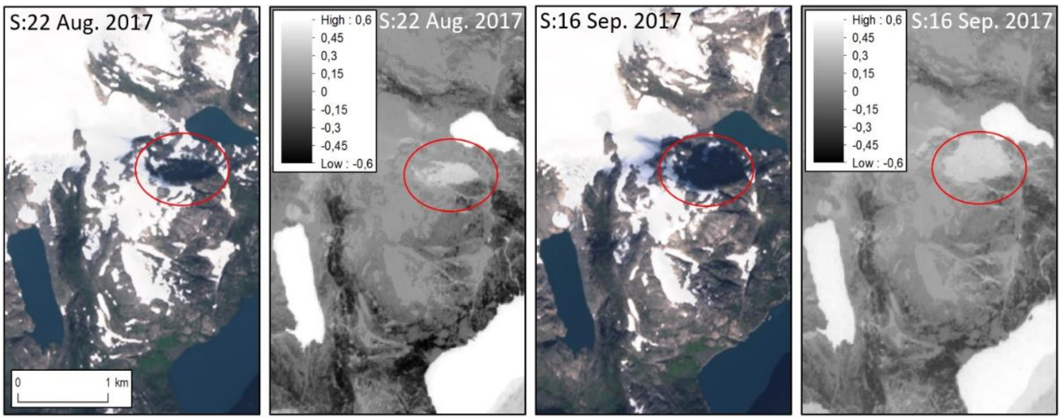

Figure 3-38. Sentinel-2 natural colour imagery and corresponding NDWI maps illustrating increased spatial extent of terrain induced shadowing in red over 25 days south of Jostefonni glacier. High-end positive NDWI values indicate presence of water. Shadowing over stable terrain manifests in increased NDWI values over non-water covered areas.

To assess the availability of useful imagery for a selection of lakes of interest, all imagery from the melting seasons 2015, 2016, 2017 and 2018 was considered. A subset of seven lakes in a N-S transect with a history of emptying events in the 21st century was selected: Sauanutvatnet, Nedre Demmevatnet, Marabreen lake, Tystigbreen lakes in southern Norway and Heiavatnet, Øvre Messingmalvatn and the Koppangsbreen lake in northern Norway. More imagery was available for the three lake sites in northern Norway due to denser Sentinel-2 observations in this part. Lake snow, ice cover and cloud cover limited the number of useful images for glacial lake monitoring. More imagery was available from 2017 and 2018 (282 images) than 2015 and 2016 (93 images). This is due to: a) doubled coverage of years 2017 and 2018 by Sentinel-2B satellite; b) Sentinel-2A sensor malfunction and irregular observations in 2015; c) difficult snow cover conditions in years 2015 and 2016. For the 4-month period 29 May – 28 September 2018 a total of 20 images could be used to detect the lake outline of Nedre Demmevatnet partly or fully. The remaining 30 images were not useful due to cloud conditions.

Glacier lake outline mapping

Ideally, for lake outline mapping, the glacier lake surface should be observed at its areal maximum, with no surface snow and ice cover. The lake perimeter should be snow free to avoid misrepresentation of the snow-covered perimeter for water or vice versa. Cloud cover as well as cloud and terrain induced shadowing should be minimal. All images used for the GLO products were visually inspected prior to selection.

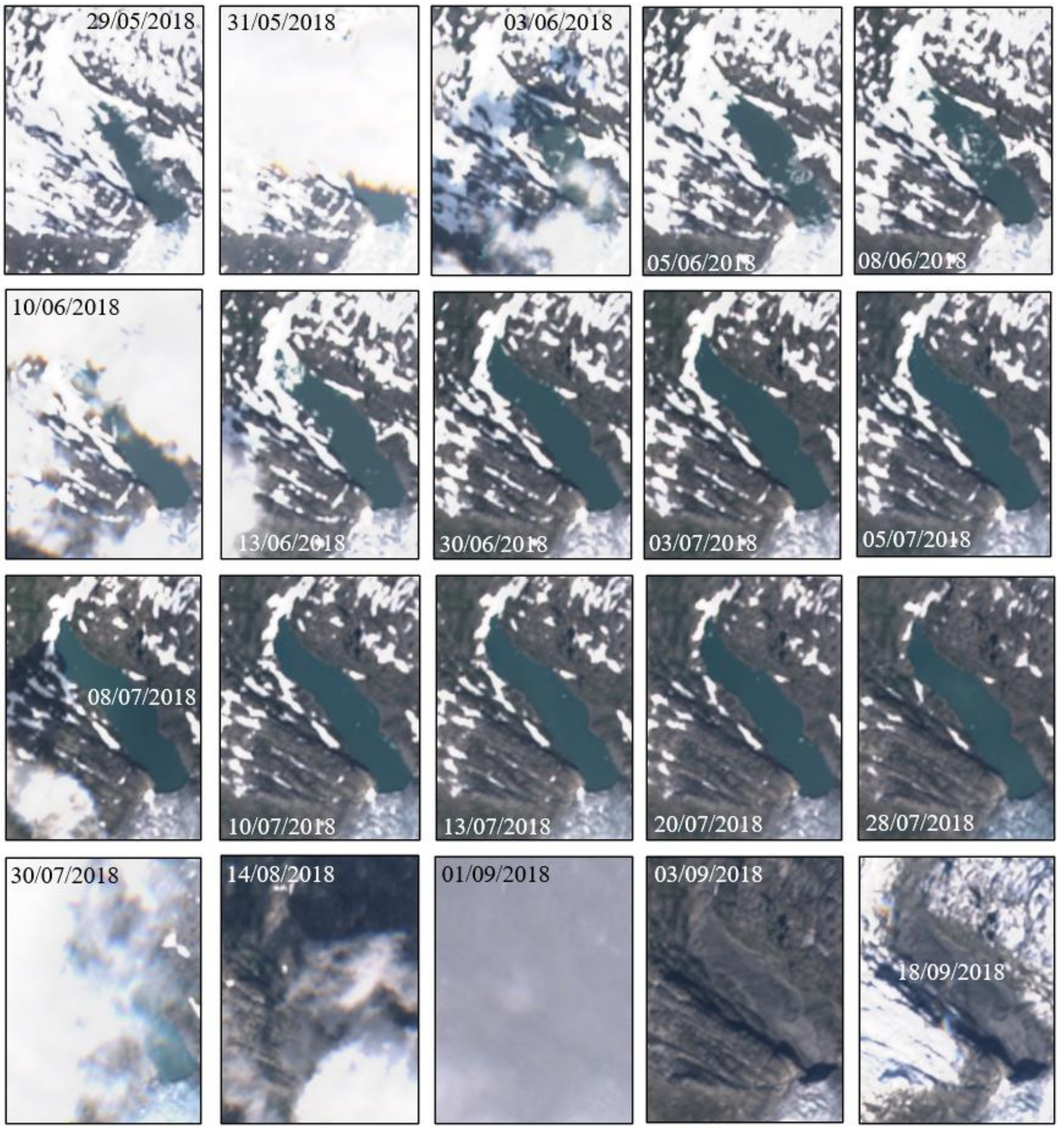

Figure 3-39. Natural colour Sentinel-2 imagery of Nedre Demmevatnet, glacier dammed lake with a history of jøkulhlaup events, from the period 29 May 2018 – 28 September 2018. Only images that were considered useful for lake outline mapping are shown. Dimensions of each of the frames are ca. 0.7 x 1.2 km. /Copernicus Sentinel data/

GLO 2014

The Landsat-8 image acquisitions used for GLO 2014 were from 9 August - 24 September 2014 and had favourable lake outline mapping conditions due to a warm summer and early onset of snow and ice melting. Manual digitisation was used to map the lake outlines. Here previous glacier lake outlines from 1999-2006 were used as basis for the mapping. Glacier lake outlines were identified as water bodies that either intersected, were within <50 m, or completely within the glacier area outline of 1999-2006 (GI_{2000}).

GLO 2018

The image acquisitions used for the GLO 2018 inventory were from the period 3 July 2018 - 8 September 2018. In total, ca. 11 % of the lakes were mapped using non-DTERRENG orthorectified imagery due to unavailability of DTERRENG orthorectified scenes. For the GLO2018 product we used a semi-automatic approach calculating the

Normalized Difference Water Index (NDWI) and applying a threshold. The NDWI maximizes the water body reflectance in the green band and minimizes its reflectance in the NIR band and is calculated as:

$$NDWI = \frac{Green - NIR}{Green + NIR} \qquad \text{(McFeeters,1996)}$$

The NDWI is commonly used for mapping lakes and were also used for the previous GLO 1999-2006 product. Sentinel-2, however, provides improved details of glacier lake outlines with its 10 m resolution of the green and NIR bands compared to Landsat 8 bands at 30m ground resolution (see Table 2-2 and Figure 2-3 for band wavelengths). Effectively, this results in a nine times sharper imagery of Sentinel-2 compared to Landsat 8 enabling to capture more details.

A threshold is needed to separate the NDWI map pixels into the water and non-water pixel (Miles et al., 2017; Watson et al., 2018; Williamson et al., 2018). The threshold value must be high enough to differentiate between ice and water, but also low enough to minimize the omission of the water pixels. To find the suitable threshold value for the glacier lake outline delineation and to assess the uncertainty of the glacier lake outline product, we used high resolution orthophotos from norgeibilder.no with almost perfect temporal overlap with Sentinel-2 imagery. Analysis of a subset of nine lakes was used to find and select a threshold of 0.23, which was then used for the further mapping as it was found to be the best compromise that would minimize the need for the lake outline digitization and also maximize the inclusion of the 'true' water pixels. Based on our findings, we estimated an uncertainty in glacier lake area of ±4% for the GLO2018 product.

In the GLO 2018 inventory, we included all lakes larger than 0.001km^2 (1000m^2) that were within ca. 100 m of the glacier perimeter, by the glacier units at least 0.25 km^2 in size. All lakes were visually inspected and categorized based on glacier-lake contact and nature of damming. Out of 414 lakes, 327 lakes (ca. 79%) were found to have an interface with the glacier ice, of which 39 lakes were found to be glacier dammed and two lakes were moraine dammed. Analysing the Sentinel-2 satellite imagery for the period 2015-2019 and available high-resolution orthophotos also revealed emptying events, which have not been recorded in the NVE database. See further details in Nagy and Andreassen (2019b).

GLO 2018-2019

An updated glacier lake product for 2018-2019 was produced to match the new 2018-2019 glacier outlines described in chap. 3.1 and to include lakes below the 0.25 km^2 threshold for glacier size that was set for the GLO 2018 product. We decided to set a lower threshold for the 2018-2019 product of 0.05 km^2 to include more glacier lakes, and we only included lake that appeared to be in contact with the glaciers. The images used for GLO 2019 were the same as used for the glacier outlines and was mainly from 27 August, but imagery from 4 August and 15 August were also used. The methods used for the glacier lake products varied.

The mapping was done a bit differently than for the NDWI derived GLO 2018 product since the semi-automatic method used for glacier outline mapping often requires manual edits to detach glacier lakes connected to the glacier outlines. The following approach was used: The glacier outline-lake interface was manually digitized as a line based on the Sentinel-2 imagery used for the glacier outline mapping. Each digitized lake interface line was given an edit code for a glacier lake, and the glacier lake was detached from the glacier by splitting the mapped polygon with the digitized line (Fig. 3-40). This often resulted in a polygon partly covering the glacier lake. For some of the smaller glacier lakes the outline was automatically mapped and was used as is after splitting, for other lakes parts of the lakes were manually digitized. To map the full glacier lake extent, the automatic mapped glacier lake was merged with the GLO2018 product or lakes from the topographic map series 1: 50 000 of Norway where available or the remaining outline just digitised manually on screen. Orthophotos from norgeibilder.no or other Sentinel-2 images were used to verify glacier lakes where newer images were available, but not all lakes were possible to verify due to snow conditions or lack of recent imagery. Supraglacial lakes were also manually digitized and assigned an edit code for easy extraction. Larger lakes were often easy to detect, but smaller newly formed lakes were more difficult to identify and were more uncertain. The lakes look dark compared to snow and ice in false colour composites (Fig. 3-38), but for very small glacier lakes it might be difficult to differentiate them from debris, part in shadow parts or braided rivers.

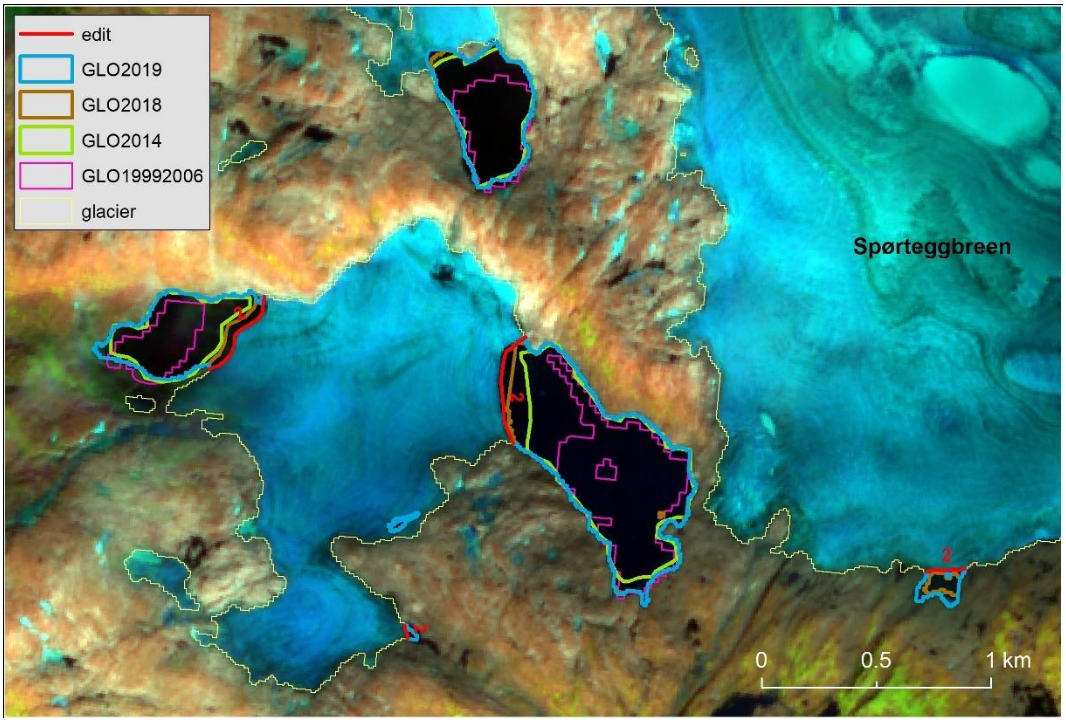

Figure 3-40. The glacier lake product (GLO) for 2018-2019 was derived from the glacier outline mapping using a Sentinel-2 image of 27 August 2019. Line edits (in red) were used to detach glacier lakes (blue)from the glacier outlines (yellow). The section shows part of south-eastern Spørteggbreen to the right and a former part of Spørteggbreen to the left. The outlines for previous GLO products are also shown clearly revealing growth of the glacier lakes. The lakes appear black in contrast to glaciers in blue in this false 11-8-4 RGB. See Table 2-1 and Figure 2-2 for wavelength of bands. The three larges lakes were mapped in all GLOs displayed, the smallest lake is only included in GLO2019, the second smallest lake are included in GLO 2018 and GLO2019. /Copernicus Sentinel data/

3.5.2 Svalbard

There are numerous lakes that lie in glaciated catchments on Svalbard. Many of the lakes form as supraglacial lakes on the surface of glaciers, others form in the confluence of glaciers (such as Setevatnet, Fig. 3-41) or downstream of rock outcrops. These lakes are in one capacity or another either entirely or partially dammed by ice. Many of these lakes drain seasonally, once a threshold is breached and the ice dam fails. This breach can be due to the seasonal filling of lakes throughout the melt season and the formation of a drainage pathway through a series of newly formed channels. These channels then entirely close up from one year to the next allowing the lake to refill. In other cases, the lakes may persist for many years without breaching any drainage threshold. This is not to say that these lakes do not have the ability to drain in the future should the conditions of their ice dam change. This could for example, include the thinning of the ice dam over time, thereby reducing the threshold for drainage to be initiated. Whilst the lakes found on Svalbard pose little threat to the limited infrastructure and inhabitants on Svalbard, they might be important for local ecosystems or pose a threat during GLOFs.

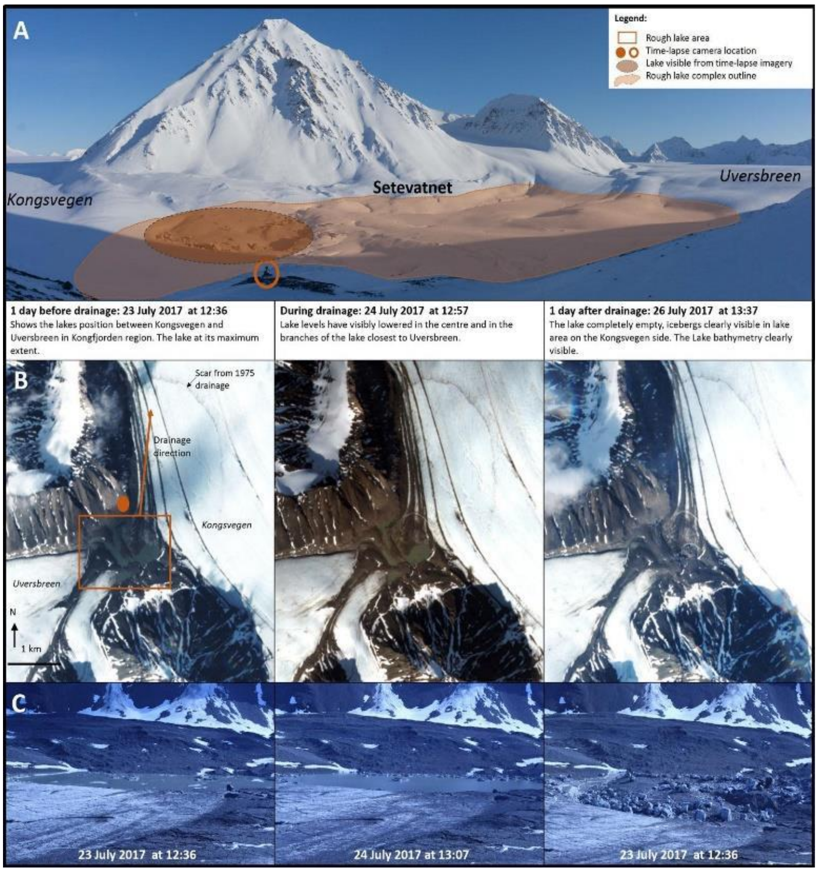

Figure 3-41. Time-series of Setevatnet GLOF in July 2017, as seen from Sentinel-2 RGB image and the time-lapse camera at Jensebu. Panel A shows an overview of the Setevatnet site as seen from Jensebu, with key outlines annotated. B shows the time series of Sentinel-2 imagery from the time-period around the drainage. C shows the closest time lapse imagery that corresponds to the Sentinel-2 imagery. /Copernicus Sentinel data/

Setevatnet (Fig. 3-41) in the Kongsfjorden region is an excellent site to test the potential of Sentinel-2 imagery for glacier lake monitoring. Setevatnet is an ice dammed lake situated between the glaciers Kongsvegen and Uversbreen and has an estimated area of ~1.5 km^2 although the exact lake extent is unknown as much of the lake is subglacial. The lake was first mapped by an expedition in 1909 (Liestøl, 1975). In 1975 when a group of scientists visited the location, they found evidence of a recent catastrophic GLOF that had left large visible features on the glacier surface downstream. The water had been forced under pressure up to the glacier surface, where it burst through, leaving a displaced crack up to 10 m high (Liestøl, 1975). The scar from this event is still visible in satellite imagery today as a black band across Kongsvegen (Fig. 3-41). Since then, researchers from NPI, who visit Kongsvegen biannually to undertake mass balance measurements, have observed the lake to be filling and draining. In 2017, a time-lapse camera was installed at Jensebu overlooking a large section of Setevatnet.

Observations from the camera show that the lake appears to fill and drain multiple times during the summer melt season. In recent years the initial and largest GLOF has occurred in mid-July. The time-lapse camera data allows for validation of Sentinel-2 imagery, and in addition enables us to pinpoint the onset of drainage with much higher temporal accuracy than solely relying on satellite imagery. In addition to refining the drainage duration to within an hour, numerous other phenomena have been observed within the camera imagery. These include unique lake filling characteristics such as the time period to fill the lake, the duration the lake remains filled, as well as observation of grounded ice being lifted to full floatation during the filling process.

Table 3-1. Overview of drainage dates for Setevatnet glacier lake as observed by Landsat-8 and Sentinel-2.

Year	Drainage Date	Sensor
2018	13/07	Landsat 8
2017	23/07 @~23:00	Sentinel-2 and camera
2016	11/07	Landsat 8
2015	Between 12/07-01/08	Landsat 8

During 2015-2018, it was possible to detect lake drainage from Landsat-8 or Sentinel-2 imagery each year although clouds prevented a precise dating in 2015 (Table 3-1). Coarse estimation of glacier lake volume was also possible by combining an ArcticDEM strip from when the lake was empty with the lake extent mapped from Landsat-8/Sentinel-2. Other glacier lakes on Svalbard can probably be monitored in the same way and following the semi-automatic glacier outline mapping with summer 2020 imagery (see Section 3.1), we are also outlining adjacent glacier lakes with goal of a complete inventory similar to mainland Norway. This will include a growing number of lakes formed behind terminal moraines when glaciers retreat and occasional lakes that have been dammed by glacier surge advances (Fig. 3-42).

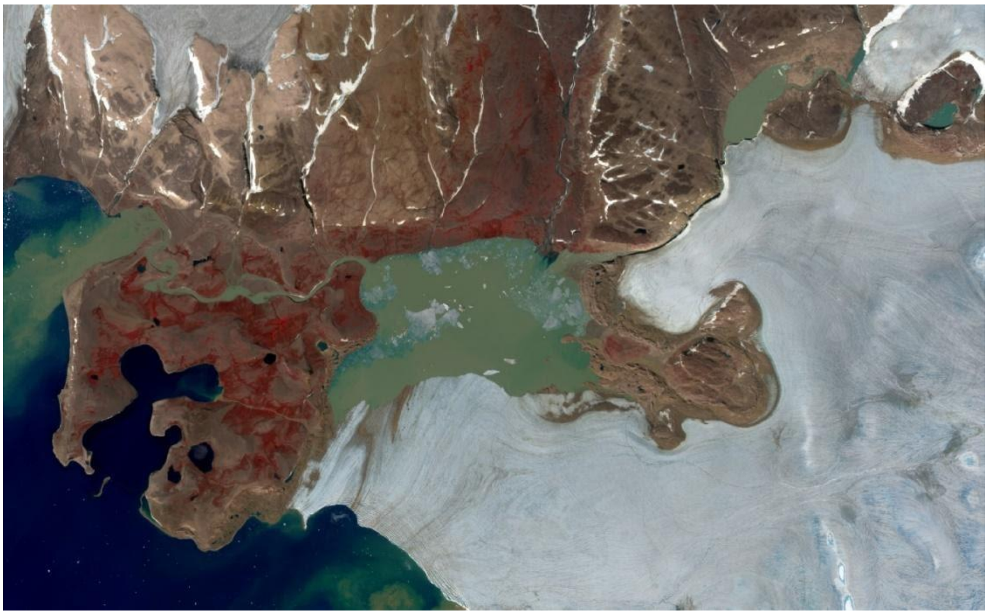

Figure 3-42. Two of the largest glacier lakes on Svalbard; Brånevatnet (left) and Flysjøen (right) at the marging of Austfonna ice cap on Nordaustlandet. Brånevatnet was likely formed when the basin Etonbreen surged around 1938 and might become a part of Wahlenbergfjorden in the future when the glacier further retreats. The image is from Sentinel-2 (False 8-4-3) on 31 July 2020. /Copernicus Sentinel data/

4 Data visualization and download

The glacier products produced in this project are made available from NPI and NVE websites (as Web Map Service's and download). Glacier outline data for mainland Norway and Svalbard will also be submitted to the GLIMS database (Global Land Ice Measurements from Space: www.glims.org). Links to data download and NVE and NPI web map services are available at the project websites:

- https://www.nve.no/hydrologi/bre/copernicus-bretjeneste/ (Norwegian)
- https://www.nve.no/hydrology/glaciers/copernicus-glacier-service/ (English)

In the following we give a short description of the services (as per February 2021).

4.1 Xgeo

Xgeo is an expert tool used for preparedness, monitoring and forecasting of floods, landslides and avalanches with maps and time base compiled data from stations and models with events and field observations. In a special edition it is now possible to also view Sentinel satellite imagery together with selected glacier data. Xgeo.no is available in both Norwegian and English versions. Sentinel-2 imagery over Svalbard was available in Xgeo from October 2019. https://xgeo.no

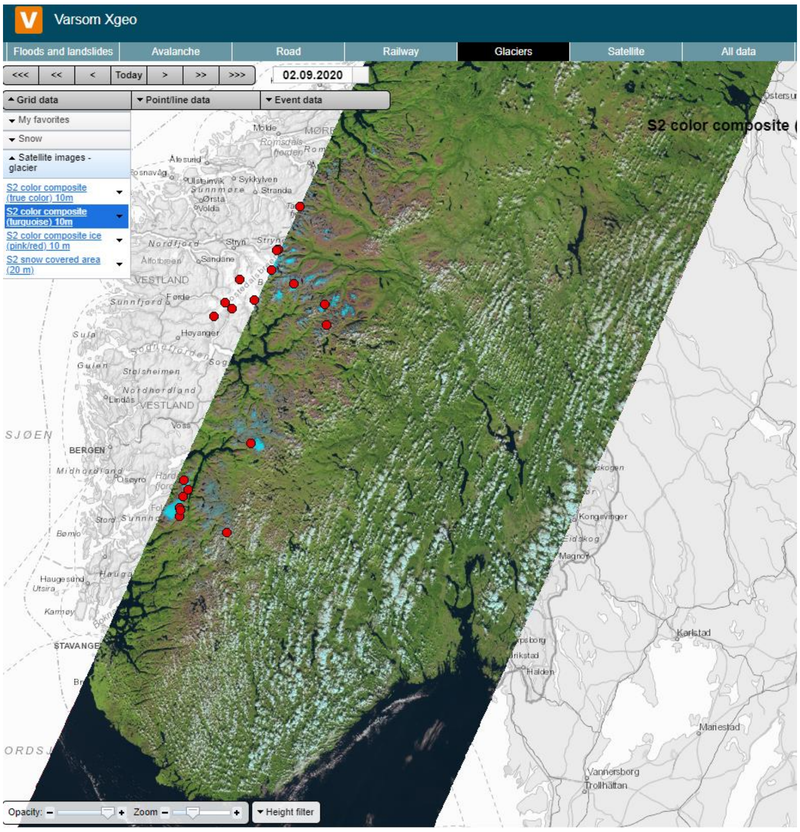

Figure 4-1. Screeenshot of xgeo displaying the S2 imagery available in southern Norway on 2 September 2020. Here we added registered sites of GLOF (Glacier Lake Outburst Flood) from the supporting map menu (not shown). The user can browse through the imagery using arrow buttons.

4.2 NVE’s digital glacier inventory

NVE’s digital glacier inventory (NVEs Breatlas) displays glacier extents together with several other glacier data. NVE’s GIS data model was updated as part of this project to allow for new data types and timeseries of glacier products. The map interface is so far only available in Norwegian. Some of the data product that have been made are already available at the map service, others will be available later in 2021.

Link: https://temakart.nve.no/tema/breatlas

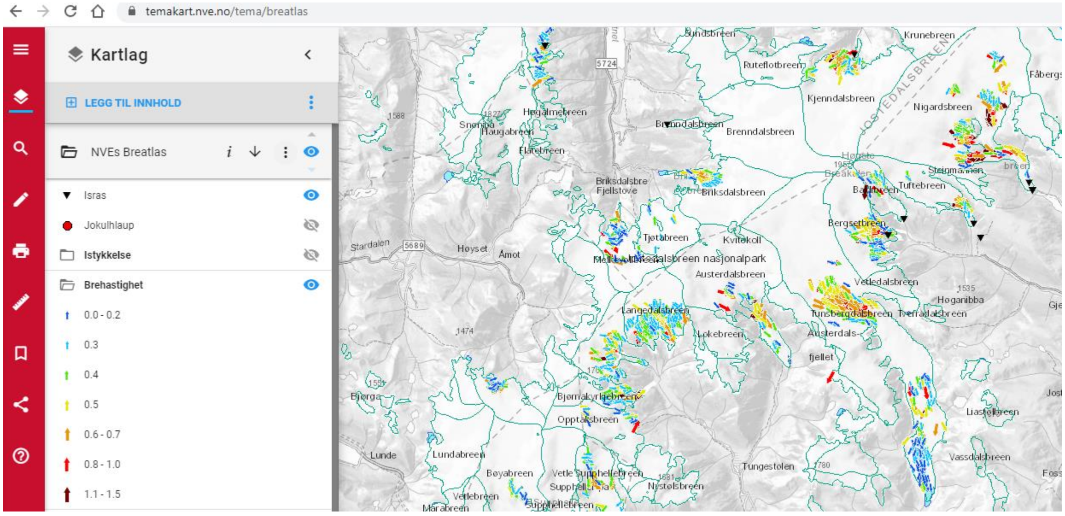

Figure 4-2. Screenshot NVE’s digital glacier inventory (NVEs temakart bre) here displaying the velocity data that was derived from Sentinel. Here also registered icefalls (‘isras’) in NVES database are shown as black triangles.

4.3 TopoSvalbard

The map and image service toposvalbard.npolar.no shows the standard maps and orthophoto products of NPI based on aerial imagery from 2008-2012, as well as seamless Sentinel-2 image mosaics from winter 2016 and summer 2020. Updated glacier calving fronts from the most recent Sentinel-2 mapping are shown as green lines in the older maps. Users can also view sea charts/bathymetry, 3D-models and historical oblique imagery from the 1930s, as well as newer local images from various overflights and field activities. The maps, orthophotos and satellite image mosaics of TopoSvalbard are also available as WMS services, see geodata.npolar.no.

Link: https://toposvalbard.npolar.no

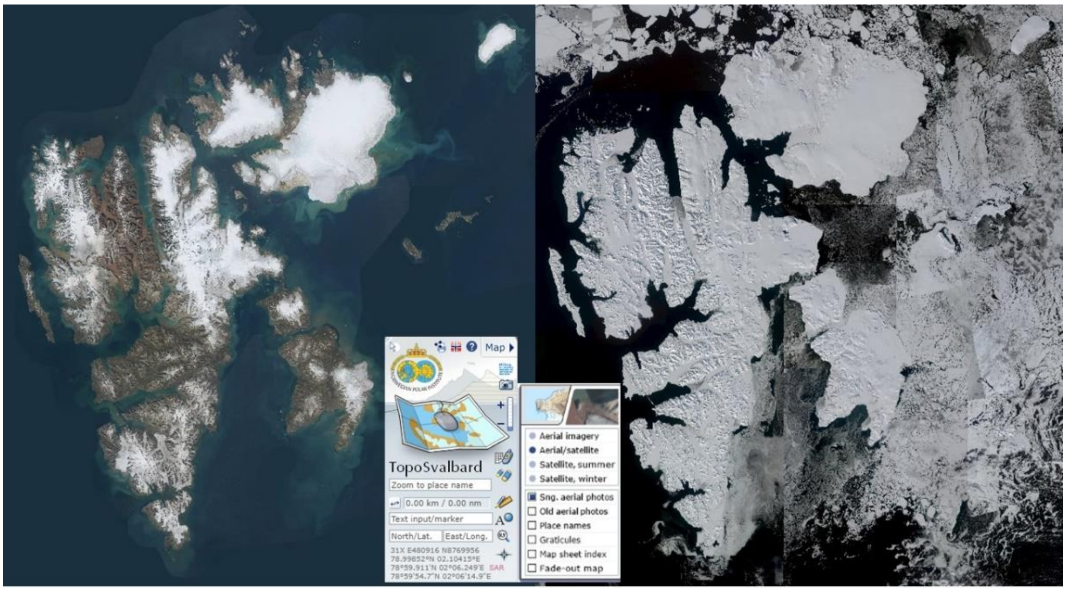

Fig. 4-3. Sentinel-2 image mosaics for summer 2020 (left) and winter 2016 (right) on toposvalbard.npolar.no.

4.4 Svalbardkartet

The map service svalbardkartet.npolar.no is a tool to visualize various thematic map layers for Svalbard together with selected background maps and aerial/satellite images as for TopoSvalbard. All glacier products can be found under the category «Sea and Ice» where the user can turn layers on/off and adjust the map layout as desired. Historical Glacier Area Outlines for 1936-1972, 1990 and 2001-2010 can be viewed, and the new glacier inventory from Sentinel-2 will be added during winter 2020. Annual calving front positions are published for the period 2012-2020 (Fig. 4.4) and will be updated annually. Derived data products of front changes, ice discharge and total frontal ablation for each calving glacier will be added when it becomes an operational monitoring time series. Glacier lake outlines from summer 2020 will be published when completed. Most thematic map layers on Svalbardkartet are also available as dynamic map services, see geodata.npolar.no.

Link: https://svalbardkartet.npolar.no

Figure 4-4. Annual glacier calving fronts for 2012-2020 as visualized on svalbardkartet.npolar.no over an area between Bjørnfjorden and Liefdefjorden, NW Spitsbergen. Background image is NPI orthophotos from 2011.

4.5 Norwegian Polar Data Centre

This is an open data portal operated by NPI for sharing environmental data, maps and publications from the polar regions. Data products for Svalbard glaciers are published in this database with a unique doi-reference that is linked to the product overview on the Copernicus Glacier Service webpage. The searchable interface makes it possible to discover other relevant datasets as well.

Link: https://data.npolar.no

5 Conclusions

In the Copernicus Glacier Service project, we have used Sentinel satellite imagery to monitor glaciers and derive glacier products for mainland Norway and Svalbard. Here we sum up the main project findings:

Sentinel-2

Sentinel-2 imagery is superior to using Landsat 8 imagery due to the higher temporal and spatial resolution. Sentinel-2 data are well suited to derive periodic glacier products and used for visual inspection of state of the glaciers and glacier lakes. Using the imagery to check the snow conditions and transient snowline elevations on the glaciers prior to fieldwork has also been helpful. The major limitation for more usage of the Sentinel-2 data is cloud cover. Both in mainland Norway and Svalbard frequent clouds reduce the useful imagery available. Although cloud-free imagery is preferable, partly cloud-cover scenes may contain much useful information. In this context, scene-averaged cloud-cover percentages might be misleading. Visual inspection of imagery is therefore needed to find the best imagery for the area of interest.

The geometric performance of Sentinel-2 was not sufficient for precise glacier applications such as velocity mapping when the previous terrain model PlanetDEM90 was used to orthorectify the imagery (used between 2015-2020). Fortunately, for many of the glacier products we received Sentinel-2 imagery orthorectified with a Norwegian terrain model processed by ESA. Copernicus/ESA have acknowledged the problem with PlanetDEM90 and have taken this into account by performing additional processing with Norwegian DEMs and by implementing a new global DEM of higher quality in future processing.

Sentinel-1

Sentinel-1 was not the primary focus of the project, but work using Sentinel.1 data proved very valuable for mapping ice velocities (only Svalbard), tracking transient snowlines, and detecting melting conditions on glaciers. Moreover, Sentinel-1 data could be used to assist glacier mapping with Sentinel-2 data. Sentinel-1 data has potential for further use in mapping crevasse fields and for detecting surging glaciers. The major advantage of Sentinel-1 data over Sentinel-2 data are the consistent time series generated due to the all-weather and day-and-night capability of radar sensors.

Glacier outline, area and calving front

We used Sentinel-2 imagery to map glacier outlines and area of mainland Norway and Svalbard using imagery from 2018-2020. Imagery in the first years of the Sentinel era (2015-2017) had too much snow to be suitable for glacier outline mapping.

It is challenging to map glacier outlines from optical imagery when a thin layer of fresh snow or much seasonal snow is present. Analyses of supporting data showed that Sentinel-1 averaged summer SAR backscatter images and Landsat-8 TIRS-derived land surface temperatures can be useful to assist the glacier mapping.

Glacier calving fronts can be efficiently mapped with Sentinel-2 although automated methods are challenged by sea ice and variable sediment content in the sea water. A reference period of one month (15 Aug. – 15 Sept) was sufficient to cover all ~200 Svalbard calving glaciers annually to derive front position changes, ice discharge and total frontal ablation for each glacier. The semi-automated method has been implemented by NPI for operational monitoring of calving fronts.

Glacier surface type and snow line

Transient snowlines and snowzones from the end of ablation season were mapped using a semi-automatic approach. Thresholds in pixel values in band 8 (NIR) of Sentinel-2 were used to differentiate between snow, firn and ice. Variability in terrain, atmospheric conditions and a range of values for snow firn and ice within single scenes necessitated the use of manual corrections. Fixed thresholding performed well over large glacier units but did not perform well over smaller valley and cirque glacier units with large variations in topography. The derivation of automatic snow lines should in all cases be carefully checked by visual inspection and manually corrected where needed.

Tests for mainland Norway and Svalbard showed that transient snowlines can also be derived from Sentinel-1A and 1B backscatter time series and be used as a data gap filler for Sentinel-2 transient snowlines. On Svalbard, use of Sentinel-1 data is the most viable way to obtain consistent time series of glacier surface type due to persistent cloud-cover in many regions during late summer.

Ice velocity

Repeated Sentinel-2 imagery was used to map glacier velocities using feature tracking. For mainland Norway, imagery over the period 2015-2018 was used. Many of the glaciers in Norway have trackable features, such as crevasses and crevasse-induced shadowing. Velocity fields are mainly obtained over glacier tongues and steep icefalls with fast flow. In total the surface velocity could be obtained from 91 out of 3143 glaciers. All glacier units in Norway were categorized into classes depending on their suitability for glacier velocity mapping using repeat Sentinel-2 imagery.

On Svalbard, glacier velocities could be derived from Sentinel-2 in most areas with faster flow. The April/May period proved to be best because of relatively clear weather and less impact from changing surface conditions which is often an issue during the summer melt season. For velocity applications year-round and in all-weather, it would be more favorable to use Sentinel-1A/B data. To test and demonstrate this, UiO has derived Svalbard-wide velocities from repeat Sentinel-1 data for the winters 2015/2016, 2017/2018, 2018/2019, and 2019/2020 using offset tracking (in principle the same method, feature tracking, as used for optical data, but with different parametrization adapted to radar data). Fast glaciers are clearly visible in the results, and comparison of the data over time allows for good detection of increasing and decreasing surges. The method proves very robust, but small glaciers are often not well resolved due to the lower resolution of radar images compared to optical images and the speckled noise of radar data.

Crevasses and surges

Sentinel-2 does not have a high enough resolution to map individual crevasses for glaciers in mainland Norway, but crevassed fields can be identified visually from the imagery or using feature tracking. On Svalbard, many new crevasse areas were discovered with Sentinel-2 in summer 2020 due to little remaining snow on the glaciers after a very warm summer. Crevasse appearances in Sentinel-2 imagery was also an efficient way to detect and confirm new glacier surges. UiO tested an automatic approach (Radon transform) to detect and map crevasse fields on Svalbard, showing promising results and a good potential for application at larger scales. Another method to detect increasing/decreasing crevassing from surge activity using stacks of Sentinel-1 backscatter data was also developed and tested. This backscatter-change method to detect surges on Svalbard agree well with the analysis of the multitemporal ice velocity maps.

Glacier lakes

Sentinel-2 imagery was shown to have a good potential for monitoring and mapping glacier lakes in mainland Norway and Svalbard. Glacier lake outlines were mapped for mainland Norway using Landsat-8 imagery for 2014 and Sentinel-2 imagery for 2018 and 2019. On Svalbard, a glacier lake inventory is being developed from summer 2020 imagery. Both manual digitization, band ratios and Normalized Difference Water Index (NDWI) maps were used to detect and map the glacier lakes. Many new glacier lakes have formed in recent years both in mainland Norway and Svalbard, and several glacier lake outburst floods were detected from repeat Sentinel-2 imagery.

Data availability & download

We have made several datasets available for download or with links to where to download from our website.

https://www.nve.no/hydrologi/bre/copernicus-bretjeneste (Norwegian)

https://www.nve.no/hydrology/glaciers/copernicus-glacier-service/ (English)

We have made Sentinel-2 imagery and selected glacier products available for viewing at xgeo.no and through NVE’s and NPI’s web map services.

6 Outlook

The work done within the Norwegian Copernicus Glacier Service (2016-2021) focused on the use of Sentinel-2 optical data, but also did some initial tests, demonstrations, and comparisons using Sentinel-1. The preliminary results using Sentinel-1 turned out promising and suggest that several important tasks of operational glacier monitoring should be based on or supported by Sentinel-1 radar data, in particular the detection and monitoring of glacier/snow facies, ice-velocity and surging. Ultimately, Sentinel-1 and Sentinel-2 complement each other very well for glacier mapping and monitoring tasks and should be used together. This large synergy potential should be investigated, developed and transferred to current and future operational activities.

Furthermore, the launch of the next Sentinel-1 and Sentinel-2 satellites (C +D) come with new possibilities and may need adaptations to processing lines.

The large amount of operational, reliably repeated and long-term data available from Sentinel-1 and Sentinel-2 is an important part of a paradigm shift in remote sensing – away from single-scene processing towards processing of massive (multisensory) image stacks. While a number of “big-data” techniques to this end are in the scientific development cycle, first techniques appear ready for operationalization, for instance stack processing for snow facies monitoring, or surge detection. Another example is repeat Sentinel-1 based ice velocity measurements over Svalbard that seem largely automatable. Operational glacier monitoring in Norway and Svalbard should actively follow the “big-data” developments and systematically test which related new methods could be useful for and implemented in operational tasks.

7 References

Altena, B. and A. Kääb. 2017. Elevation Change and Improved Velocity Retrieval Using Orthorectified Optical Satellite Data from Different Orbits. Remote Sensing, 9(3), 300. https://doi.org/10.3390/rs9030300

Andreassen, L.M., S.H. Winsvold, F. Paul and J.E. Hausberg. 2012. Inventory of Norwegian Glaciers. NVE Rapport 38, Norwegian Water Resources and Energy Directorate.

Andreassen, L.M. (red.), M. Callanan, T. Saloranta, B. Kjøllmoen og T. Nagy. 2020a. FonnSat - Fonner, arkeologi og satellittdata. NVE Rapport 41-2020, 65 s.

Andreassen, L.M., H. Elvehøy, B. Kjøllmoen, J.M.C. Belart. 2020b. Glacier change in Norway since the 1960s – an overview of mass balance, area, length and surface elevation changes. Journal of Glaciology, 1–16. https://doi.org/10.1017/jog.2020.10

Bhardwaj, A., L. Sam, S. Singh and R. Kumar. 2016. Automated detection and temporal monitoring of crevasses using remote sensing and their implications for glacier dynamics. Annals of Glaciology, 57(71), 81- 91. https://doi.org/10.3189/2016AoG71A496

Björnsson, H., Y. Gjessing, S.E Hamran, J.O Hagen., O. Liestøl, F. Palsson and B. Erlingsson. 1996. The thermal regime of sub-polar glaciers mapped by multi-frequency radio-echo sounding. Journal of Glaciology, 42, 23−32.24. https://doi.org/10.3189/S0022143000030495

Blaszczyk, M., J.A. Jania and J.O. Hagen. 2009. Tidewater glaciers of Svalbard: Recent changes and estimates of calving fluxes, Pol. Polar Res., 30, 85-142.

Cogley, J. G., Hock, R., Rasmussen, L. A., Arendt, A. A., Bauder, A., Braithwaite, R. J., Jansson, P., Kaser, G., Möller, M., Nicholson, L., and Zemp, M. 2011. Glossary of Glacier Mass Balance and Related Terms, IHP-VII Technical Documents in Hydrology No. 86, IACS Contribution No. 2, Paris, UNESCO-IHP, 114 pp.

Cooley, S.W., L.C. Smith, J.C. Ryan, L.H. Pitcher and T.M. Pavelsky. 2019. Arctic-Boreal lake dynamics revealed using CubeSat imagery. Geophysical Research Letters, 46. https://doi.org/10.1029/2018GL081584

Copland, L., M.J. Sharp and J.A. Dowdeswell. 2003. The distribution and flow characteristics of surge-type glaciers in the Canadian High Arctic. Ann. Glaciol., 36, 73–81. https://doi.org/10.3189/172756403781816301

Dehecq, A., N. Gourmelen and E. Trouve. 2015. Deriving large-scale glacier velocities from a complete satellite archive: Application to the Pamir–Karakoram–Himalaya. Remote Sens. Environ., 162, 55–66. https://doi.org/10.1016/j.rse.2015.01.031

Dozier, J. 1989. Spectral signature of alpine snow cover from the Landsat Thematic Mapper. Remote Sens. Environ., 28, 9–22, https://doi.org/10.1016/0034-4257(89)90101-6

Dunse, T., T.V. Schuler, J.O. Hagen, and C.H. Reijmer. 2012. Seasonal speed-up of two outlet glaciers of Austfonna, Svalbard, inferred from continuous GPS measurements. The Cryosphere, 6, 453–466, https://doi.org/10.5194/tc-6-453-2012

Dunse, T., T. Schellenberger, , J.O. Hagen, A. Kääb, T.V. Schuler, and C.H. Reijmer. 2015. Glacier-surge mechanisms promoted by a hydro-thermodynamic feedback to summer melt. The Cryosphere, 9, 197–215, https://doi.org/10.5194/tc-9-197-2015

Dyurgerov, M., M.F. Meier and D.B. Bahr. 2009. A new index of glacier area change: a tool for glacier monitoring. J. Glaciol. 55, 710–716, https://doi.org/10.3189/002214309789471030

Engeset, R.V., J. Kohler, K. Melvold and B. Lundén. 2002. Change detection and monitoring of glacier mass balance and facies using ERS SAR winter images over Svalbard. Int. J. Remote Sens., 23, 2023–2050, https://doi.org/10.1080/01431160110075550

Engeset, R.V., T.V. Schuler and M. Jackson. 2005. Analysis of the first jökulhlaup at Blåmannsisen in northern Norway and implications for future events. Annals of Glaciology, 42, 35–41, https://doi.org/10.3189/172756405781812600

ESA. http://www.esa.int/Applications/Observing_the_Earth/Copernicus/Overview4. (Date viewed: 2020-01-05).

Fahnestock, M., T. Scambos and R.A. Bindschadler. 1992. Semi-automated ice velocity determination from satellite imagery. EOS, 73, 493

Farinotti, D. et al. 2017. How accurate are estimates of glacier ice thickness? Results from ITMIX, the Ice Thickness Models Intercomparison Experiment. The Cryosphere, 11, 949-970, doi:10.5194/tc-11-949-2017

Fürst, J.J., F. Navarro, F. Gillet-Chaulet, M. Huss, G. Moholdt, X. Fettweis, C. Lang, T. Seehaus, S. Ai, T.J Benham, D.I. Benn, H. Björnsson, J.A. Dowdeswell, M. Grabiec, J. Kohler, I. Lavrentiev, K. Lindbäck, K. Melvold, R. Pettersson, … M.H. Braun. 2018. The ice-free topography of Svalbard. Geophysical Research Letters, 45, 11,760–11,769, https://doi.org/10.1029/2018GL079734

Gardner, A. S., G. Moholdt, T. Scambos, M. Fahnstock, S. Ligtenberg, M. van den Broeke, and J. Nilsson, 2018: Increased West Antarctic and unchanged East Antarctic ice discharge over the last 7 years, Cryosphere, 12(2), 521–547.

Gascon, F. 2016. Sentinel-2: Products Data Quality and Evolutions. Available from: http://www.eurosdr.net/workshops/2nd-workshop-preparation-sentinel-2-europe.

Girod, L., C. Nuth, A. Kääb, R. McNabb and O. Galland. 2017. MMASTER: Improved ASTER DEMs for Elevation Change Monitoring. Remote Sensing, 9(7), 704. https://doi.org/10.3390/rs9070704

Gong, Y., T. Zwinger, J. Åström, B. Altena, T. Schellenberger, R. Gladstone and J.C. Moore. 2018. Simulating the roles of crevasse routing of surface water and basal friction on the surge evolution of Basin 3, Austfonna ice cap. The Cryosphere, 12, 1563–1577. https://doi.org/10.5194/tc-12-1563-2018

Hagen, J.O., O. Liestol, E. Roland, T. Jorgensen. 1993. Glacier atlas of Svalbard and Jan Mayen vol 129. Norwegian Polar Institute, Oslo

Hall, D. K., G.A. Riggs and V.V. Salomonson. 1995. Development of methods for mapping global snow cover using moderate resolutionimaging spectroradiometer data. Remote Sensing of Environment, 54, 127–140, https://doi.org/10.1016/0034-4257(95)00137-P

Heid T. and A. Kääb A. 2012. Evaluation of existing image matching methods for deriving glacier surface displacements globally from optical satellite imagery. Remote Sensing of Environment, 118, 339-355.

How, P., D.I. Benn, N.R.J. Hulton, B. Hubbard, A. Luckman, H. Sevestre, W. J. J. van Pelt, K. Lindbäck, J. Kohler, and W. Boot. 2017. Rapidly changing subglacial hydrological pathways at a tidewater glacier revealed through simultaneous observations of water pressure, supraglacial lakes, meltwater plumes and surface velocities. The Cryosphere, 11, 2691–2710.

Jackson, M., I.A. Brown and Elvehøy, H. 2005. Velocity measurements on Engabreen, Norway. Ann. Glaciol., 42, 29–34. https://doi.org/10.3189/172756405781812655

Jackson, M. and G. Ragulina. 2014. Inventory of glacier-related hazardous events in Norway. Norwegian Water Resources and Energy Directorate, NVE report 83-2014, 218p.

Jiskoot, H., T. Murray and P. Boyle. 2000. Controls on the distribution of surge-type glaciers in Svalbard. J. Glaciol., 46(154), 412-422. https://doi.org/10.3189/172756500781833115

Kääb A. and M. Vollmer M. 2000. Surface geometry, thickness changes and flow fields on creeping mountain permafrost: automatic extraction by digital image analysis. Permafrost and Periglacial Processes.11, 315-326.

Kääb, A., T. Bolch, K. Casey, T. Heid, J.S. Kargel, G.J. Leonard, F. Paul and B.H. Raup. 2014. Glacier Mapping and Monitoring Using Multispectral Data, in: Global Land Ice Measurements from Space, edited by J.S. Kargel, G.J. Leonard, M.P. Bishop, A. Kääb,A., and B.H. Raup. 2014. Springer Praxis Books, pp. 75–112, Springer Berlin Heidelberg, doi:10.1007/978-3-540-79818-7_4.

Kääb, A., S.H. Winsvold, B. Altena, C. Nuth, T. Nagler and J. Wuite. 2016. Glacier Remote Sensing Using Sentinel-2. Part I: Radiometric and Geometric Performance, and Application to Ice Velocity. Remote Sensing, 8(7), 598, https://doi.org/10.3390/rs8070598

Kartverket. 2018. DTM 10 Terrengmodell. https://kartkatalog.geonorge.no/metadata/kartverket/dtm-10-terrengmodell-utm33/dddbb667-1303-4ac5-8640-7ec04c0e3918, accessed: 23.03.2018

Kelly, R., R.V. Engeset, M. Kennett, E.C. Barrett and W. Theakstone. 1997. Characteristic snow and ice properties of a Norwegian ice cap determined from complex ERS SAR. Proceedings, 3rd ERS Symposium (ESA), Florence, Italy, CD-ROM.

Kienholz, C., R. Hock, M. Truffer, P. Bieniek and R. Lader. 2017. Mass balance evolution of Black Rapids Glacier, Alaska, 1980–2100, and its implications for surge recurrence. Frontiers in Earth Sciences - Cryospheric Sciences, 5, 56, https://doi.org/10.3389/feart.2017.00056

Kjøllmoen, B. 2018. Glasiologiske undersøkelser på Blåmannsisen 2002-2017, NVE-Rapport 3- 2018, 49 pp.

Kjøllmoen, B. (Ed.), L.M. Andreassen, H. Elvehøy, M. Jackson. 2020. Glaciological investigations in Norway 2019. NVE Rapport 34-2020, 86 pp +app.

Klingenberg, T.F. 2017. Evaluation of Sentinel-2: Case Study of Land Cover Classification and Ice Velocity, Masters thesis, p. 118.

König, M., J.G. Winther, J. Kohler and F. König. 2004. Two methods for firn-area and mass-balance monitoring of Svalbard glaciers with SAR satellite images. Journal of Glaciology, 50(168), 116-128, https://doi.org/10.3189/172756504781830286

Leigh, J.R, C.R. Stokes, D.J.A. Evans, R.J. Carr and L.M. Andreassen. 2020. Timing of 'Little Ice Age' maxima and subsequent glacier retreat in northern Troms and western Finnmark, northern Norway. Arctic, Antarctic, and Alpine Research, 52:1, 281-311, doi: 10.1080/15230430.2020.1765520

Li, J. and Y. Sheng. 2012. An automated scheme for glacial lake dynamics mapping using Landsat imagery and digital elevation models: a case study in the Himalayas. International Journal of Remote Sensing, 33(16), 5194-5213. https://doi.org /10.1080/01431161.2012.657370

Li, J. and D.P. Roy. 2017. A global analysis of Sentinel-2A, Sentinel-2B and Landsat-8 data revisit intervals and implications for terrestrial monitoring. Remote Sens., 9, 902. https://doi.org/10.3390/rs9090902

Liestøl, O. 1956. Glacier dammed lakes in Norway. Norsk geografisk tidsskrift, Bind 15, Oslo, p. 122-149.

Liestøl, O. 1962. List of the area and number of glaciers. In A. Hoel and W. Werenskiold, eds. Glaciers and snowfields in Norway. Norsk Polarinstitutt Skrifter, 114.

Liestøl, O. 1967. Storbreen glacier in Jotunheimen, Norway. Norsk Polarinstitutt Skrifter, 141, p. 63.

Loveland, T.R. and J.R. Irons. 2016. Landsat 8: The plans, the reality, and the legacy. Remote Sens. Environ., 185, 1–6, https://doi.org/10.1016/j.rse.2016.07.033

Luckman, A., D. Jansen, B. Kulessa, E.C. King, P. Sammonds and D.I. Benn,. 2012. Basal crevasses in Larsen C Ice Shelf and implications for their global abundance, The Cryosphere, 6, 113–123, https://doi.org/10.5194/tc-6-113-2012.

Lydersen, C. and 12 others. 2014. The importance of tidewater glaciers for marine mammals and seabirds in Svalbard, Norway. Journal of Marine Systems, 129, 452-471.

Main-Knorn, M., B. Pflug, J. Louis, V. Debaecker, U. Müller-Wilm and F. Gascon. 2017. Sen2Cor for Sentinel-2. In Image and Signal Processing for Remote Sensing XXIII

Conference; International Society for Optics and Photonics, Warsaw, Poland, 2017. https://doi.org/10.1117/12.2278218

Maton, J. 2019. First precise dataset recording front lines positions of all Svalbard tidewater laciers from the last 7 years (2013-2019). Internship report 2019-2020, Norwegian Polar Institute and Université Libre de Bruxelles, Belgium.

McFeeters, S.K. 1996. The use of the Normalized Difference Water Index (NDWI) in the delineation of open water features. International J. of Remote Sens., 17:7, 1425-1432. https://doi.org/10.1080/01431169608948714

Messerli, A. and A. Grinsted. 2015. Image georectification and feature tracking toolbox: ImGRAFT. Geosci. Instrum. Methods Data Syst., 4, 23–34. https://doi.org/10.5194/gi-4-23-2015

Miles, K.E., I.C. Willis, C.L. Benedek, A.G. Williamson and M. Tedesco. 2017. Toward monitoring surface and subsurface lakes on the Greenland Ice Sheet using Sentinel-1 SAR and Landsat 8 OLI imagery. Frontiers in Earth Sciences - Cryospheric SciencesFrontiers in Earth Sciences - Cryospheric Sciences, 5, 1–17. https://doi.org/10.3389/feart.2017.00058

Morris, A., G. Moholdt and L. Gray. 2020. Spread of Svalbard Glacier Mass Loss to Barents Sea Margins Revealed by CryoSat-2. Journal of Geophysical Research: Earth Surface, 125(8).

Mouginot, J. and E. Rignot. 2015. Ice motion of the Patagonian Icefields of South America: 1984-2014. Geophys. Res. Lett., 42, 1441–1449. https://doi.org/10.1002/2014GL062661

Nagy, T., L.messerliM. Andreassen, R. A. Duller and P. J. Gonzalez. 2019. SenDiT: A Sentinel-2 Displacement Toolbox with application to glacier surface velocities. Remote Sensing, 11, 1151. https://doi.org/10.3390/rs11101151

Nagy, T. and L.M. Andreassen. 2019a. Glacier surface velocity mapping with Sentinel-2 imagery in Norway. NVE Rapport 37-2019, 35 p.

Nagy, T. and L. M. Andreassen. 2019b. Glacier lake mapping with Sentinel-2 imagery in Norway. NVE Rapport 40-2019, 54 s.

Nie, Y., Y. Sheng, Q. Liu, L. Liu, S. Liu, Y. Zhang and C. Song. 2017. A regional-scale assessment of Himalayan glacial lake changes using satellite observations from 1990 to 2015. Remote Sens. Environ., 189, 1–13. https://doi.org/10.1016/j.rse.2016.11.008

Norsk Polarinstitutt. 2018. Svalbard DTM 20. https://kartkatalog.geonorge.no/metadata/norsk-polarinstitutt/svalbard-dtm-20/9d118d31-182c-495b-b7be-d819cc7444b1, accessed: 03.23.2018.

Nuth, C., J. Kohler, M. König, A. von Deschwanden, J. O. Hagen, A. Kääb, G. Moholdt and R. Pettersson. 2013. Decadal changes from a multi-temporal glacier inventory of Svalbard. Cryosphere, 7(5), 1603–1621. https://doi.org/10.5194/tc-7-1603-2013

O’Neel, S., W. T. Pfeffer, R. Krimmel and M. Meier. 2005. Evolving force balance at Columbia Glacier, Alaska, during its rapid retreat. J. Geophys. Res., 110, F03012, https://doi.org/10.1029/2005JF000292

Paul F., A. Kääb. 2005. Perspectives on the production of a glacier inventory from multispectral satellite data in Arctic Canada: Cumberland Peninsula, Baffin Island Annals of Glaciology, 42, 59-66.

Paul, F., S.H. Winsvold, A. Kääb, T. Nagler and G. Schwaizer. 2016. Glacier Remote Sensing Using Sentinel-2. Part II: Mapping Glacier Extents and Surface Facies, and Comparison to Landsat 8. Remote Sensing, 8, 575, https://doi.org/10.3390/rs8070575

Pelto, M. 2011. Utility of late summer transient snowline migration rate on Taku Glacier, Alaska. Cryosphere, 5, 1127–1133, https://doi.org/10.5194/tc-5-1127-2011

Pfeffer W.T., A.A. Arendt, A. Bliss, T. Bolch, J.G. Cogley, A.S. Gardner, J. Hagen, R. Hock, G Kaser, C. Kienholz, E.S. Miles, G. Moholdt, N. Mölg, F Paul, V. Radić, P. Rastner, B.H. Raup, J. Rich and M.J. Sharp. 2014. The Randolph Glacier Inventory: a globally complete inventory of glaciers. Journal of Glaciology, 60:537-552, https://doi.org/10.3189/2014JoG13J176

Porter, C. and 28 others.2018. ArcticDEM, Harvard Dataverse. doi:10.7910/DVN/OHHUKH.

Rabatel, A., J.P. Dedieu and C. Vincent. 2005. Using remote-sensing data to determine equilibrium-line altitude and mass-balance time series: Validation on three French glaciers, 1994–2002. Journal of Glaciology, 51, 539–546, https://doi.org/10.3189/172756505781829106

Rabatel, A., P. Sirguey, V. Drolon, P. Maisongrande, Y. Arnaud, E. Berthier, L. Davaze, J.-P. Dedieu and M. Dumont. 2017. Annual and seasonal glacier wide surface mass balance quantified from changes in glacier surface state: a review on existing methods using optical satellite imagery. Remote Sensing, 9 (5), 507, doi: 10.3390/rs9050507.

Racoviteanu A.E., K. Rittger and R. Armstrong. 2019. An Automated Approach for Estimating Snowline Altitudes in the Karakoram and Eastern Himalaya From Remote Sensing. Front. Earth Sci., 7, 220, https://doi.org/10.3389/feart.2019.00220

Rastner, P., R. Prinz, C. Notarnicola, L. Nicholson, R. Sailer, G. Schwaizer and F. Paul. 2019. On the Automated Mapping of Snow Cover on Glaciers and Calculation of Snow Line Altitudes from Multi-Temporal Landsat Data. Remote Sens., 11, 1410. https://doi.org/10.3390/rs11121410

Raup, B., A. Kääb, J.S. Kargel, M.P. Bishop, G. Hamilton, E. Lee, F. Paul, F. Rau, D. Soltesz, S.J.S. Khalsa, M. Beedle, C. Helm. 2007. Remote sensing and GIS technology in the global land ice measurements from space (GLIMS) project Comput Geosci 33:104-125,. 10.1016/j.cageo.2006.05.015

Redpath, T. A. N., P. Sirguey, S.J. Fitzsimons and A. Kääb. 2013. Accuracy assessment for mapping glacier flow velocity and detecting flow dynamics from ASTER satellite imagery: Tasman Glacier, New Zealand. Remote Sens. Environ, 133, 90–101, https://doi.org/10.1016/j.rse.2013.02.008

safetravel.is/crevasse-maps: Crevasse maps of Icelandic glaciers. Accessed on: 20/03/2020

Schellenberger, T., T. Dunse, A. Kääb, J. Kohler, and C.H. Reijmer. 2015. Surface speed and frontal ablation of Kronebreen and Kongsbreen, NW Svalbard, from SAR offset tracking. The Cryosphere, 9, 2339–2355, https://doi.org/10.5194/tc-9-2339-2015.

Schellenberger, T., W. Van Wychen, L. Copland, A. Kaab and L. Gray. 2016. An Inter-Comparison of Techniques for Determining Velocities of Maritime Arctic Glaciers, Svalbard, Using Radarsat-2 Wide Fine Mode Data, Remote Sens-Basel, 8, https://doi.org/ARTN 78510.3390/rs8090785, 2016.

Schuler T.V., J. Kohler, N. Elagina, J.O.M. Hagen, A.J Hodson, J.A Jania, A. Kääb, B. Luks, J. Małecki, G. Moholdt, V.A. Pohjola, I. Sobota and W.J.J. Van Pelt. 2020. Reconciling Svalbard Glacier Mass Balance. Front. Earth Sci. 8:156, https://doi.org/10.3389/feart.2020.00156

Sund, M., T.R. Lauknes, and T. Eiken. 2014. Surge dynamics in the Nathorstbreen glacier system, Svalbard, The Cryosphere, 8, 623–638, https://doi.org/10.5194/tc-8-623-2014.

Sund, M., T. Eiken, J.O. Hagen, and A. Kääb. 2009. Svalbard surge dynamics derived from geometric changes. Annals of Glaciology, 50(52), 50-60, https://doi.org/10.3189/172756409789624265

Thakur, P.K., S.P. Aggarwal, G. Arun, S. Sood, A.S. Kumar and S. Mani. 2017. Estimation of snow cover area, snow physical properties and glacier classification in parts of Western Himalayas using C-Band SAR data. J. Indian Soc. Remote Sens., 45, 525–539, https://doi.org/10.1007/s12524-016-0609-y

Wangensteen, B., O.M. Tønsberg, A. Kääb, T. Eiken and J.O. Hagen. 2006. Surface Elevation Change and High Resolution Surface Velocities for Advancing Outlets of Jostedalsbreen. Geografiska Annaler, Series A: Physical Geography, 88(1), 55–74.

Watson, C.S., O. King, E.S. Miles and D.J. Quincey. 2018. Optimising NDWI supraglacial pond classification on Himalayan debris-covered glaciers. Remote Sens. Environ., 217, 414–425, https://doi.org/10.1016/j.rse.2018.08.020

Weber, P., C.M. Boston, H. Lowell, L.M. Andreassen. 2019. Evolution of the Norwegian plateau icefield Hardangerjøkulen since the 'Little Ice Age'. The Holocene, 1-21, doi/10.1177/0959683619865601

Weber, P., L.M. Andreassen, C. M. Boston, H. Lovell and S. Kvarteig. 2020a. An ~1899 glacier inventory for Nordland, northern Norway, produced from historical maps. Journal of Glaciology, 1-19. https://doi.org/10.1017/jog.2020.3

Weber, P. H. Lovell, L.M. Andreassen and C.M. Boston. 2020b. Reconstructing the Little Ice Age extent of Langfjordjøkelen, northernmost Arctic Norway, as a baseline for assessing centennial-scale icefield recession. Polar Research, 39, https://doi.org/10.33265/polar.v39.4304

WGMS. 2020. Global Glacier Change Bulletin No. 3 (2016-2017). Zemp, M., I. Gärtner-Roer, S.U. Nussbaumer, J. Bannwart, P. Rastner, F. Paul and M. Hoelzle (eds.). ISC(WDS)/IUGG(IACS)/UNEP/UNESCO/WMO, World Glacier Monitoring Service, Zurich, Switzerland, 274 pp., publication based on database version: doi:10.5904/wgms-fog-2019-12

Whillans, I. and Y. Tseng. 1995. Automatic tracking of crevasses on satellite images. Cold Reg. Sci. Technol., 23, 201–214, https://doi.org/10.3189/S0022143000016452

Williamson, A.G., A.F. Banwell, I.C. Willis and N.S. Arnold. 2018. Dual-satellite (Sentinel-2 and Landsat 8) remote sensing of supraglacial lakes in Greenland. Cryosphere, 12, 3045-3065, https://doi.org/10.5194/tc-12-3045-2018

Winsvold, S.H. 2017. Mapping glaciers using time-series of remote sensing data, PhD thesis, University of Oslo. Available from: https://www.duo.uio.no/handle/10852/55631

Winsvold, S.H. and L.M. Andreassen. 2012. Glacier Lake Outline – Norway, v1.0. NVE. http://arcus.nve.no/data/bre/GLO/zip/. Delivered by CryoClim service.

Winsvold, S.H., L.M. Andreassen and C. Kienholz. 2014. Glacier area and length changes in Norway from repeat inventories. Cryosphere, 8, 1885–1903,https://doi.org/10.5194/tc-8-1885-2014

Winsvold, S.H., A. Kääb, C. Nuth, L.M. Andreassen, W.J. Van Pelt and T. Schellenberger. 2018. Using SAR satellite data time series for regional glacier mapping. Cryosphere, 12, 867–890, https://doi.org/10.5194/tc-12-867-2018

Wouters, B., A.S. Gardner and G. Moholdt. 2019. Global Glacier Mass Loss During the GRACE Satellite Mission (2002-2016). Front. Earth Sci. 7:96, doi: 10.3389/feart.2019.00096

Zhou, C., E. Dongchen, Z. Wang and L. Sun. 2008. Remote sensing application in Antarctic inland areas. Int. Arch. Photogramm. Remote Sens. Spatial Inf. Sci., 37(B8), 819–824.

Østrem, G. 1975. ERTS data in glaciology - an effort to monitor glacier mass balance from satellite imagery. Journal of Glaciology, 15, 403–415.

Østrem, G., K. Dale Selvig and K. Tandberg. 1988. Atlas over breer i Sør-Norge. Meddelelse, 61, Hydrologisk avdeling, Norges Vassdrags- og Elektrisitetsvesen, Oslo, Norway.

Østrem, G., N. Haakensen and O. Melander. 1973. Atlas over breer i Nord-Skandinavia. Meddelelse, 22, Hydrologisk avdeling, Norges Vassdrags- og Energiverk, Oslo, Norway.

Østrem, G., O. Liestøl and B. Wold. 1976. Glaciological investigations at Nigardsbreen, Norway. Norsk Geografisk Tidskrift (Norwegian Journal of Geography), 30(1), 187–209.

Østrem, G. and T. Ziegler. 1969. Atlas over breer i Sør-Norge. Meddelelse, 20, Hydrologisk avdeling, Norges Vassdrags- og Elektrisitetsvesen, Oslo, Norway.

Appendix: List of publications

Here we list publications and selected presentations related to Copernicus Glacier Service.

List of peer-reviewed publications

1. Kääb, A., S.H. Winsvold, B. Altena, C. Nuth, T. Nagler and J. Wuite. 2016. Glacier Remote Sensing Using Sentinel-2. Part I: Radiometric and Geometric Performance, and Application to Ice Velocity. Remote Sensing, 8(7), 598, https://doi.org/10.3390/rs8070598

2. Paul, F., S. H. Winsvold, A. Kääb, T. Nagler and G. Schwaizer. 2016. Glacier Remote Sensing Using Sentinel-2. Part II: Mapping Glacier Extents and Surface Facies, and Comparison to Landsat 8. Remote Sensing, 8, 575. https://doi.org/10.3390/rs8070575

3. Schellenberger, T., W. Van Wychen, L. Copland, A. Kääb and L. Gray. 2016. An Inter-Comparison of Techniques for Determining Velocities of Maritime Arctic Glaciers, Svalbard, Using Radarsat-2 Wide Fine Mode Data. Remote Sensing, 8(9), 785, https://doi.org/10.3390/rs8090785

4. Altena, B. and A. Kääb. 2017. Elevation change and improved velocity retrieval using orthorectified optical satellite data from different orbits. Remote Sensing, 9(3), 300, https://doi.org 10.3390/rs9030300

5. Altena B. and Kääb A. 2017. Weekly glacier flow estimation from dense satellite time series using adapted optical flow technology. Frontiers in Earth Sciences - Cryospheric Sciences, 5, 53, https://doi.org/10.3389/feart.2017.00053

6. Strozzi, T., A. Kääb and T. Schellenberger. 2017. Frontal destabilization of Stonebreen, Edgeøya, Svalbard. Cryosphere, 11, 553-566, https://doi.org/10.5194/tc-11-553-2017

7. Strozzi T., F. Paul, A. Wiesmann, T. Schellenberger and A. Kääb. 2017. Circum-Arctic changes in the flow of glaciers and ice caps from satellite SAR data between the 1990s and 2017. Remote Sensing, 9(9), 947, https://doi.org/10.3390/rs9090947

8. Winsvold, S. H., A. Kääb, C. Nuth, L. M. Andreassen, W. van Pelt and T. Schellenberger. 2018. Using SAR satellite data time-series for regional glacier mapping. Cryosphere, 12, 867-890, https://doi.org/10.5194/tc-12-867-2018

9. Stokes, S., L. M. Andreassen, M. R. Champion and G. D. Corner. 2018. Widespread and accelerating glacier retreat on the Lyngen Peninsula, northern Norway, since their 'Little Ice Age' maximum. Journal of Glaciology, 64(243), 100-118. https://doi.org/10.1017/jog.2018.3

10. Girod, L., N. I. Nielsen, F. Couderette, C. Nuth and A. Kääb. 2018. Precise DEM extraction from Svalbard using 1936 high oblique imagery. Geoscientific

Instrumentation, Methods and Data Systems, 7, 277-288, https://doi.org/10.5194/gi-7-277-2018 (pdf)

11. Nagy, T., L. M. Andreassen, R. A. Duller and P. J. Gonzalez. 2019. SenDiT: A Sentinel-2 Displacement Toolbox with application to glacier surface velocities. Remote Sensing, 11, 1151, https://doi.org/10.3390/rs11101151

12. Nuth, C., A. Gilbert, A. Köhler, R. McNabb, T. Schellenberger, H. Sevestre, C. Weidle, L. Girod, A. Luckman and A. Kääb. 2019. Dynamic vulnerability revealed in the collapse of an Arctic tidewater glacier. Scientific Reports. 9(1), 5541, https://doi.org/10.1038/s41598-019-41117-0

13. Weber, P., C.M. Boston, H. Lowell and L.M. Andreassen. 2019. Evolution of the Norwegian plateau icefield Hardangerjøkulen since the 'Little Ice Age'. The Holocene, 29, 1-21, https://doi.org/10.1177%2F0959683619865601

14. Leigh, J.R, C.R. Stokes, R.J. Carr, I.S. Evans, L.M. Andreassen and D.J.A. Evans. 2019. Identifying and mapping very small (<0.5 km^2) mountain glaciers on coarse to high-resolution imagery. Journal of Glaciology, 65, 873-888, https://doi.org/10.1017/jog.2019.50

15. Weber, P., L. M. Andreassen, C. M. Boston, H. Lovell and S. Kvarteig. 2020. An ~1899 glacier inventory for Nordland, northern Norway, produced from historical maps. Journal of Glaciology, 66, 259-277, https://doi.org/10.1017/jog.2020.3

16. Leigh, J.R, C.R. Stokes, D.J.A. Evans, R.J. Carr and L.M. Andreassen. 2020. Timing of 'Little Ice Age' maxima and subsequent glacier retreat in northern Troms and western Finnmark, northern Norway. Arctic, Antarctic, and Alpine Research, 52:1, 281-311, doi: 10.1080/15230430.2020.1765520

17. Weber, P. H. Lovell, L.M. Andreassen and C.M. Boston. 2020. Reconstructing the Little Ice Age extent of Langfjordjøkelen, northernmost Arctic Norway, as a baseline for assessing centennial-scale icefield recession. Polar Research, 39, https://doi.org/10.33265/polar.v39.4304

18. Haga, O., R. McNabb, R., C. Nuth, B. Altena, T. Schellenberger and A. Kääb. 2020. From high friction zone to frontal collapse: Dynamics of an ongoing tidewater glacier surge, Negribreen, Svalbard. Journal of Glaciology, 1-13, doi:10.1017/jog.2020.43.

19. Morris, A., G. Moholdt, & L. Gray. 2020. Spread of Svalbard glacier mass loss to Barents Sea margins revealed by CryoSat-2. Journal of Geophysical Research, 125, doi:10.1029/2019JF005357

Theses

1. Klingenberg, T. F. 2017. Evaluation of Sentinel-2: Case Study of Land Cover Classification and Ice Velocity. Master thesis. Physical Geography, Hydrology and geomatics, University of Oslo.

2. Winsvold, S. H. 2017. Mapping glaciers using time-series of remote sensing data. Doctor thesis. Department of Geosciences, Faculty of Mathematics and Natural Sciences, University of Oslo.

List of reports

1. Nagy, T. and L.M. Andreassen. 2019. Glacier surface velocity mapping with Sentinel-2 imagery in Norway. NVE Rapport 37-2019, 35 p.

2. Nagy, T. and L.M. Andreassen. 2019. Glacier lake mapping with Sentinel-2 imagery in Norway. NVE Rapport 40-2019, 54 p.

3. Andreassen, L.M. (red.), M. Callanan, T. Saloranta, B. Kjøllmoen og T. Nagy. 2020. FonnSat - Fonner, arkeologi og satellittdata. NVE Rapport 41-2020, 65 s

4. Andreassen, L.M. (ed.), G. Moholdt, A. Kääb, A. Messerli, T. Nagy and S.H. Winsvold. 2021. Monitoring glaciers in mainland Norway and Svalbard using Sentinel. NVE Rapport 3-2021, 94 p.

List of popular literature and medialized articles

1. Barth, V. L., S. H. Winsvold and A. Kääb. 2016. COPERNICUS: Norge i rødt, grønt og blått, Posisjon-3-2016. Magasinet for Geomatikk, p 6-7.

2. News: Satellittbilder viser nye ras på Svalbard. 17. November 2016, Titan, Universitetet i Oslo.

3. News: Vi har mistet 11 kvadratkilometer isbre årlig. 18. September 2017, Titan, Universitetet i Oslo.

4. News: "Vårflommen" i høst – sett fra radarsatellitter. 19. October 2018, Titan, Universitetet i Oslo.

5. News: Isbreene smelter: Ny øy på Svalbard. 7. September 2019, NRK.

6. Andreassen, L. M. and P. Weber. Historiske kart over Norge avslører breenes utvikling. 29. October 2019, Aftenposten.

7. Andreassen, L. M and T. Nagy. 2019. Sentinel satellittbilder til å kartlegge og overvåke breer. Posisjon, nr. 4, 2019, p. 7.

Presentations (selection)

1. Solveig H. Winsvold, Andreas Kääb, Christopher Nuth, Ward van Pelt, Liss M. Andreassen and Thomas Schellenberger. Glacier mapping using combined optical and SAR time-series. Oral presentation, Nordic Branch Meeting, International Glaciological Society, 26-28. October 2016, Tromsø, Norway.

2. Alexandra Messerli and Geir Moholdt. Velocity Products from Landsat-8 and Sentinel-2 using ImGRAFT. Poster presentation, Nordic Branch Meeting, International Glaciological Society, 26-28. October 2016, Tromsø, Norway.

3. Solveig H. Winsvold, Andreas Kääb, Christopher Nuth, Liss M. Andreassen, Ward van Pelt and Thomas Schellenberger. Regional Glacier Mapping by Combination of Dense Optical and SAR Satellite Image Time-Series. Oral presentation. AGU fall meeting, 12-16. December 2016, San Fransisco, USA.

4. Liss M. Andreassen, Andreas Kääb, Ferdinand Klingenberg, Alexandra Messerli, Geir Moholdt and Solveig H. Winsvold. Oral presentation, GLIMS Meeting at AGU fall Meeting, 13. December 2016, San Fransisco, USA.

5. Solveig H. Winsvold, Andreas Kääb, Christopher Nuth and Bas Altena. Landsat time-series analysis opens new approaches for regional glacier mapping. Oral presentation (Invited). AGU fall meeting, 12-16. December 2016, San Francisco, USA.

6. Alexandra Messerli and Geir Moholdt. Norwegian Copernicus Glacier Service: Svalbard Velocity using ImGRAFT. Poster presentation. EARSeL workshop "Remote Sensing of Land Ice and Snow", 7-9. February 2017, Bern, Switzerland.

7. Liss M. Andreassen, Solveig H. Winsvold, Ferdinand Klingenberg, Paul Weber, Joaquin M. C. Belart. Status of GLIMS work NVE, Norway. Oral presentation, GLIMS workshop, 11-13. August 2017, Boulder, Colorado, USA.

8. Solveig H. Winsvold, Andreas Kääb, Christopher Nuth, Liss M. Andreassen, Ward van Pelt and Thomas Schellenberger. Mapping glaciers using time-series of SAR data. Oral presentation, GLIMS workshop, 11-13. August 2017, Boulder, Colorado, USA.

9. Solveig H. Winsvold, Liss M. Andreassen, Andreas Kääb, Alexandra Messerli and Geir Moholt. Using the Sentinel satellites for glacier monitoring in Norway. Oral presentation. Nordic IGS branch meeting. 25-27. October 2017, Uppsala, Sweeden.

10. A. Messerli and G. Moholdt. Norwegian Copernicus Glacier Service: Glacier products for Svalbard using Sentinel-2. Poster presentation, Svalbard Science Forum, 6.-8. November 2017, Oslo, Norway.

11. R. McNabb, A. Kääb, C. Nuth and L. Girod. Exploiting satellite archives to estimate global glacier volume changes (case study Norway). Presentation, AGU fall meeting, December 2017, San Fransisco, USA.

12. T. F. Klingenberg. Quality assessment of PlanetDEM90 in Norway and its effect on the geometric performance of Sentinel. 2nd Sentinel-2 validation team meeting, ESA-ESRIN, 29-31. January 2018, Frascati, Italy.

13. S. H. Winsvold. Bruk av Sentinel-satellittene i Norges vassdrags- og energidirektorat. Oral presentation. NIFRO-seminar «Anvendt bruk av satellittdata i Norge – nå og i framtiden» at Space Dinner, 13. February 2018, Grand Hotel, Oslo, Norway.

14. S. H. Winsvold, L. Andreassen, K. Melvold, K. Müller, M. Sund and Nils K. Orthe. Sentinel-satellittene gir nye muligheter for hydrologisk kartlegging. Oral presentation. Norsk Hydrologiråds fagmøte «Ny teknologi for hydrologiske observasjoner», 5. April 2018, SWECO, Oslo, Norway.

15. S. H. Winsvold, A. Kääb, L. M. Andreassen, K. Melvold, K. Müller, M. Sund and Nils K. Orthe. Overvåkning av Norges vannressurser med Sentinel-satellittene. Oral presentation. Geomatikkdagene, 13-15. March 2018, Stavanger, Norway.

16. A. Kääb. Glacier instabilities on Svalbard. Oral presentation, Centre of Earth Evolution and Dynamics, 1. June 2018, Oslo, Norway.

18. L. M. Andreassen, S. H. Winsvold, A. Kääb, A. Messerli, G. Moholdt, T. F. Klingenberg and N.K. Orthe Copernicus Glacier Service – monitoring glaciers in Svalbard and mainland Norway using Sentinel. Poster presentation, Polar 2018, 20. June 2018, Davos, Switzerland.

19. Geir Moholdt. Sentinel-2 for glacier monitoring on Svalbard. Nordic Branch Meeting, International Glaciological Society, 24-25. October 2018, Rovaniemi, Finland.

20. Paul Weber. Response of Norwegian plateau icefields to climate warming since the little ice age. Oral presentation. Workshop on mass budget of Arctic glaciers, International Association of Cryospheric Sciences, 21-23. January 2019, Geilo, Norway.

21. Ashley Morris. Svalbard glacier elevation and mass changes from Cryosat data. Oral presentation. Workshop on mass budget of Arctic glaciers, International Association of Cryospheric Sciences, 21-23. January 2019, Geilo, Norway.

22. Liss M. Andreassen. From historical maps to high resolution satellite imagery – mapping the present state and changes of Norway's glaciers. Oral presentation. 7. March 2019, Durham, United Kingdom.

23., Kjetil Melvold, Karsten Muller, Teodor Nagy, Nils K. Orthe. Using the Sentinels to detect glacier lake outburst floods, snow avalanches and the glacier, lake ice and snow cover in Norway. Poster presentation. European Geosciences Union Meeting, Session, 7-12. April 2019, Vienna, Austria.

24. Teodor Nagy, Liss M. Andreassen, R. A. Duller and P. J. Gonzalez. SenDiT: The Sentinel-2 Displacement Toolbox with application to glacier surface velocities. Poster presentation. European Space Agency Living Planet Symposium, 13-17. May 2019, Milano, Italy.

25. Bas Altena. Bringing together remote sensing data to produce region-wide glacier velocities. Oral presentation. European Space Agency Living Planet Symposium, 13-17. May 2019, Milano, Italy.

26. Liss M. Andreassen, Kjetil Melvold, Karsten Muller, Teodor Nagy, Nils K. Orthe. Monitoring glacier, snow and ice in Norway using the Sentinels. Poster presentation.

International Union of Geodesy and Geophysics Assembly, 8-18. July 2019, Montreal, Canada.

27. Bas Altena. Techniques to reveal inter-annual glacier flow from optical remote sensing. Oral presentation. International Union of Geodesy and Geophysics Assembly, 8-18. July 2019, Montreal, Canada.

28. Robert McNabb, Christopher Nuth, Luc Girod, Romain Hugonnet and Andreas Kääb. Multi-decadal elevation changes of Arctic glaciers. Arctic DEM workshop, 11. October 2019. Reykavik, Iceland.

29. Teodor Nagy and Liss M. Andreassen. Mapping of glacier surface velocity, glacier lakes and jøkulhlaups with Sentinel-2 imagery in mainland Norway. Nordic IGS Branch meeting. Oral presentation. 30. October-1. November 2019. Reykholt, Iceland.

30. Liss M. Andreassen, Hallgeir Elvehøy, Bjarne Kjøllmoen and Teodor Nagy. Glacier mapping using high-resolution satellite imagery and LIDAR, Nordic IGS Branch. Oral presentation. 30. October-1. November 2019. Reykholt, Iceland.

31. Geir Moholdt, Jack Kohler, Josephine Maton and Ashley Morris. Marine mass balance of Svalbard glaciers, Svalbard Science Conference. Oral presentation. 6-7. November 2019, Oslo, Norway.

32. Ashley Morris, Geir Moholdt, Jack Kohler, Alex Messerli, Josephine Maton and Marta Majerska. The Copernicus Glacier Service: An integrated observing system for Svalbard glacier mass balance, Svalbard Science Conference. Poster presentation. 6-7. November 2019, Oslo, Norway.

33. Josephine Maton, Geir Moholdt, Jack Kohler, Ashley Morris, Alex Messerli and Marta Majerska. Record of frontlines positions of Svalbard tidewater glaciers for the last 7 years, Svalbard Science Conference. Poster presentation. 6-7. November 2019, Oslo, Norway.

34. Geir Moholdt, Jack Kohler, Ashley Morris, Josephine Maton, Alex Gardner and Johannes Fürst. Recent increase in marine ablation of Svalbard glaciers. IACS Workshop on the dynamics and mass budget of Arctic glaciers. Oral presentation. 28-30. January 2020, Obergurgl, Austria.

35. Liss M. Andreassen and Teodor Nagy. Mapping glacier extent in Norway using Sentinel-2. IASC Workshop on the dynamics and mass budget of Arctic glaciers. Oral presentation. 28-30. January 2020, Obergurgl, Austria.

36. Liss M. Andreassen, Geir Moholdt and Andreas Kääb. Mapping and monitoring glaciers in mainland Norway and Svalbard using Sentinel. 17. February. Oral presentation on zoom.

NVE

Norges vassdrags- og energidirektorat

MIDDELTHUNS GATE 29
POSTBOKS 5091 MAJORSTUEN
0301 OSLO
TELEFON: (+47) 22 95 95 95